014311-1-S

COO-1407-64
068670-3-S

Microphysical Response of Cloud Droplets in a Fluctuating Updraft

DUANE D. HARDING

A. NELSON DINGLE
Project Director

July 1977

U.S. Energy Research & Development Administration
Contract No. AT(11-1)-1407
Argonne, Illinois
and
National Aeronautics and Space Administration
Langley Research Center
NASA Grant NSG 1243
Hampton, Virginia

Department of Atmospheric and Oceanic Science

THE UNIVERSITY OF MICHIGAN

COLLEGE OF ENGINEERING
Department of Atmospheric and Oceanic Science

MICROPHYSICAL RESPONSE OF CLOUD DROPLETS IN A FLUCTUATING UPDRAFT

Duane D. Harding

A. Nelson Dingle
Project Director

under contract with:

U.S. ENERGY RESEARCH & DEVELOPMENT ADMINISTRATION
CONTRACT NO. AT(11-1)-1407
ARGONNE, ILLINOIS

and

NATIONAL AERONAUTICS AND SPACE ADMINISTRATION
LANGLEY RESEARCH CENTER
NASA GRANT NSG 1243
HAMPTON, VIRGINIA

administered through:

OFFICE OF RESEARCH ADMINISTRATION ANN ARBOR

July 1977

PREFACE

The technology of cloud microphysics was greatly advanced in 1949 by the work of Howell who first computed the growth pattern of droplets formed in rising air on a population of condensation nuclei. It was advanced somewhat again by Mason's (1957) derivation of a "growth equation" for droplets. Subsequent applications of this equation to models of the development of cloud led to the observation that cloud droplets growing in a steady updraft tend in time to progress toward an increasingly narrow size spectrum. Although most workers in the field have agreed that the microphysical result of the Mason growth equation is "reasonable," nearly all, including Mason, et al. (1962, 1974) have observed that the maximum cloud droplet sizes generated in 20 to 30 minutes of steady rise are too small and/or too few to generate precipitation by the coalescence process. This is a basic question regarding the fidelity of simulation.

In his Ph.D. Dissertation, D. D. Harding has explored two distinct approaches to the correction of the above deficiency. The first is to note that cumuli in general are not produced by steady updrafts but rather are characterized by turbulent eddies, and to create a simulation using synthetic eddies (alternately increasing and decreasing saturation ratios) with Mason's growth equation (the implicit model). The result is clear: within certain domains of amplitude and frequency of the fluctuations of the saturation ratio, the largest droplets of a population continue to grow almost steadily, the

smallest evaporate and recondense with the fluctuations, and in toto, a shift of water mass toward the largest sizes takes place.

The second approach is a reconsideration of the growth equation in which it is noted that Mason's simplifying assumptions tend to create a systematic bias favoring growth of the small particles with respect to the large ones. Although in the context of conventional analytic derivations, Mason's assumptions appear quite reasonable, the particular process being considered appears to demand greater fidelity. In any event, the explicit model proposed here restores appropriate growth potential to the large droplet end of the cloud particle spectrum. By this means and by considerations of the turbulent nature of cumuli, the explicit microphysical model is capable of simulating natural rain-generation more adequately than prior models.

An additional benefit is derived from the explicit model in that vapors other than water vapor can be included in the microphysical simulation. Although the basic data on properties of dilute solutions, diffusion and sticking coefficients, and latent- and solution-energies are not always available, they will be determined as the need is shown. The field of atmospheric chemistry now demands and justifies these necessary determinations.

A. Nelson Dingle

MICROPHYSICAL RESPONSE OF CLOUD DROPLETS IN A FLUCTUATING UPDRAFT

by

Duane Douglas Harding

A dissertation submitted in partial fulfillment
of the requirements for the degree of
Doctor of Philosophy
(Atmospheric Science)
in The University of Michigan
1977

Doctoral Committee:

Professor A. Nelson Dingle, Chairman
Professor Ferdinand Baer
Associate Professor S. Roland Drayson
Professor Marc H. Ross

ACKNOWLEDGEMENTS

I am grateful to many people who helped during this endeavor. Uppermost is Dr. A. N. Dingle, chairman, tutor, logophile, and friend; you and your wife and have been very supportive.

My committee members, Drs. Baer, Drayson, and Ross have been very helpful. Dr. Dennis Baker also helped from the start, but was unable to attend the defense.

Thanks also go to Mr. Hsiao-ming Hsu for many useful discussions and suggestions. Brian Heikes and Mike Lebeis have been helpful by tracking down information and asking questions. Gary Rizzo helped do some of the early plotting. Jim Geyer has been indispensable for keypunching, editing, plotting, proofreading, and doing many of the small jobs necessary for this work.

I am also grateful to Dave Kraemer for moral support; good luck on your dissertation!

I thank Mrs. Barbara Walunas for the seemingly inhuman task of translating my disjointed scribbles into readable typescript.

And to my wife, Debi, a wonderful person...
...thank you for being you.

Duane

ABSTRACT

MICROPHYSICAL RESPONSE OF CLOUD DROPLETS IN A FLUCTUATING UPDRAFT

by
Duane Douglas Harding

Chairman: A. Nelson Dingle

The effect of a fluctuating updraft upon a distribution of cloud droplets is examined. Computations are performed for fourteen vertical velocity patterns; each allows a closed parcel of cloud air to undergo downward as well as upward motion. Droplet solution and curvature effects are included. It is found that with suitable conditions, adiabatic warming during downward motion causes small droplets to evaporate, and large, unactivated droplets to continue growing. Periods of long, slow, downward motion followed by uplifting can result in a broadening of the droplet size distribution in the lowest 100 meters of cloud height. The results depend upon the frequency and amplitude of the vertical velocity fluctuations.

The classical equation for the growth rate of an individual droplet by vapor condensation relies on simplifying assumptions. Those assumptions are isolated and examined. One result of the assumptions is that the classical equation underestimates by a few percent the actual growth rate of the largest droplets. Since the droplet temperature does not appear in the final equation,

the classical approach is called here the "implicit model." A unique approach is presented in which all energy sources and sinks of a droplet may be considered. Since direct calculation of the droplet temperature is required, the new approach is termed the "explicit model." Though details differ, both models yield similar results for the growth of ammonium sulfate solution droplets in the lowest 100 meters of cloud height. It is speculated that the explicit model may enhance the growth of large droplets at greater heights. The advantage of the explicit model is that it is the first capable of computing the growth rate of droplets in the presence of more than one volatile component. Such a model is beneficial to the studies of pollution scavenging and acid rain.

TABLE OF CONTENTS

ACKNOWLEDGEMENTS ii

ABSTRACT iii

LIST OF TABLES vii

LIST OF FIGURES viii

GLOSSARY OF SYMBOLS xii

CHAPTER I: INTRODUCTION 1

1.1 Background 1
1.2 Objectives 13

CHAPTER II: IMPLICIT MODEL 15

2.1 General Statement of the model 15
2.2 Pressure Equation 16
2.3 Temperature Equation 17
2.4 Conservation of Mass 18
2.5 Energy Budget of a Droplet 18
2.6 Droplet Growth Equation 19
2.7 Initial Conditions 23
2.8 Dry Particle Distribution 24
a. Chemical composition
b. Surface impurities
c. Particle shape
d. Discrete classification
2.9 Distribution of Droplets at the Cloud Base 28
2.10 Integration of the Equations 33
a. Method of integration
b. Stability
c. Roundoff error
d. Efficiency of integration

CHAPTER III: RESULTS WITH IMPLICIT MODEL 37

3.1 Introduction 37
3.2 Steady Updraft 38
a. Growth of droplets
b. Temperature and liquid water content
c. Breadth of distribution
d. Droplet equilibrium vapor pressure
e. Droplet growth time
f. Selective evaporation and activation
g. Radial growth rate

3.3 Fluctuating Updraft 52
a. Vertical velocity patterns
b. Growth of droplets
c. Dispersion of the droplet size distribution
d. Droplet size distribution
e. Single loop: Case 4
f. Double loops: Cases 5 and 6

CHAPTER IV: EXPLICIT MODEL 93

4.1 Introduction 93
4.2 Energy Budget of a Droplet 94
4.3 Droplet Growth Equation 97
4.4 Integration Technique 97
4.5 Review of Implicit and Explicit Equations 101
4.6 Results with Explicit Model 104
a. Droplet size distribution
b. Droplet temperature elevation
c. Droplet equilibrium supersaturation
d. Energy terms
4.7 Conclusion 113

CHAPTER V: CONCLUDING REMARKS 117

5.1 Summary 117
5.2 Suggestions for Further Research 122

APPENDIX 124

REFERENCES 133

LIST OF TABLES

Table		Page
I	Distribution of $(NH_4)_2SO_4$ particles and of cloud base droplets	32
II	Estimated times for a droplet to grow from r_n to $r_{s=0}$ and r_c. Temperature is 283.16 K. Supersaturation is 1.0%.	49
III	Vertical velocity patterns.	55
IV	Mean radius, $\bar{r}$, standard deviation, σ, and dispersion, δ, of droplet distributions 100 meters above cloud base.	71
V	Selected statistics for Cases 1,4,5, and 6.	85
VI	Coefficient of dispersion for mixed parcels.	88

LIST OF FIGURES

Figure		Page
1.	Cumulative distribution of dry $(NH_4)_2SO_4$ particles.	29
2.	Nucleus radius, droplet radius at cloud base, and radius in equilibrium at 100% relative humidity	31
3.	Growth of cloud droplets in a steady updraft of 1 m/s: Case 1. The size of the dry sulfate nucleus for each droplet size class is indicated at the bottom of the scale.	39
4.	Growth of cloud droplets in a steady updraft of 4 m/s: Case 2.	40
5.	Growth of cloud droplets in a steady updraft of 10 m/s: Case 3.	41
6.	Temperature and liquid water content within steady updrafts of 1, 4, and 10 m/s (Cases 1, 2, and 3). Also shown are the dry and moist adiabatic lapse rates. Marks on temperature curves indicate height at which maximum supersaturation is achieved.	43
7.	Critical supersaturation, S_c, critical radius, r_c, and equilibrium radius at 100% relative humidity, $r_{S=0}$, for droplets containing a nucleus of $(NH_4)_2SO_4$ at 10°C.	46
8.	Equilibrium supersaturation for two droplets.	50
9.	Radial growth rate of droplets ascending at 1 m/s from cloud base (Case 1). Curve labels indicate time (sec). Included is a line showing r^{-1} relationship.	53
10.	Growth of cloud droplets for indicated square wave velocity pattern: Case 4.	58
11.	Growth of cloud droplets for indicated square wave velocity pattern: Case 5.	59

Figure		Page
12.	Growth of cloud droplets for indicated square wave velocity pattern. Only odd-numbered size classes are shown: Case 6.	60
13.	Growth of cloud droplets for indicated square wave velocity pattern. Only odd-numbered size classes are shown: Case 7.	61
14.	Growth of cloud droplets for indicated sinusoidal velocity pattern. Only odd-numbered size classes are shown: Case 8.	63
15.	Growth of cloud droplets for indicated sinusoidal velocity pattern. Only odd-numbered size classes are shown: Case 9.	64
16.	Growth of cloud droplets for indicated sinusoidal velocity pattern. Only odd-numbered size classes are shown: Case 10.	65
17.	Growth of cloud droplets for indicated sinusoidal velocity pattern. Only odd-numbered size classes are shown: Case 11.	66
18.	Growth of cloud droplets for indicated sinusoidal velocity pattern. Only odd-numbered size classes are shown: Case 12.	67
19.	Growth of cloud droplets for indicated sinusoidal velocity pattern. Only odd-numbered size classes are shown: Case 13.	68
20.	Growth of cloud droplets for indicated sinusoidal velocity pattern. Only odd-numbered size classes are shown: Case 14.	69

Figure		Page
21.	Coefficient of dispersion of cloud droplets, from Warner (1969a).	72
22.	Droplet size distributions 100 meters above cloud base. Curve labels refer to case number.	74
23.	Droplet size distributions 100 meters above cloud base. Curve labels refer to case number.	75
24.	Droplet size distributions 100 meters above cloud base. Curve labels refer to case number.	76
25.	Droplet size distributions 100 meters above cloud base. Curve labels refer to case number.	77
26.	Equilibrium supersaturation for selected droplets: Case 4. Curve labels are the droplet size classes. Dashed line is the ambient supersaturation.	80
27.	Radial growth rate of droplets: Case 4.	83
28.	Droplet size distributions at several times and heights: Case 4.	84
29.	Mass of water associated with each size class for Cases 4, 5, and 6 relative to that of Case 1. Height is 100 meters above cloud base.	87
30.	Total mass of water/(gm air) on each size class at indicated height and time: Case 4.	90
31.	Droplet size distributions computed by implicit and explicit models for Case 1. Height is 100 meters above cloud base.	105
32.	Droplet size distributions computed by implicit and explicit models for Case 4. Height is 100 meters above cloud base.	107

Figure		Page
33.	Droplet temperature elevation with respect to the ambient air: Case 1. Curve labels are time in seconds from cloud base.	109
34.	Droplet temperature elevation with respect to the ambient air: Case 4. Curve labels are time in seconds from cloud base.	110
35.	Droplet equilibrium supersaturation: Case 1. Curve labels are meters above cloud base. ——— Explicit model. - - - Implicit model.	112
36.	Indicated energy term relative to internal energy, Q_T, 10 meters above cloud base in steady updraft of 1 m/s.	114
37.	Correction factor for vapor diffusion at 10°C and 900 mb. Curve labels indicate value of condensation coefficient.	127
38.	Correction factor for thermal diffusion at 10°C and 900 mb. Curve labels indicate value of thermal accomodation coefficient.	130
39.	Thickness of parietal layer of 10°C and 900 mb. The mean free path lengths for air and water molecules are 0.071 and 0.064 μm, respectively.	132

GLOSSARY OF SYMBOLS

a activity
c specific heat, ergs $gm^{-1}K^{-1}$
C vapor concentration, gm cm^{-3}
D diffusivity, $cm^2 sec^{-1}$
e vapor pressure, dynes cm^{-2}
E equivalent gray body emissivity
F correction factor (Fuchs, 1959)
g acceleration of gravity, cm sec^{-2}
h enthalpy of solution per unit mass
K thermal conductivity of air, ergs $cm^{-1}sec^{-1}K^{-1}$
L latent heat of condensation, ergs gm^{-1}
m mass, gm
M molecular mass, gm $mole^{-1}$
n number density of particles, cm^{-3}
N number density of particles, gm^{-1}
p pressure, dynes cm^{-2}
r radius of droplet, cm
R specific gas constant, ergs $gm^{-1}K^{-1}$
$\bar{r}$ arithmetic mean droplet radius, μm
S supersaturation
t time, sec
T temperature, K
V ventilation coefficient (Squires, 1952)
w vertical velocity
x mixing ratio, gm per gm of dry air
z height, cm

α condensation coefficient
β ratio of molecular masses of water and air
γ accomodation coefficient
δ coefficient of dispersion
λ mean free path, cm
μ molality
μ_f molecular viscosity of air, gm $cm^{-1}sec^{-1}$

ρ density, gm cm^{-3}

σ surface energy, ergs cm^{-2}

σ standard deviation of droplet size distribution, m

σ_R Stefan-Boltzmann constant, ergs $cm^{-2}sec^{-1}K^{-4}$

Subscripts

a ambient

c critical

d dry air

i size category

k heat

m moist air

n nucleus

r droplet or droplet surface

s saturation

v water vapor

w liquid water

Other symbols are defined in text as needed.

CHAPTER I

INTRODUCTION

1.1 Background

Current interest in energy conversion, and the anticipated shift to the further use of coal as a fuel source, have increased attention to the removal of effluents. Contaminants, once released to the atmosphere by either anthropogenic or natural sources, are beyond the limits of man's pollution controls. Rather, their removal is dependent on the rates and efficiencies of the atmospheric cleansing processes that determine the self-renewal capability of the air. Among the important atmospheric scavenging processes are those associated with clouds and precipitation (Sartor and Jiusto, 1976). Of these, the formation of cloud droplets upon condensation nuclei is prominent.

At the same time, nucleation of droplets is the initial step for cloud development and precipitation generation. It has been realized for many years that the colloidal stability of a cloud is related to the early growth of cloud droplets by condensation of water vapor. The growth of droplets is generally expected to depend on such things as the size distribution of nuclei and the updraft speed.

To determine how long growth by vapor diffusion must continue in order to produce rain, and to assess the

impact of varying conditions on the nucleation of droplets, it is logical to study the early growth of a population of droplets by means of a numerical model.

Howell (1949) was the first to calculate the growth of droplets by condensation. He described the growth of an individual droplet with an ordinary differential equation that included the droplet radius, supersaturation, and nucleus mass. His model consisted of a parcel of air, containing a discrete size distribution of sodium chloride particles, rising adiabatically within a steady updraft. Because of the mutual relationship between cooling rate, vapor consumption, and supersaturation, he was able to perform hand calculations for only three cases; his updraft velocities ranged from 0.015 to 0.6 m/sec.

Howell recognized that the rate of consumption of water vapor depends on the total surface area of the droplet size distribution. Until the droplets reach appreciable size, the rate of condensation is slow. He found with his model that as adiabatic cooling began, the supersaturation increased until the aerosol reached some tens of meters above the cloud base. At that point, the supersaturation determined the smallest salt particle size that could surpass its critical radius (Köhler, 1926) and become an activated cloud droplet.

Continued cooling resulted in further growth of the activated droplets and reduction of the supersaturation.

Small droplets that failed to activate began to evaporate and were carried along as haze droplets.

Howell discovered that because the radial growth rate of an individual droplet decreases with increasing droplet size, a droplet size distribution narrows with age in the case of a simple steady updraft. He postulated that condensation might be the dominating process creating homogeneous distributions found in some young clouds. Also, he suspected that this process might be the cause of the brilliant iridescence seen in altocumulus clouds of uniform composition. Finally, he concluded that the updraft speed is most important in determining the shape of the droplet size distribution, whereas the particle size distribution has a minor effect. Although no further calculations were performed, he suggested that evaporation or turbulent mixing might create a broader size distribution.

Cloud droplet size distributions in convective clouds have been observed (Diem, 1942; Weickmann and aufm Kampe, 1953; Warner, 1969a; Spyers-Duran, 1972) to be considerably broader than those computed from the microphysical model of Howell. The problem of modelling the generation of cloud droplets with size distributions similar to those observed has been addressed by several authors.

Following the increase in the number of particle measurements and the development of computers, Mordy (1959)

made further calculations. He included droplet sedimentation, but concluded that the effect is important only if the updraft velocity is less than 10 cm/sec or if there are extremely high concentrations of giant particles.

After including larger particles than did Howell, Mordy concluded that the particle size distribution is as important as the updraft speed in determining the final droplet population. Because of the relatively slow radial growth rate, the largest droplets lagged behind their respective equilibrium size, whereas the smallest droplets were able to react quickly to environmental changes. In a fast updraft, then, the droplet spectrum was narrow; the spectrum was broader in a slow updraft, in which the large droplets could approach further their equilibrium size.

Mason and Ghosh (1957) showed that large droplets may be formed on giant ($r>1$ μm) salt nuclei. This may be acceptable for maritime clouds, but does not explain the observed droplet size distributions in continental clouds where giant salt nuclei are extremely rare or nonexistent.

Kornfeld (1970) considered growth upon a particle size distribution that included both salt nuclei and insoluble discs. The particle distributions used were not representative of those found in the atmosphere. In several cases, the salt particles had only one size

(r = 1 μm). At most, they were distributed among three sizes (r = 0.25, 0.5, and 1.0 μm). After 800 seconds, the inclusion of insoluble particles broadened the size distribution somewhat. Whereas the presence of insoluble particles may be instrumental in broadening the range of droplet sizes, Kornfeld's particle size distributions were not realistic enough to evaluate properly their effect. Furthermore, Paluch (1971) showed that by replacing the insoluble discs with small salt particles ($r \gtrsim 0.1$ μm), she could approximate the results of Kornfeld.

Fitzgerald (1972) measured droplet size distributions at the 200 to 300-meter level for fifteen clouds in Minnesota and Florida and compared them to his computed droplet size distributions. Nucleus size distributions were inferred from the measured supersaturation spectra. He found fairly good agreement between the measured and computed droplet size distributions, but his efforts were limited to small or medium sized nonprecipitating cumulus clouds of nearly uniform composition. An extension of his study to cumulus congestus clouds is desirable.

Other authors have augmented the Howell model in laminar conditions to explain the observed broad spectra. Most of them considered turbulent mixing.

Instead of assuming a steady updraft speed, Neiburger and Chien (1960) employed vertical velocities based on the results of the Thunderstorm Project (Byers and Braham,

1949). Their model produced, after 2400 seconds, 20 μm-radius droplets at a concentration of 1/liter. They concluded that coalescence could take place after that time. Even so, as with those of Mordy and Howell, their droplet size distributions narrowed with age and did not resemble measured droplet spectra.

Warner (1969a,b) measured droplet size spectra at various levels in several cumulus clouds near the Australian coast. Although most of the clouds had maritime origins, some were likely influenced by continental sources. Average droplet concentrations measured by Warner may differ from those of North American continental clouds, but the behavior of the droplet distributions is of interest.

Warner found that when the environment was unstable, the measured droplet size distribution was often bimodal. The frequency of bimodal distributions increased with increasing height and decreasing stability. During more stable conditions, the bimodal feature was not as common. It was suggested that mixing of cloud and environmental air might produce the observed bimodal distributions.

The argument is that when a distribution of cloud droplets with a single mode is mixed with drier, polluted environmental air, the supersaturation is reduced and the small droplets evaporate. Large droplets may evaporate or continue growing depending on the mixed supersaturation. As the parcel continues to rise, the small

droplets are not as likely to become reactivated. Instead, water condenses on the smaller numbers of large droplets. If this aerosol is subsequently mixed with cloud air, a bimodal distribution might be produced.

During horizontal passes through the cloud, Warner found that the bimodal nature was not confined strictly to the edges of the cloud. If entrainment through the sides of the cloud were the principal mixing mechanism, he speculated that horizontal uniformity would not be expected. Warner suggests that the primary mixing might occur at the top of the growing cloud.

Mason and Chien (1962) developed a model assuming turbulent mixing between cloud droplets and unactivated particles at the cloud edge. Squires (1958) suggested a similar model in which dry air entered the cloud top and produced regions of low humidity. Both of these processes are expected to be more efficient near the cloud boundaries, and thus are not likely to account for the broad spectra and the abundance of small droplets within the interior (Paluch, 1971).

Warner (1973) improved somewhat the model of Mason and Chien. His turbulent model produced, 150 meters above the cloud base, droplet distributions that characteristically had a mode near 6 μm-radius, and a nearly constant number density of smaller droplets which he called a "plateau." The mode was a result of the growth of droplets that formed at the cloud base, whereas

the lower plateau was caused by the introduction of fresh nuclei into the cloud edges. However, Warner stated that the plateau is not normally found in cloud measurements. He concluded that although entrainment of polluted air results in a broader spectrum, it does not yield realistic size distributions. Moreover, he presented evidence that the rate of entrainment, as indicated by the ratio of the measured and adiabatic liquid water contents, does not have an obvious direct relationship to the dispersion (standard deviation divided by the mean radius) of the measured distribution.

Mason and Jonas (1974) advanced the single thermal model of Mason and Chien. In their model, a thermal rose by virtue of its own buoyancy and then fell back as a result of entrainment of dry environmental air. A second thermal was allowed to rise and mix with the residue of the first. They concluded that their model successfully predicted droplet size spectra which closely resembled observations. Their maritime cloud model produced droplets of 25 μm in radius in 30 minutes; however, the continental cloud model, with its greater number of particles, did not result in a significant number of 20 μm-radius droplets within a reasonable time. Warner (1975) criticized the model because it predicted liquid water contents in the lower regions of the cloud much greater than those measured. Mason (1975) replied

that measurements refer to averages across a cloud and not to a single active thermal.

Srivastava and Roy (1962) investigated the effects of turbulence within a cloud. Droplets at a given height were assumed to have experienced different trajectories and hence different growth times. Their size distributions were broader than those calculated within a uniform updraft, but it was assumed that the supersaturation was constant. Fitzgerald (1972) pointed out that if the supersaturation had not been assumed constant, then the size distribution would have been much narrower than that predicted by Srivastava and Roy.

Belyaev (1961) and Sedunov (1965) studied the growth of droplets in an updraft of fluctuating speed and supersaturation. Particles entering the cloud scattered about and experienced different growth times and growth rates. Although the size distributions were broader, they could not be related to those at a fixed height.

Paluch (1971) developed a model which included small humidity variations along the vertical axis of an updraft. Droplets within each region of the updraft grew at different rates. Large droplets were allowed to settle into regions of low humidity originally occupied by small droplets, thus retarding their growth rate. The high humidity region, then void of large droplets, resulted in rapid growth of the remaining small droplets. This process was able to maintain local variations of droplet

concentration and relative humidity. Although she did include turbulence which could counter this effect somewhat, observations (e.g., Warner, 1969a) indicate that turbulence is not extensive enough to completely homogenize a cloud.

There are several features of the observed microstructure of a cloud (Warner, 1969a) that should be explained by a comprehensive model, namely:

1. the range of droplet radii i.e., the formation within reasonable time limits of droplets large enough to coalesce ($r \gtrsim 25$ μm), and the presence of droplets less than 5 μm in radius;
2. the bimodal nature of the spectrum, which is not confined to the cloud edges;
3. the measured dispersion (standard deviation divided by the mean size) of the spectrum;
4. regions of low or zero liquid water content; and
5. regions in which the liquid water content is larger than the adiabatic value (this is not a common occurrence, however.)

To arrive at a calculated distribution different from that first obtained by Howell, one must impose a physical situation other than laminar flow. The most common approach has been to use a diabatic, or "open parcel" model such as entrainment, turbulence, and/or droplet settling.

To date, no model has reproduced all aspects of the observed distributions, especially for a continental cloud. Those models which consider entrainment appear to offer the best promise, particularly when wetted nuclei are introduced along with the entrained air. However, they are most applicable near the cloud boundaries. Despite its shortcomings, the model of Mason and Jonas, in which a spent thermal is mixed with the active cloud, is the most successful.

A complete cloud model must include both microphysics and dynamics in time and space coordinates. Many investigators of cloud systems, (e.g., Ogura and Takahashi, 1971; Murray and Loenig, 1972) model the dynamics and parameterize the thermodynamics of condensation (Silverman and Glass, 1973). Inasmuch as a comprehensive model is not now attainable because of the limits of available computer capacity (Lilly, 1970), an equally plausible approach is to parameterize the dynamics (e.g., by specifying particle trajectories, etc.) and to investigate in detail the microphysical processes and how they are affected by the motion field. This would seem to be one approach to evaluate the microphysical feedback to the local and overall dynamic process, and thus to indicate the requirements for parameterization of the microphysics.

For this purpose a one dimensional model is useful. A few authors have used an adiabatic parcel to investigate the direct effect of a selected oscillating updraft speed upon a distribution of droplets.

Saad, et al. (1976) modelled the early growth of droplets in a simulation chamber. They included oscillating updraft speeds of $w = 100 + 100 \sin(t)$ and $w = 100 + 100 \sin(0.1t)$ [cm/sec] and found no appreciable difference between the resulting droplet size distribution and those predicted under steady updraft conditions. It should be pointed out that the selected velocities did not allow downdraft and consequent evaporation.

Storebø and Dingle (1974) have calculated the growth and washout of particles moving up and over a land barrier. Under adiabatic compression of an air parcel, the relative humidity decreased enough to initiate evaporation from small activated droplets. At the same time, larger ones continued to grow as long as the humidity was high enough. These findings led them to speculate that if the parcel were then lifted again, the droplet size spectrum might have broadened.

Kornfeld (1970) included in her model an unsteady updraft velocity. Periodic fluctuations about a mean velocity did not produce a spectrum significantly different from that within a steady updraft. Paluch (1973), however, suggested that the results might depend

to a large degree on the amplitude and frequencies of the velocity variations.

1.2 Objectives of Research

This research is divided into two parts. The first is to use currently acceptable techniques to determine whether a fluctuating updraft has any effect upon a population of droplets within the lower regions of a cloud. The movement of a parcel of air in a convective cloud is a complicated pattern of upward, downward, and lateral motions of varying speeds and reversal frequencies. For the purpose of this study, turbulence is characterized by either a sinusoidal velocity pattern or alternating steady upward and downward motion. Modifying effects of entrainment and droplet settling are not included.

The second part is to develop an alternative approach to model droplet growth by condensation. The classical approach (chiefly attributed to Mason, 1957, 1971) presented in the first part makes use of certain assumptions and approximations to arrive at a single equation for the growth rate of a droplet. Since the droplet temperature is never actually determined in the classical approach, it is called here the "implicit model." An alternative method presented here, which includes all the known heat sources and sinks, makes direct use of the droplet temperature and so is called the

"explicit model." The advantage of the explicit model is that it has the capacity to treat more than one diffusing vapor.

CHAPTER II

IMPLICIT MODEL

2.1 General Statement of the Model

The modelling begins at cloud base with an aerosol of moist air and droplets. Each droplet contains one nucleus of ammonium sulfate, $(NH_4)_2SO_4$; the amount of water on each droplet depends on the cloud base conditions and the size of the nucleus.

The parcel of cloud air is allowed to rise or fall according to an imposed vertical velocity. The intent is to limit the study to the direct response of the droplet growth rate to a fluctuating updraft. Processes such as coalescence and impaction by raindrops are not considered. Further, it is assumed that droplet interaction may be ignored (Carstens, et al., 1970; Williams and Carstens, 1971). No mixing is allowed with other cloud elements or with the outside air so that the parcel expands or contracts adiabatically but the mass remains constant. For these reasons, all equations are written in terms of unit mass of dry air to ensure that the number of particles and the total mass of water are unchanged throughout the integration.

The implicit model consists of five equations. They are expressions for:

1. the change of pressure within the parcel,
2. the change of air temperature,

3. the conservation of water mass,

4. the energy budget of an individual droplet, and

5. the rate of growth of a droplet.

2.2 Pressure Equation

The air parcel is assumed to have an unsteady vertical velocity, w. The pressure equation, then, is

$$\frac{dp_m}{dz} = -\rho_m\left(g + \frac{dw}{dt}\right)$$

where

p_m = pressure of moist air,

ρ_m = density of moist air,

g = acceleration of gravity,

w = updraft speed, and

z = height.

Using the ideal gas law and multiplying by dz/dt, this transforms to

$$\frac{dp_m}{dt} = -\frac{p_m}{R_m T_a}\left(g + \frac{dw}{dt}\right)w, \qquad (2.1)$$

where T_a = air temperature. The gas constant for moist air is (Fleagle and Businger, 1963)

$$R_m = \left[1 + \left(\frac{1}{\beta} - 1\right)\frac{x}{1+x}\right]R_d,$$

where

x = water vapor mixing ratio,

β = ratio of the molecular masses of water and air, and

R_d = gas constant for dry air.

2.3 Temperature Equation

The parcel is assumed to contain one gram of air, x grams of water vapor, and x_w grams of liquid water. Then the first law is (Haltiner and Martin, 1957)

$$dq = (1+x)[c_{pm}dT_a - \frac{1}{\rho_m} dp_m],$$

where

q = heat, and

c_{pm} = specific heat of moist air.

There are two sources of heat:

1. the heat released by condensation

$$dq_1 = -Ldx$$

2. the sensible heat due to the cooling of the droplets

$$dq_2 = -x_w c_w dT_a$$

where

c_w = specific heat of liquid water, and

L = latent heat of condensation. In units of ergs/gm it is

$$L = 2.503 \times 10^{10} - 2.425 \times 10^{7} (T_a - 273.16).$$

Combining, and substituting the pressure equation (2.1), yields

$$\frac{dT_a}{dt} = - \frac{(1+x)(g + \frac{dw}{dt})\ w + L \frac{dx}{dt}}{c_{pd}+xc_{pv}+x_w c_w} \qquad (2.2)$$

Here, c_{pm} was replaced by the equivalent expression $(c_{pd} + x\ c_{pv})/(1+x)$, in which c_{pv} is the specific heat of water vapor, and c_{pd} is the specific heat of dry air.

2.4 Conservation of Mass

Since the total mass of water in the parcel is constant,

$$dx = -dx_w.$$

For a discrete distribution of droplets,

$$\frac{dx}{dt} = - \sum_i N_i \frac{dm_{wi}}{dt}\ , \qquad (2.3)$$

where

N_i = number of droplets in the i^{th} radius interval, and

m_{wi} = mass of water in a droplet of the i^{th} radius interval.

2.5 Energy Budget of a Droplet

In the implicit model, it is assumed that all of the heat supplied to the droplet by condensation of the vapor is returned to the air by conduction. Thus

$$L \frac{dm_w}{dt} = 4\pi r K F_K (T_r - T_a) V \qquad (2.4)$$

where

K = coefficient of conduction. In units of ergs $cm^{-1} K^{-1} sec^{-1}$,

$K = 2395. + 8.0375 \ (T_a - 273.16)$;

F_K = Fuchs' (1959) correction for thermal diffusion, (see Appendix A),

r = droplet radius,

T_r = droplet temperature, and

V = ventilation factor (Squires, 1952).

It is assumed that the droplet is homogeneous so that the droplet temperature is represented by the surface temperature.

Squires' values for the ventilation factor were fit to the curve

$$V = 1.0 + 36.8r + 3012.0r^2$$

for droplet radius in centimeters.

2.6 Droplet Growth Equation

Consider a spherical droplet of radius r. The flux of vapor along the radial distance is

$$\frac{dm_w}{dt} = 4\pi r D F_v (C_a - C_r) V,$$

where

C_a = ambient vapor density,

C_r = vapor density at the droplet surface,

F_v = Fuchs' (1959) correction for vapor diffusion (Appendix A), and

D = coefficient of diffusion of water vapor in air. In units of cm^2/sec it is (Dorsey, 1940)

$$D = (.219 + .0015(T-273.16)) \times 1.01325 \times 10^6 / p_a.$$

The growth rate equation as given above is for a steady state situation; however, the droplet radius and the ambient conditions are variable. It is generally assumed (Sedunov, 1974) that the growth of a droplet is quasisteady, so that the growth rate at any particular time can be represented by the steady state equation. The implication is that the droplet radius and the ambient conditions vary slowly relative to the establishment of the vapor density and temperature gradients. Kirkaldy (1958) studied nonstationary diffusion theory and arrived at the same growth rate expression as that of the quasi-steady approximation. He points out, however, that the agreement is not a justification of the quasisteady concept. Philip (1965) studied the nonstationary theory and concluded that the quasisteady model is sufficient for most problems.

Using the ideal gas law and the assumption that $T_a/T_r \approx 1.0$, the growth rate equation is transformed

$$\frac{dm_w}{dt} = \frac{4\pi r D F_v}{R_v T_a} V(e_a - e_r) \qquad (2.5)$$

where

R_v = gas constant for water vapor,

e_a = ambient vapor pressure, and

e_r = vapor pressure at the droplet surface.

The ambient vapor pressure is related to vapor mixing ratio with

$$e_a = \frac{x}{\beta+x} p_m.$$

The vapor pressure in equilibrium with a droplet containing a soluble particle is

$$e_r = e_s(T_r)\ a \exp \frac{2\sigma_r}{r\rho_r R_v T_r}, \qquad (2.6)$$

where

ρ_r = density of the droplet,

σ_r = surface tension of the droplet, and

a = water activity (Low, 1969a,b).

Here, the water activity is used to quantify the vapor pressure reduction by the solute because it is more accurate than Raoult's Law, particularly for droplets in the activation stage (McDonald, 1953; Vohra and Nair, 1971). Low's tables of activity are presented as a function of molality. The activities are insensitive enough to temperature and pressure (Harned and Owens, 1958) that the published values are used without modification.

To determine the solution surface tension it is assumed here that temperature and molality act independently on the surface tension, viz:

$$\sigma_r(T,\mu) = \sigma_o(T) + \Delta\sigma(\mu),$$

where

μ = molality,

σ_o = surface energy of pure water, and

$\Delta\sigma$ = correction due to the presence of an electrolyte.

Values of σ_o are interpolated between those given by Weast (1968). The correction term is fit to the data of Dean (1973). For ammonium sulfate it is

$$\Delta\sigma = 2.18$$

Tolman (1949) and Dufour and Defay (1963) have shown that for droplets of 0.01 μm-radius, the reduction of the surface tension due to the radius of curvature is of the order of only 2%. For droplets of 1.0 μm-radius, the reduction is about 0.03%. The influence of the radius of curvature is ignored in this study.

The solution density, ρ_r, is taken from tabulated values of Hodgeman (1961). Between the listings, linear interpolation is used.

The saturation vapor pressure for pure water is computed from the Murray (1967) formulation

$$e_s(T) = 6107.8 \exp \frac{17.2693882(T-273.16)}{T-35.86} \qquad (2.7)$$

with T in units of K and e_s in dynes/cm^2. At 283.16 K, it predicts a value 0.057% greater than that given by the Goff-Gratch formulation (List, 1968).

To eliminate the droplet temperature from the calculations, the equilibrium vapor pressure at the droplet surface is first related to the air temperature by (2.7) so that

$$e_s(T_r) = e_s(T_a)\ \exp\left[\frac{T^*(T_r-T_a)}{(T_a-35.86)(T_r-35.86)}\right]$$

where $T^* = 4098.03$ K. Since the difference between the droplet and air temperatures is small, one can use

$$e_s(T_r) = e_s(T_a)\left[1 + \frac{T^*(T_r-T_a)}{(T_a-35.86)^2}\right] \tag{2.8}$$

The droplet temperature elevation is determined by the heat budget (2.4):

$$T_r - T_a = \frac{L}{4\pi r K F_K V}\frac{dm_w}{dt} \tag{2.9}$$

Finally, by combining (2.5), (2.6), (2.8) and (2.9), one arrives at the rate of growth for an individual droplet

$$\frac{dm_w}{dt} = 4\pi r V\ \frac{e_a - e_s(T_a)a\ \exp\left(\frac{2\sigma_r}{r\rho_r R_v T_a}\right)}{\frac{R_v T_a}{DF_v} + \frac{T^* L\ e_s(T_a)a\ \exp\left(\frac{2\sigma_r}{r\rho_r R_v T_a}\right)}{KF_K(T_a-35.86)^2}} \tag{2.10}$$

2.7 Initial Conditions

The model is envisioned in the following manner. A parcel of air with a population of wet particles starts

at the base of a cloud at 900 mb and 283.16 K. In nature, the amount of water associated with each nucleus depends on the particular history of each particle before entering the cloud. In this model, the precloud histories are not specified; rather, dry particles are placed artificially into the cloud base and allowed to approach equilibrium with the environment. During this adjustment period, the temperature and pressure are constant and the relative humidity is held steady at 100%. This procedure is not intended to duplicate nature exactly, but to give a representative distribution of droplets at the cloud base.

The parcel composed of one gram of dry air and its associated vapor and droplets is then raised according to a preselected velocity pattern to a height of 100 meters. The distribution resulting from a steady updraft is used as a standard to compare those created by the turbulent motion.

2.8 Dry Particle Distribution

a. Chemical composition

There is evidence (e.g., Twomey, 1971; Junge, 1963; Williamson, 1973) that ammonium sulfate, $(NH_4)_2SO_4$, is a common constituent of atmospheric particles. In this study, spherical particles of pure ammonium sulfate are assumed.

The effects of including insoluble matter within an aerosol and of using another pure salt, sodium chloride NaCl, were discussed in reports by Junge and McLaren (1971) and Fitzgerald (1974). Junge and McLaren concluded that mixed particles containing both soluble and insoluble matter behave essentially as soluble particles as long as they have at least 10% by volume of soluble material.

Fitzgerald performed further numerical computations to study the effect of the chemical composition. Solubilities ranged from 1% to 90% throughout a particle distribution. He also used distributions of pure ammonium sulfate and pure sodium chloride. His results showed that increasing the proportion of insoluble matter lowered the maximum concentration of droplets and correspondingly raised the mean droplet size. However, a change in the chemical composition of the particles did not significantly alter the breadth of the resultant droplet distribution. Also, both pure salt distributions produced similar droplet spectra. His conclusion reinforced that of Junge and McLaren that a change of shape of the particle distribution has a greater effect than the chemical composition on the dispersion of the droplet size spectrum.

b. Surface impurities

In theoretical models it is assumed that there is

no energy barrier to the initial condensation of vapor onto the dry crystal surface. Experiments by Knight (1971) indicated that early diffusion of vapor to sodium chloride particles results in the formation of droplets on the surface rather than a uniform liquid layer. The crystals used were apparently quite large (tens and hundreds of microns) and it is uncertain how the behavior he reported is to be applied to the nucleation of particles found in the atmosphere.

Katz and Kocmond (1973) concluded from their experiments with sodium chloride that particles must be two to three times larger than predicted by theory to become activated at a particular supersaturation. This may be related to the non-zero contact angle between the liquid water and the crystal, evident in Knight's work.

However, there were no claims by either author of purity of the salt surface. Adsorption of organic or other matter onto the surface of the crystals can lead to an energy barrier to the initial condensation. In nature there is no guarantee that nuclei are uncontaminated. Impurities can either increase or reduce the surface energy.

c. Particle shape

Atmospheric nuclei are likely to be irregular agglomerates rather than spherical particles. This

agglomeration creates cracks and crevices in the surface which can contain concave water surfaces that accept condensing vapor readily due to a negative curvature effect.

Because of all the uncertainties of the physical and chemical properties of particles within an aerosol, it is assumed for this study that the nuclei are pure spherical particles of ammonium sulphate with zero contact angle.

d. Discrete classification

Particle sizes are continuous in a natural aerosol, but must be distributed in a discrete manner for modelling. The particle sizes used here are defined such that the mass, m, of a particle increases by a factor y from one size to the next. Then if i is the size class number,

$$\frac{m_{i+1}}{m_i} = y, \text{ or}$$

$$d(\ln r) = \ln r_{i+1} - \ln r_i = \frac{1}{3} \ln y.$$

With a constant d(ln r),

$$r_i = \exp(\ln r_1 + (i-1)\, d(\ln r)).$$

Particle sizes can be readily calculated by specifying r_1, the smallest particle radius, and y. In this study

r_1 = 0.015 μm and y = 1.9. The distribution is represented by 27 size classes so that the largest particle has a dry radius of 3.908 μm.

The particle number densities are distributed according to a formulation similar to that found by Junge (1963),

$$n_i = \text{constant} \qquad r \leq 0.08 \times 10^{-4} \text{ cm}$$

$$n_i = br_i^{-J} \qquad r \geq 0.08 \times 10^{-4} \text{ cm}$$

If the total particulate mass is M, then

$$b = \frac{3M}{4\pi\rho_n \left(\sum_{i=1}^{7} r_i^3 (0.08\times10^{-4})^{-J} + \sum_{i=8}^{27} r_i^3 \, r_i^{-J}\right)}$$

where ρ_n is the density of the nucleus salt. For the aerosol modelled, the total particulate loading is 3 μg/m^3 and J = 3. Figure 1 represents the distribution of dry particles.

2.9 Distribution of Droplets at the Cloud Base

The particles at the cloud base are not all at their respective equilibrium sizes because the largest particles grow in radius very slowly and thus lag behind their equilibrium sizes. For dilute droplets, the supersaturation, S, in equilibrium with a droplet is (Fletcher, 1966)

$$S = \frac{2\sigma_r}{\rho_r R_v T_a} \frac{1}{r} - \frac{iM_w\rho_n}{M_n\rho_r} \frac{r_n^3}{r^3},$$

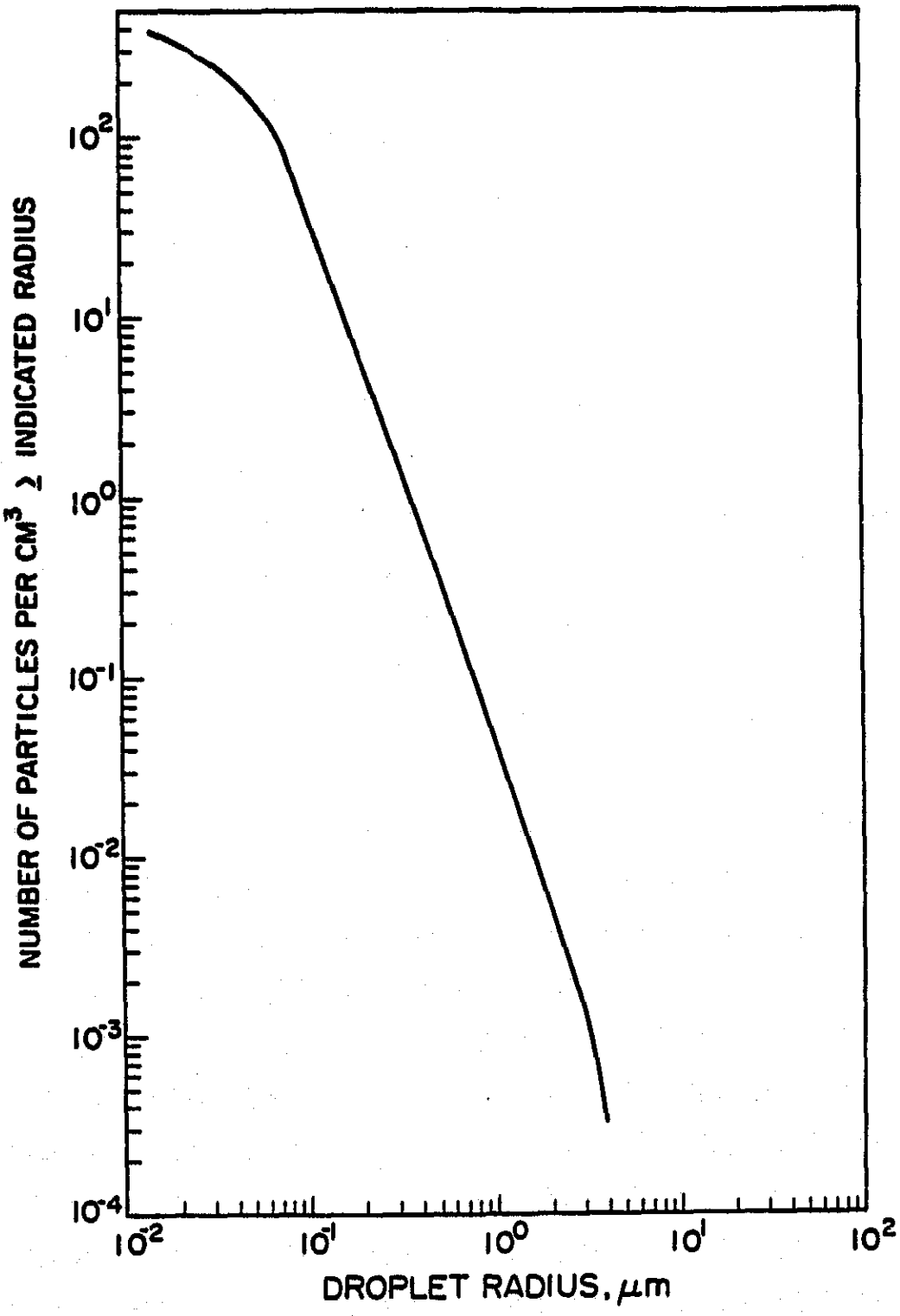

Figure 1. Cumulative distribution of dry $(NH_4)_2SO_4$ particles.

where the subscript n refers to the nucleus. The van't Hoff factor is i. To find the equilibrium droplet size at 100% relative humidity, set S = 0. Then

$$r_{s=0} \propto r_n^{3/2} .$$

Thus the droplet size distribution at the cloud base is broader than that of the dry particles if the droplets are at or near their equilibrium sizes.

To estimate how long the dry particles should be adjusted to the cloud base environment, a distribution of droplets growing on sodium chloride particles was allowed to approach equilibrium and was compared periodically to the cloud base droplet distributions used by Mordy (1959) and Fitzgerald (1972). From this study it was judged that an adjustment time of 60 seconds would give a representative distribution. During the adjustment period the temperature and relative humidity are held constant, so the adjustment time can not be compared directly to a pre-cloud history of the particles.

The distribution of droplets at the cloud base is shown graphically in Figure 2. Also shown are the equilibrium sizes at cloud base. Nuclei of radius less than 0.13 μm are at equilibrium with the saturated environment, whereas the largest particles are at their 99% relative humidity equilibrium size.

The distributions of dry particles and of cloud droplets are listed in Table I.

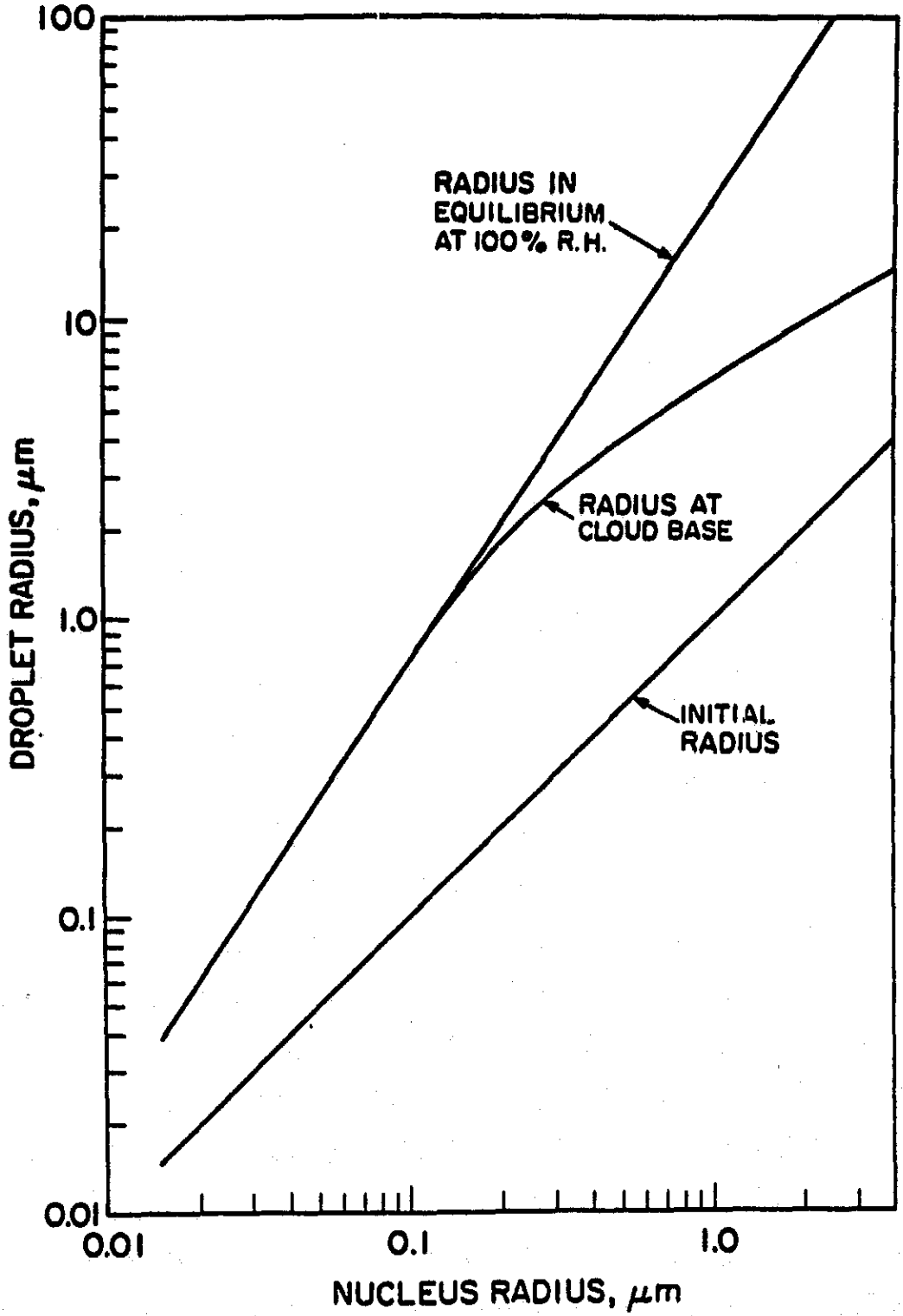

Figure 2. Nucleus radius, droplet radius at cloud base, and radius in equilibrium at 100% relative humidity.

TABLE I

Distribution of $(NH_4)_2SO_4$ Particles and of Cloud Base Droplets.

Size Class	Nucleus Radius, μm	Nucleus Mass, gm	Radius at Cloud Base	Concentration cm^{-3}	Concentration gm^{-1}
1	0.0150	2.501×10^{-15}	0.0388	39.07	3.578×10^{4}
2	0.0186	4.752×10^{-15}	0.0538	39.07	3.578×10^{4}
3	0.0230	9.028×10^{-15}	0.0747	39.07	3.578×10^{4}
4	0.0285	1.715×10^{-14}	0.1038	39.07	3.578×10^{4}
5	0.0353	3.259×10^{-14}	0.1446	39.07	3.578×10^{4}
6	0.0437	6.192×10^{-13}	0.2008	39.07	3.578×10^{4}
7	0.0541	1.177×10^{-13}	0.2801	39.07	3.578×10^{4}
8	0.0671	2.235×10^{-13}	0.3854	39.07	3.578×10^{4}
9	0.0831	4.247×10^{-13}	0.5306	34.90	3.196×10^{4}
10	0.1029	8.070×10^{-13}	0.7307	18.37	1.682×10^{4}
11	0.1274	1.533×10^{-12}	1.0034	9.668	8.852×10^{3}
12	0.1578	2.913×10^{-12}	1.3488	5.089	4.659×10^{3}
13	0.1955	5.535×10^{-12}	1.7436	2.678	2.452×10^{3}
14	0.2421	1.052×10^{-11}	2.1734	1.410	1.291×10^{3}
15	0.299	1.998×10^{-11}	2.6389	0.7419	679.3
16	0.3714	3.797×10^{-11}	3.1470	0.3905	357.5
17	0.4600	7.214×10^{-11}	3.7071	0.2055	188.2
18	0.5698	1.371×10^{-10}	4.3300	0.1082	99.03
19	0.7057	2.604×10^{-10}	5.0271	5.693×10^{-2}	52.12
20	0.8741	4.948×10^{-10}	5.8105	2.996×10^{-2}	27.43
21	1.0826	9.401×10^{-10}	6.6930	1.572×10^{-2}	14.44
22	1.3408	1.786×10^{-9}	7.6884	8.300×10^{-3}	7.599
23	1.6607	3.394×10^{-9}	8.8100	4.368×10^{-3}	4.000
24	2.0569	6.448×10^{-8}	10.073	2.299×10^{-3}	2.105
25	2.5475	1.225×10^{-8}	11.508	1.210×10^{-3}	1.108
26	3.1553	2.328×10^{-8}	13.139	6.369×10^{-4}	0.5831
27	3.9080	4.423×10^{-8}	14.994	3.352×10^{-4}	0.3069

2.10 Integration of the Equations

a. Method of integration

To integrate, it is assumed that during a time step each droplet category responds to the environment independently of the others. The interaction of the droplets is treated by resetting the vapor mixing ratio by (2.3) at the end of each time step. The equations to be integrated, then, are a growth equation (2.10) for each of the 27 size classes, the temperature equation (2.2), and the pressure equation (2.1).

All equations are integrated using a fourth order Kutta-Simpson Method (Ralston & Wilf, 1960). This method gives a good degree of accuracy without requiring calculations of higher than the first derivative. Then, if

$$\frac{dm}{dt} = f(m,T,p,x)$$

the predicted value of the mass of the droplet is

$$m(t+\Delta t) = m(t) + \frac{\Delta t}{6}(F_1+2F_2+2F_3+F_4),$$

where

$$F_1 = f[m(t),T(t),p(t),x(t)]$$

$$F_2 = f[m(t) + \frac{\Delta t}{2} F_1,\ T(t+\frac{\Delta t}{2}),p(t+\frac{\Delta t}{2}),\ x(t+\frac{\Delta t}{2})]$$

$$F_3 = f[m(t) + \frac{\Delta t}{2} F_2,\ T(t+\frac{\Delta t}{2}),p(t+\frac{\Delta t}{2}),\ x(t+\frac{\Delta t}{2})]$$

$$F_4 = f[m(t) + \Delta t F_3,\ T(t+\Delta t),\ p(t+\Delta t),\ x(t+\Delta t)].$$

The temperature and pressure equations are integrated first to get values at $t+\Delta t$. Linear interpolation is

used to get the temperature and pressure at $t+\frac{\Delta t}{2}$. There is no differential equation for the vapor mixing ratio; the quantities $x(t+\frac{\Delta t}{2})$ and $x(t+\Delta t)$ are extrapolated by using the value of dx/dt of the previous time step.

b. Stability

All 29 equations could be solved simultaneously, but because of stability problems, a slightly different approach is used.

The smallest droplets are nearly in equilibrium with the environment. If the time step is too large, they tend to overshoot their equilibrium size. Successive time steps lead to oscillations of size and to numerical instability. The integration here follows the suggestion of Paluch (1971) that good accuracy can be maintained if the time step is chosen such that the increase of mass of any droplet is less than 0.5% during the time step. Further, in the present study, the time step is increased if no droplet is found to grow by more than 0.2% of its mass.

At the beginning of each time step, the temperature and pressure are integrated first. Next integrated is the growth equation for the droplet with the greatest value for F_1. If the change of mass is between 0.2 and 0.5%, the integration is continued, otherwise the time

step is altered accordingly and only three equations need to be reintegrated.

Because the growth rate of a droplet is related to the vapor pressure gradient, the length of the time step is linked to the supersaturation in such a way that the time step decreases as the supersaturation increases. For the case of a steady updraft of 1 m/s, the time step decreases from 0.1 seconds to 0.014 seconds and increases after surpassing the maximum supersaturation to 0.16 seconds at the 100 meter level.

c. Roundoff error

In addition to stability, the other concern is roundoff error. The temperature, for instance, changes only a few ten thousandths of one percent in a 0.1 meter altitude shift. To have this change be meaningful, it is necessary to use double precision (16 significant digits) throughout. Computations are performed on an Amdahl 470 at the University of Michigan.

d. Efficiency of integration

Other schemes of integration may be more efficient but have not been pursued. Árnason and Brown (1971) and Brown and Árnason (1973) use another approach put forward by Liniger and Willoughby (1970). Their technique, however, is not useful during activation.

Also, convergence is not assured during evaporation. For these reasons their method is not used here.

CHAPTER III

RESULTS WITH IMPLICIT MODEL

3.1 Introduction

This chapter is divided into two parts. The first is an overview of droplet behavior in a steady updraft. The effects of a steady updraft are studied for the following reasons:

i. To understand in detail how a population of droplets responds to a variable supersaturation and temperature. In particular, each nucleus size class has its own set of physical characteristics and responds to the environment accordingly.

ii. To use (i) as a basis to suggest mechanisms that might result in substantial modification of the droplet growth behavior.

iii. To arrive at a droplet size distribution at the 100-meter level for each of three steady updraft cases. These are used as standards for comparison with the droplet size distributions produced in the fluctuating updraft.

The second part discusses the consequences of a fluctuating updraft.

3.2 Steady Updraft

a. Growth of droplets

Figure 3 illustrates the modelled growth of the droplets from the cloud base to a height above cloud base of 100 meters in a steady updraft of 1 m/s (Case 1). All droplets grow slowly through the first few meters until the supersaturation peaks some 18 meters above cloud base with a value of 0.71%, at which time the droplets grow quite rapidly. Subsequently, the supersaturation decreases and the growth rate slows. In this case particles of the first two size classes do not become active cloud droplets but evaporate as the supersaturation decreases and are carried along as haze particles. Included at the bottom of the figure are the nucleus radii of the 27 size classes.

In a faster updraft, the droplet behavior pattern is similar, but details differ. For a steady updraft of 4 m/s (Case 2), the maximum supersaturation is higher (1.56%) as is the height at which the maximum is achieved (40 meters). The growth of the droplets for Case 2 is shown by Figure 4. Figure 5 represents droplet growth in a steady updraft of 10 m/s (Case 3). In this case, the supersaturation attains an extremely high value of 2.7% at a height of some 70 meters above cloud base. This case probably represents an upper limit of sustained updraft speed.

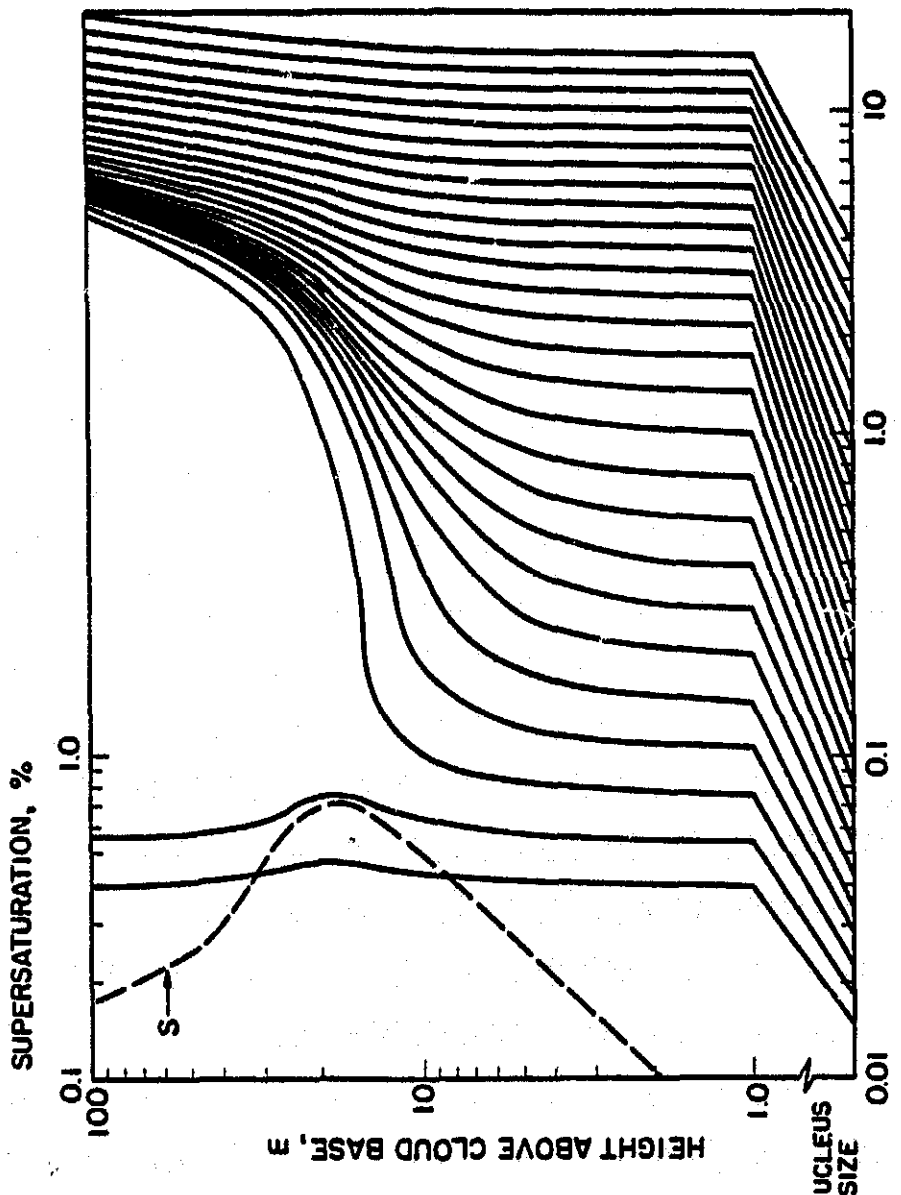

Figure 3. Growth of cloud droplets in a steady updraft of 1 m/s: Case 1. The size of the dry ammonium sulfate nucleus for each droplet size class is indicated at the bottom of the scale.

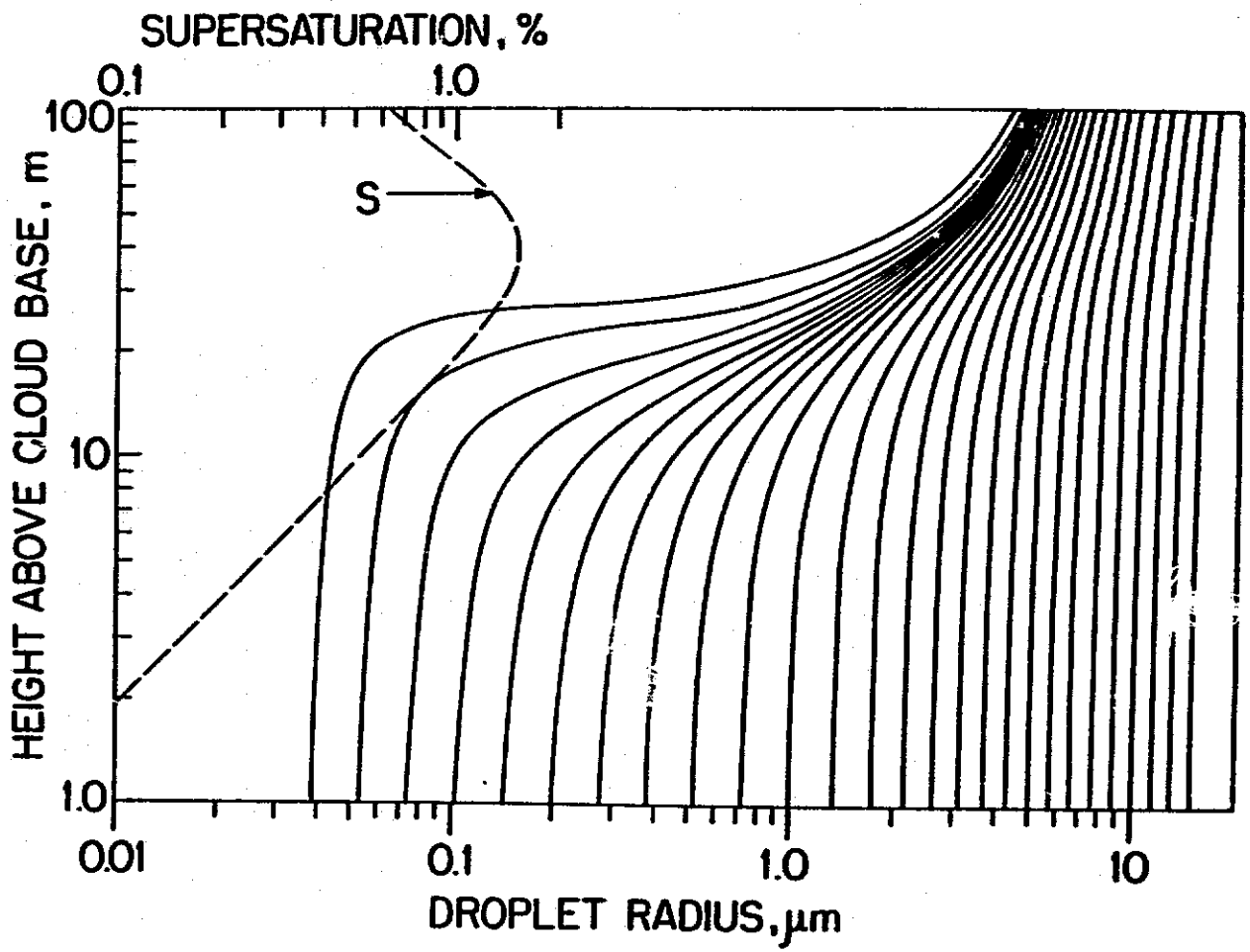

Figure 4. Growth of cloud droplets in a steady updraft of 4 m/s: Case 2.

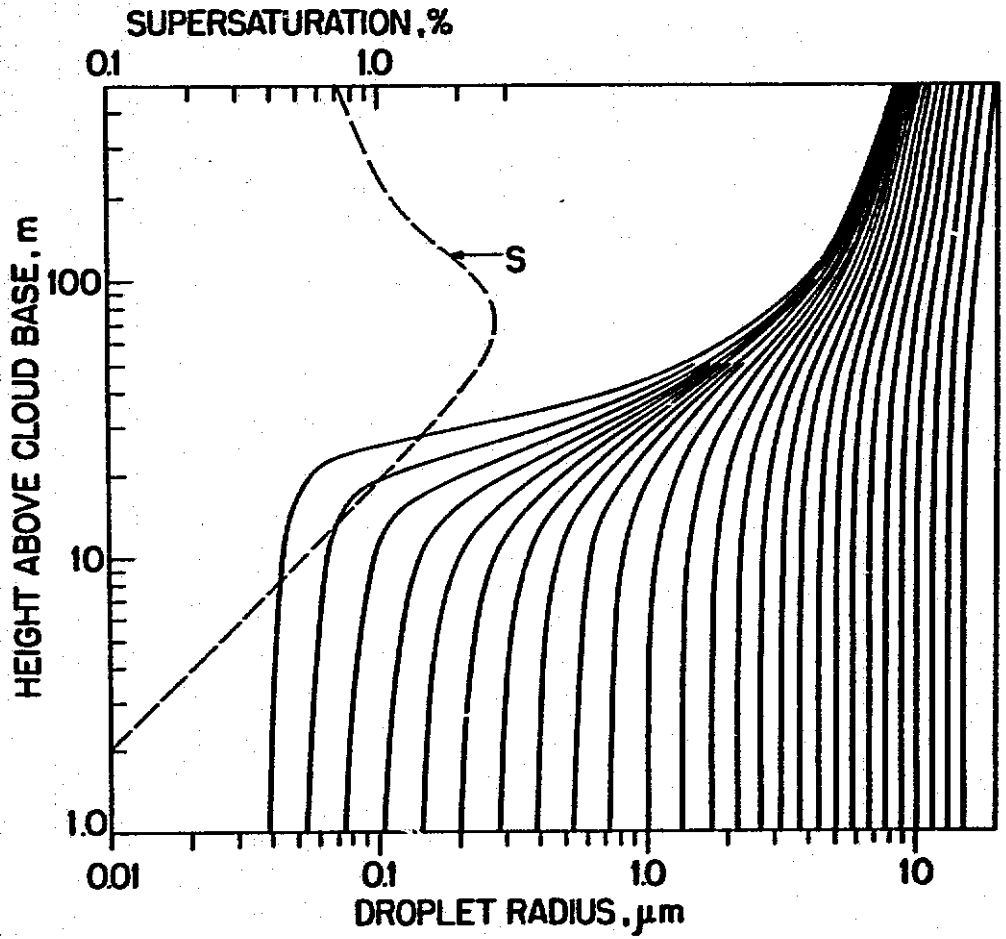

Figure 5. Growth of cloud droplets in a steady updraft of 10 m/s: Case 3.

b. Temperature and liquid water content

Because the growth rate of the droplets is slow in the lower regions of the cloud, the temperature initially decreases at a rate close to the dry adiabatic cooling rate (Figure 6). The liquid water content increases slowly during that time. Shortly after the supersaturation peaks, the rate of consumption of water vapor increases markedly and the temperature decay approaches the moist adiabatic cooling rate asymptotically. The liquid water content at the 100-meter level decreases with increasing updraft speed. Correspondingly, the temperature at the 100-meter level decreases with increasing updraft speed.

c. Breadth of distribution

The narrowing of the droplet size distribution visible in Figures 3, 4, and 5 is mainly a result of plotting droplet size on a logarithmic scale, for the actual size difference between the largest and smallest active cloud droplets increases slightly with height in the lower region of the cloud. For example, in Case 1, the difference in radius between size classes 3 and 27 is 14.7 μm at the cloud base and 14.9 μm at the 100-meter level.

A more useful indicator of the breadth of a droplet size distribution is the coefficient of dispersion (standard deviation of droplet sizes divided

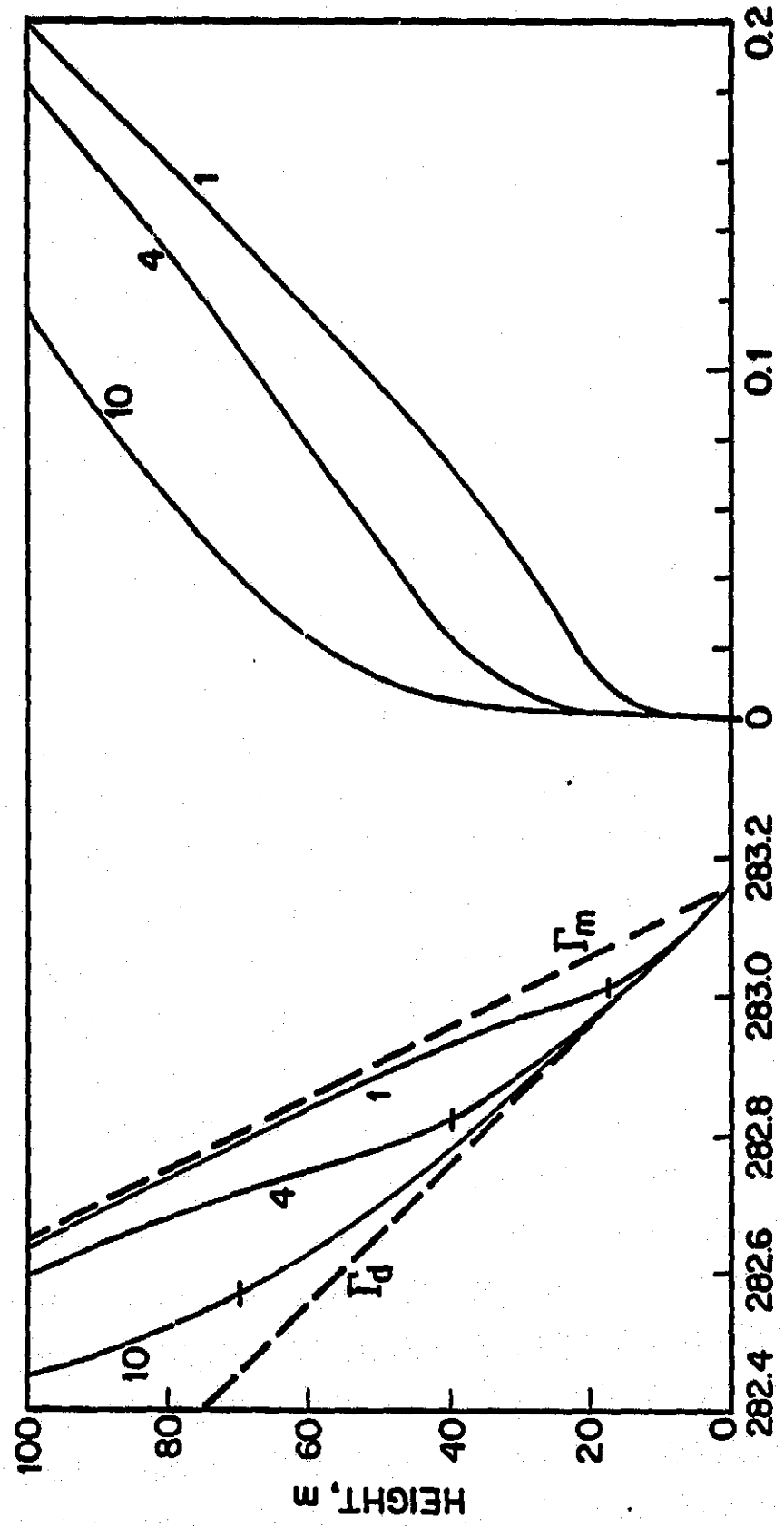

Figure 6. Temperature and liquid water content within steady updrafts of 1, 4, and 10 m/s (Cases 1, 2, and 3). Also shown are the dry and moist adiabatic lapse rates. Marks on temperature curves indicate height at which maximum supersaturation is achieved.

by the mean size), referred to in this report as simply the dispersion. In Case 1, the dispersion decreased considerably from 0.387 at the cloud base to 0.072 at the 100-meter level. The dispersion at the 100-meter level for Case 2 is 0.067 and for Case 3 is 0.060. Thus, by the dispersion criterion, the droplet size distribution narrows substantially with time.

From (2.10) it is easy to show that the radial growth rate, dr/dt, is inversely proportional to the radius. This 1/r relationship is the cause of the narrowing of the droplet size distribution. At the same time, the radial growth rate is proportional to the water vapor pressure difference (e_a-e_r) near the individual droplet. The vapor pressure of the environment, e_a, is a function of the air pressure and the vapor mixing ratio, whereas the vapor pressure at the droplet surface, e_r, is a function of the droplet size and nucleus mass and thus varies over the size spectrum.

d. Droplet equilibrium vapor pressure

The convex surface of a droplet requires that the equilibrium vapor pressure over the droplet be greater than it would be over a flat surface of pure water. Concurrently, the presence of a salt lowers the equilibrium vapor pressure over the droplet. The combination results in an equilibrium vapor pressure over the droplet (Köhler, 1926) given by (2.6). The

equilibrium supersaturation for a droplet is $(e_r/e_s - 1.0)$. When a droplet first starts to condense water, it has a high molality and can grow under less than saturated conditions. As it increases in size and becomes more dilute, the curvature term becomes important and the atmosphere must be supersaturated for the droplet to continue growing. If growth continues, both the curvature and solution effects decrease.

The maximum value of the equilibrium supersaturation is the critical supersaturation, S_c. The corresponding critical radius is r_c. Once a droplet exceeds its critical radius, the droplet is said to be activated. The physical significance of the critical radius will be made clear in a later paragraph. Figure 7 shows the critical values for aqueous ammonium sulfate droplets at 10°C. Also included is the radius, $r_{s=0}$, at which the droplet would be in equilibrium with an environment of 100% relative humidity. It can be shown that $r_c \approx \sqrt{3}\, r_{s=0}$.

It is of interest that a very small nucleus of 0.01 μm-radius must increase its radius by a factor of 3.8 to reach its critical radius. This means that the volume must be increased by a factor of $3.8^3 = 54.9$. On the other hand, the critical radius for a 1.0 μm radius salt nucleus is 38.3 μm; the volume of the particle is increased roughly by a factor of $(38)^3 = 5.5 \times 10^4$.

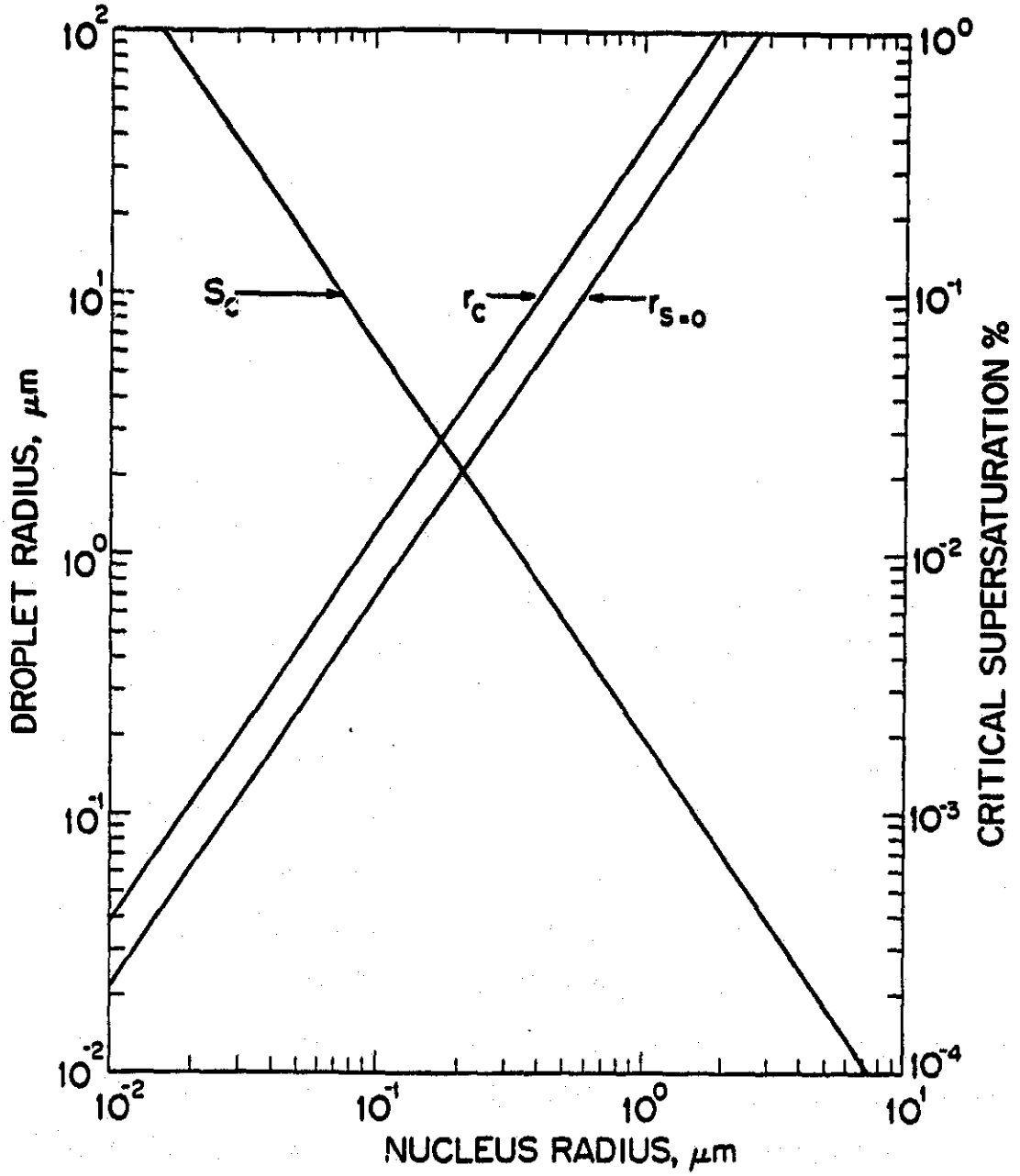

Figure 7. Critical supersaturation, S_c, critical radius, r_c, and equilibrium radius at 100% relative humidity, $r_{S=0}$, for droplets containing a nucleus of $(NH_4)_2SO_4$ at 10°C.

e. Droplet growth time

A very crude estimate can be made of the time required for a particle to grow from r_n to $r_{s=0}$ or r_c. If the assumption is made that solution and curvature effects are negligible, then for a given temperature and constant saturation ratio, (2.10) can be integrated. The time it takes a droplet to reach its critical radius is approximately

$$\Delta t = \frac{\frac{\rho_r R_v T_a}{De_s} + \frac{T^* L \rho_r}{K(T-35.86)^2}}{2(S-1)} (r_c^2 - r_n^2)$$

Admittedly, this does not give accurate results, especially for a small nucleus. It does, however, allow order of magnitude estimates which appear in Table II. The supersaturation used here was 1%. Since this is a high value, the listings in Table II represent the minimum time a nucleus must remain in a cloud to become activated. A droplet with 0.1 μm-radius nucleus will activate in less than one second under the high humidity conditions. On the other hand, a 10.0 μm-radius nucleus would have to be in a cloud at least 10 days to activate, and at least 3 days to reach its equilibrium radius $r_{s=0}$. A large droplet, then, will not reach equilibrium with cloud conditions.

f. Selective evaporation and activation

Figure 8 shows the equilibrium supersaturation for two droplets of nucleus size $r_n^{(1)}$ and $r_n^{(2)}$. The

critical points S_c and r_c are indicated, as well as $r_{s=0}$. It is to be remembered that the Köhler curves of Figure 8 are loci of equilibrium points. Whether a droplet will tend to grow or evaporate depends on both environment and droplet conditions. It has already been shown that a large droplet will not reach equilibrium in a cloud. Only small droplets can be expected to react quickly enough to be near equilibrium with a changing environment.

Suppose the environment to have a supersaturation of A in Figure 8. Suppose further that the two droplets have particular radii such that their conditions are represented by the points $A^{(1)}$ and $A^{(2)}$ respectively. For both droplets the ambient supersaturation is greater than the equilibrium value so both would grow along the indicated arrows (constant ambient conditions assumed). If the ambient supersaturation were lowered to B, the first droplet would evaporate, while the second one would continue to grow. This is the basis of selective evaporation within the droplet distribution.

Selective evaporation is apparent in Figure 3. Droplets of the smallest two size classes evaporate as the supersaturation decreases.

Once a droplet exceeds its critical radius, it is said to be activated, since it will continue to grow even though the ambient supersaturation decreases, as long as the ambient value does not go below the

TABLE II

Estimated times for a droplet to grow from r_n to $r_{s=0}$ and r_c. Temperature is 283.16 K. Supersaturation is 1.0%.

r_n	$r_{s=0}$	$t_{s=0}$	r_c	t_0
0.1 μm	0.7 μm	0.3 sec	1.2 μm	0.8 sec
0.3	3.6	7.6	6.3	23
0.5	7.8	36	13.5	108
1.0	22	290	38	860
3.0	115	7,800	199	23,000
5.0	247	36,000	428	109,000
10.0	699	290,000	1,210	870,000

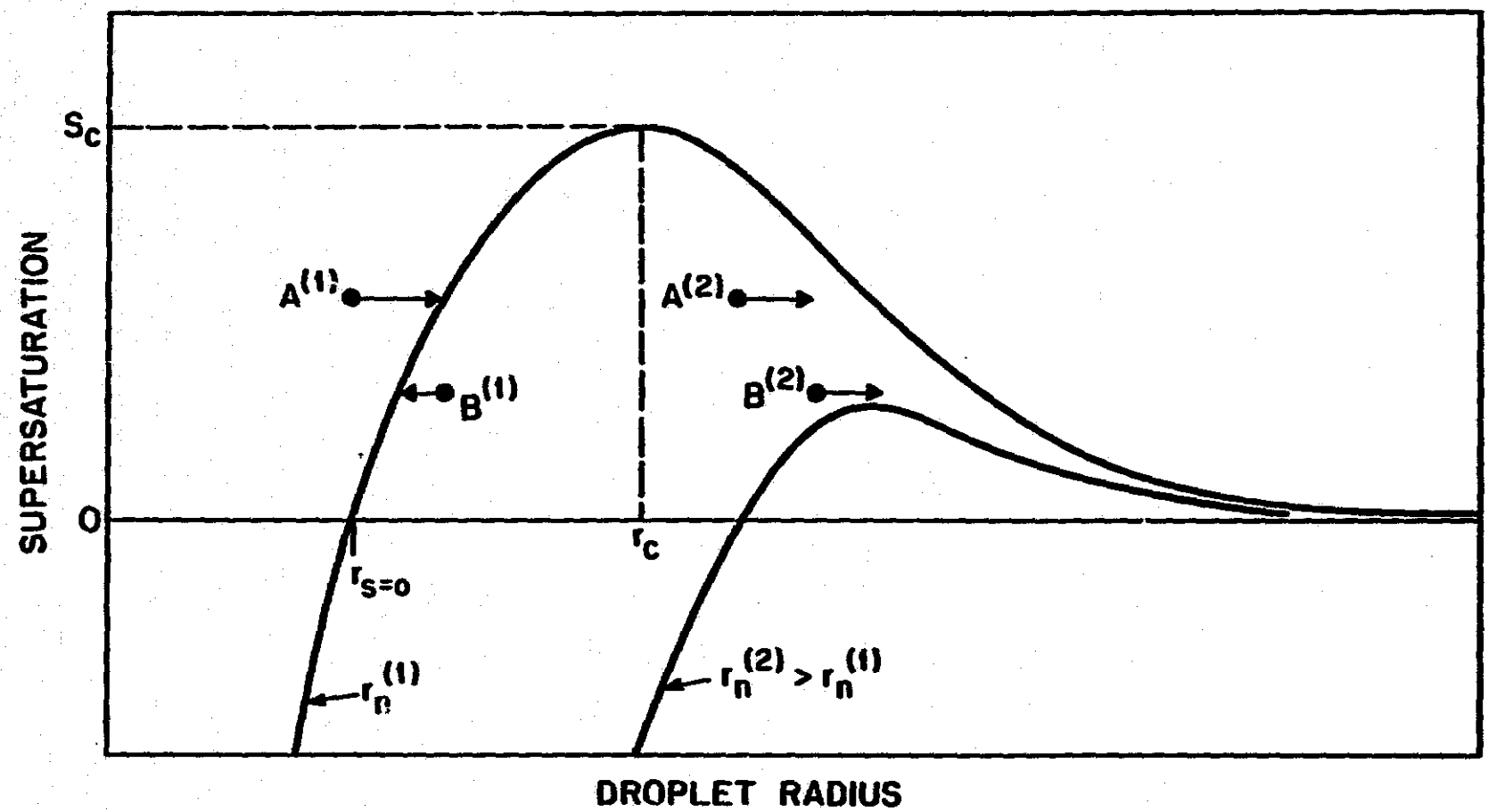

Figure 8. Equilibrium supersaturation for two droplets.

equilibrium value for that droplet. A droplet will activate if two conditions are met: the supersaturation of the environment exceeds the critical supersaturation for the droplet; and the droplet is given sufficient time under supersaturated conditions to grow beyond its critical size.

Not all droplets activate. A large droplet, by virtue of its slow growth, does not activate despite its low critical supersaturation. In contrast, the smallest droplet, even though it has a small critical radius, does not activate if the ambient supersaturation does not exceed the droplet equilibrium supersaturation. As a result, the first droplets to activate in Case 1 (Figure 3) are those of size class 7 (r_n= 0.054 μm) after 7 seconds. With time, the threshold of activated droplets spreads outward to larger and smaller sizes. At the time of maximum supersaturation, droplets of size classes 3 to 13 (r_n = 0.023 to 0.195 μm) are activated. Even as the ambient supersaturation decreases, size classes 14 and 15 (r_n = 0.24 and 0.30 μm) become activated.

g. Radial growth rate

The effect of the dependence of the vapor pressure difference (e_a-e_r) on the droplet properties is that the radial growth rate of a droplet is not related simply to the inverse of the radius. Droplets containing a small nucleus are able to respond quickly

to changes in the environment; hence they are nearly in equilibrium and maintain a small vapor pressure difference with a corresponding low growth rate. Conversely, a droplet with a large nucleus lags well behind its equilibrium size and has a large vapor gradient near it.

Figure 9 illustrates the radial growth rate of the droplets at various times for Case 1. The curve at 5 seconds has two maxima: one at about 0.8 μm and the other at about 15 μm. The first is due to the dominance of the 1/r relationship and the second to that of the vapor pressure difference, $e_a - e_r$. Only after 20 seconds, which is just beyond the maximum supersaturation, does the smallest (class 3) droplet have the fastest radial growth rate.

3.3 Fluctuating Updraft

The growth rate of a droplet depends on two properties: the droplet radius and the ambient supersaturation. Taken together, these give rise to a vapor pressure difference ($e_a - e_r$) for each droplet. It has been demonstrated that the radial growth rate of a droplet is inversely proportional to the droplet radius and directly proportional to the vapor pressure difference. To produce a droplet size spectrum broader than that obtained in a steady updraft, there needs to be a mechanism which slows the growth rate of the small

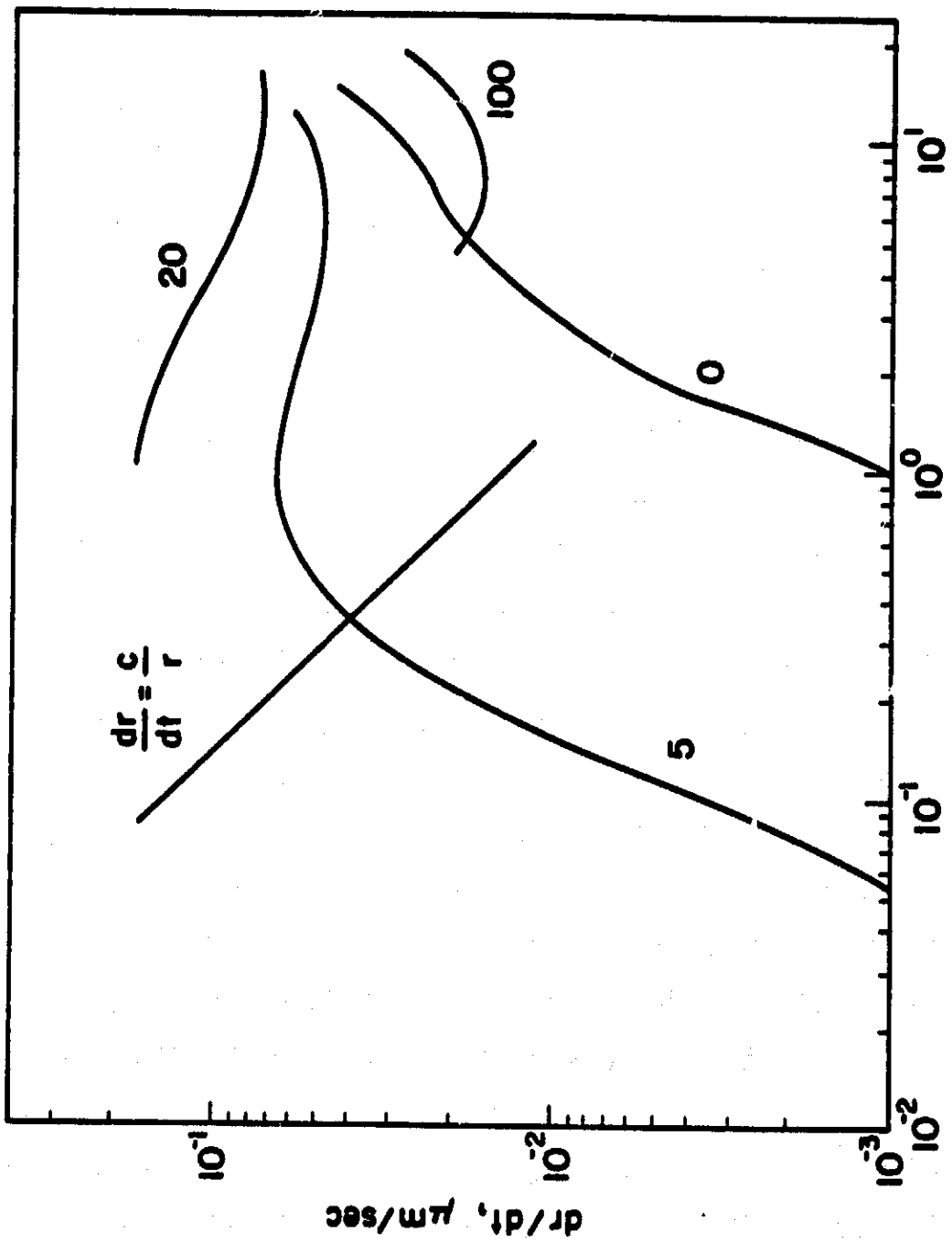

Figure 9. Radial growth rate of droplets ascending at 1 m/s from cloud base (Case 1). Curve labels indicate time (sec). Included is a line showing r^{-1} relationship.

droplets and allows the large droplets to continue growing. The key is to discover a naturally occurring process which alters the spectral variation of the vapor pressure difference in such a way that broadening of the droplet size spectrum is achieved.

Consider, then, the effect of alternating upward and downward motions. As a parcel of cloud air is raised, the smaller droplets activate while larger ones grow toward equilibrium. As the parcel of cloud air is then lowered, some of the smallest droplets deactivate, whereas the largest ones continue to grow for some time. Subsequent uplifting produces renewed growth, but growth upon a size distribution broader than the original one. The overall effect on the droplet size distribution is expected to depend on the eddy size and frequency and on the speed of the parcel.

a. Vertical velocity patterns

To test the above idea, studies with two types of vertical velocity patterns are presented. The velocities for 14 cases are listed in Table III.

One velocity group simulates a parcel of cloud air that leaves the updraft, falls, and subsequently reenters the updraft. A steady updraft of 1.0 m/s is combined with a steady downdraft, usually of -0.2 m/s. Velocities of this group are referred to as square wave velocity patterns to distinguish them from sinusoidal patterns.

TABLE III

Vertical velocity patterns

Steady Updraft

Case Number	Vertical velocity (m/s)	Time to reach 100-meter level (s)
1	1	100
2	4	25
3	10	10

Square wave

Case Number	Height (m)	Vertical velocity (m/s)	Time to reach 100-meter level (s)
4	0-20	1.0	
	20-0	-0.2	
	0-100	1.0	220
5	0-20	1.0	
	20-0	-0.2	
	0-20	1.0	
	20-0	-0.2	
	0-100	1.0	340
6	0-20	1.0	
	20-0	-0.2	
	0-30	1.0	
	30-10	-0.2	
	10-100	1.0	340
7	0-10	1.0	
	10-0	-1.0	
	0-20	1.0	
	20-10	-1.0	
	10-30	1.0	
	30-20	-1.0	
	20-40	1.0	
	40-30	-1.0	
	30-50	1.0	
	50-40	-1.0	
	40-60	1.0	
	60-50	-1.0	
	50-100	1.0	220

TABLE III Continued

Sinusoidal

Case Number	Velocity (m/s)	Maximum updraft speed (m/s)	Eddy diameter (m)	Time to reach 100 meter level(s)
8	0.25+0.75 cos(0.032t)	1	25	375
9	1.0+3.0 cos(0.13t)	4	25	100
10	1.0+3.0 cos(0.064t)	4	50	100
11	1.0+3.0 sin(0.15t)	4	40	61
12	2.5+7.5 cos(1.6t)	10	5	40
13	2.5+7.5 cos(0.32t)	10	25	40
14	2.5+7.5 cos(0.16t)	10	50	40

Sinusoidal velocities make up the second group of velocity patterns. They are used to relate the eddy size and frequency to the dispersion of the droplet size distribution. Maximum updrafts of 1, 4, or 10 m/s are used. The maximum downdraft speed is half the maximum updraft speed. Various descent lengths (eddy diameter) of 5, 25, and 50 meters are used.

b. Growth of droplets

The effects of alternating steady upward and downward motion (Cases 4-7) are illustrated in Figures 10-13. In Figure 10, the cloud parcel rises to the 20 meter level at 1 m/s, descends to the cloud base at -0.2 m/s, and rises again to the 100 meter level at 1 m/s. With downward motion of the parcel the supersaturation drops below zero to a minimum of -0.12%. Small droplets undergo substantial evaporation during that time. It will be shown later that droplets of size class 22(r_n = 1.34 μm) through 27(r_n = 3.9 μm) grow throughout the entire cycle. As the parcel is again lifted, the supersaturation reaches a peak of 0.59%, a value somewhat lower than the first maximum of 0.71%.

Case 5 (Figure 11) differs from Case 4 in that there are two loops between the cloud base and the 20 meter level. Again, selective evaporation is apparent. In Case 6, the second loop is between the 10 meter level and the 30 meter level. The droplet behavior is shown in Figure 12. (In this figure, and

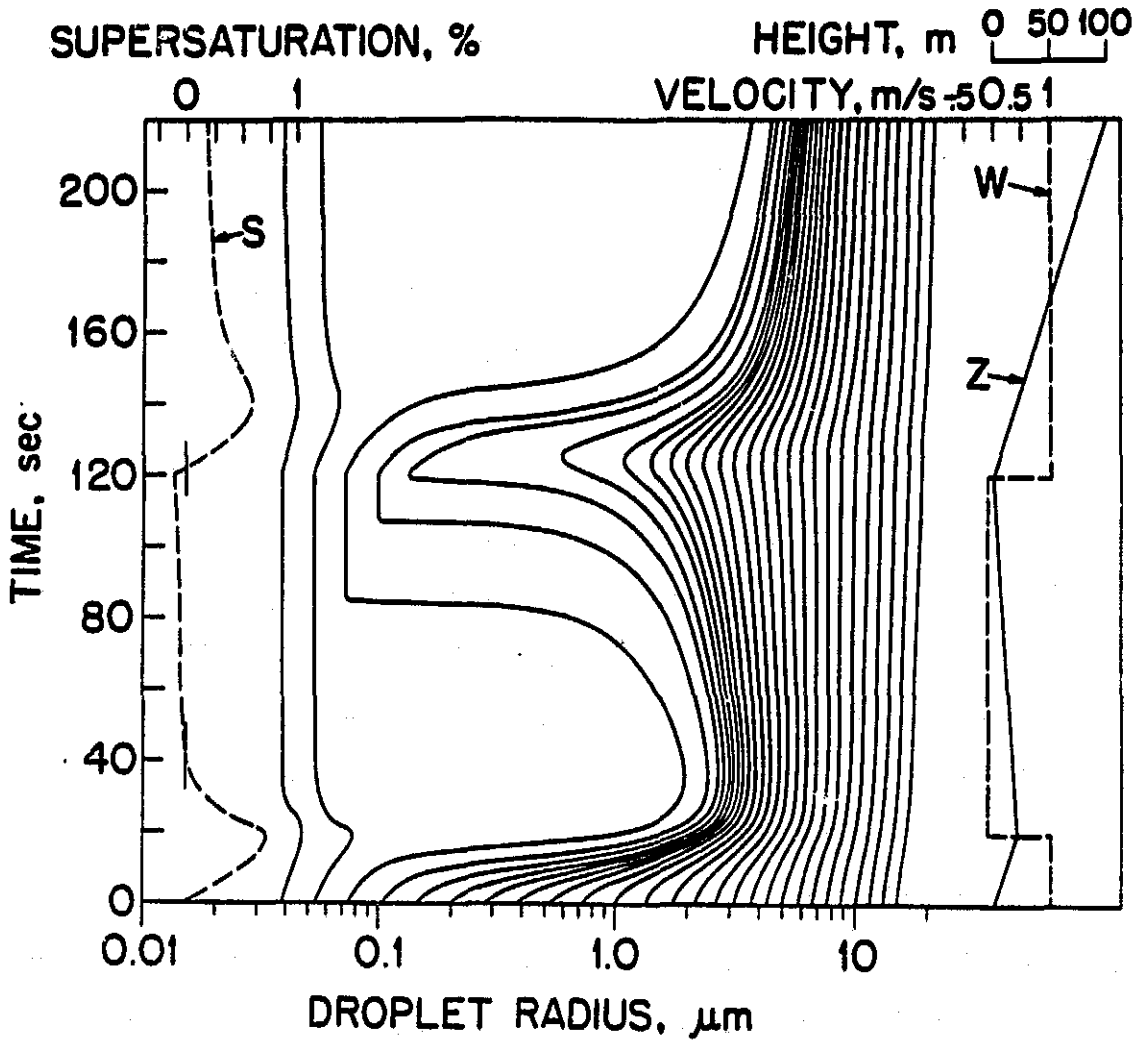

Figure 10. Growth of cloud droplets for indicated square wave velocity pattern: Case 4.

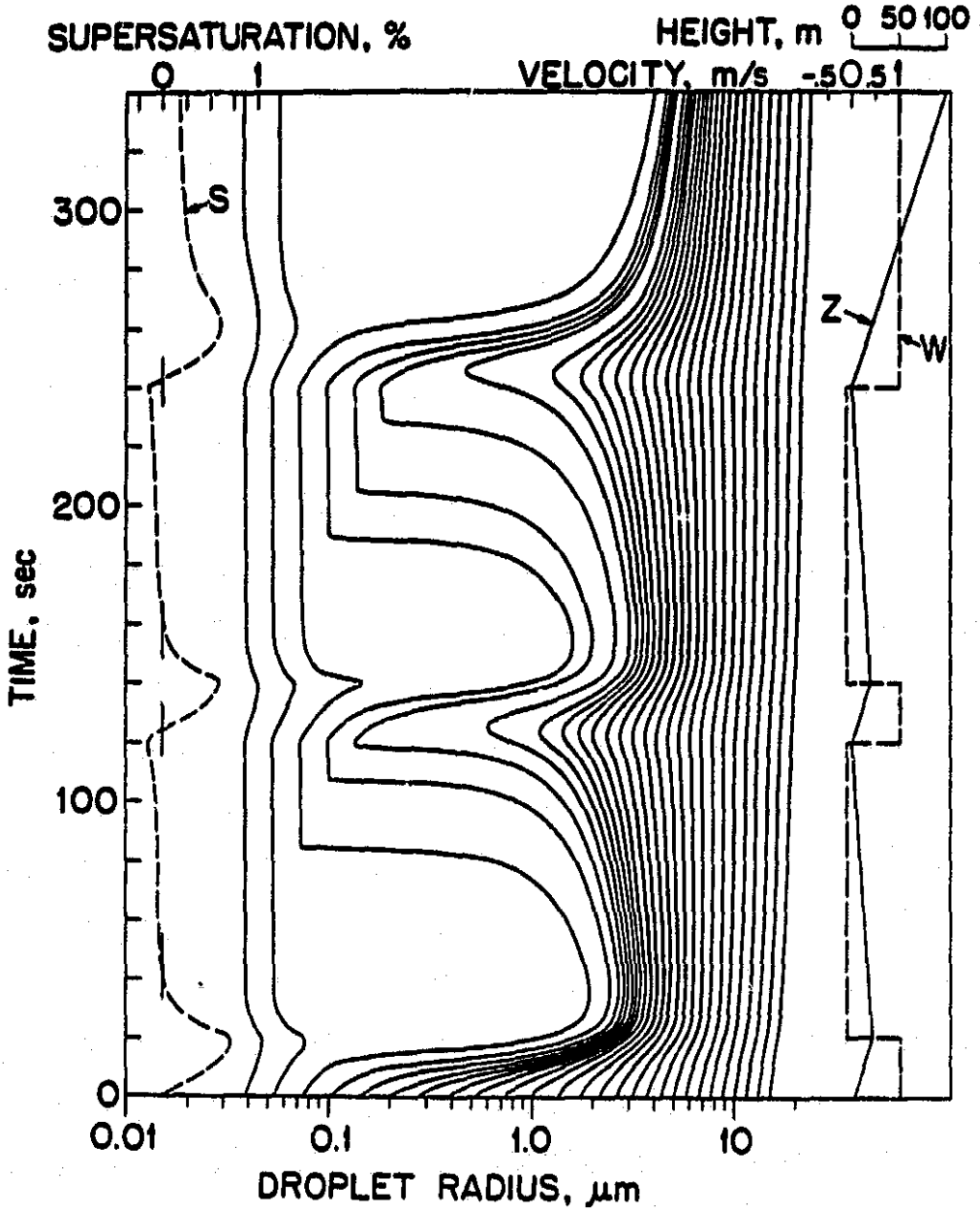

Figure 11. Growth of cloud droplets for indicated square wave velocity pattern: Case 5.

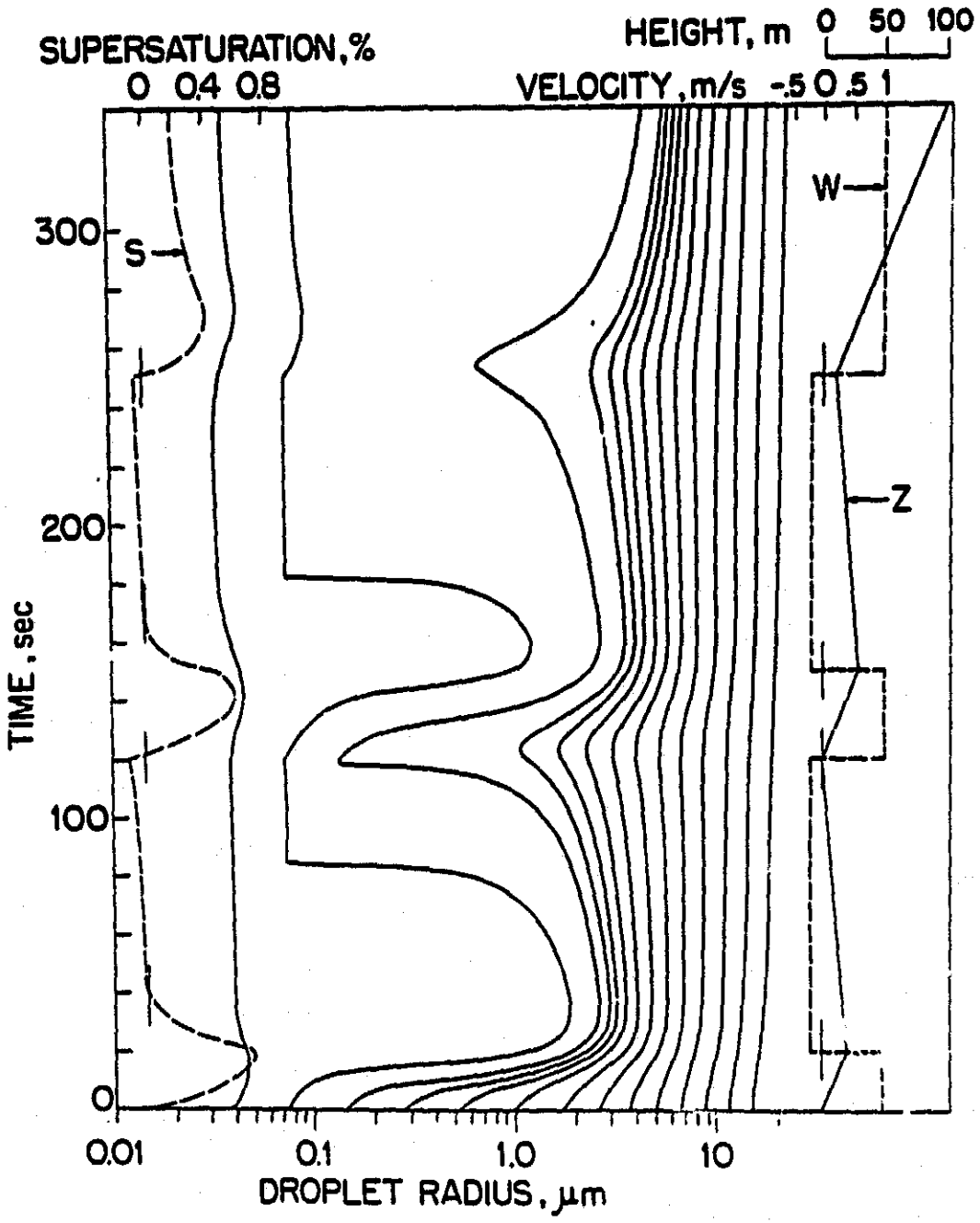

Figure 12. Growth of cloud droplets for indicated square wave velocity pattern. Only odd-numbered size classes are shown: Case 6.

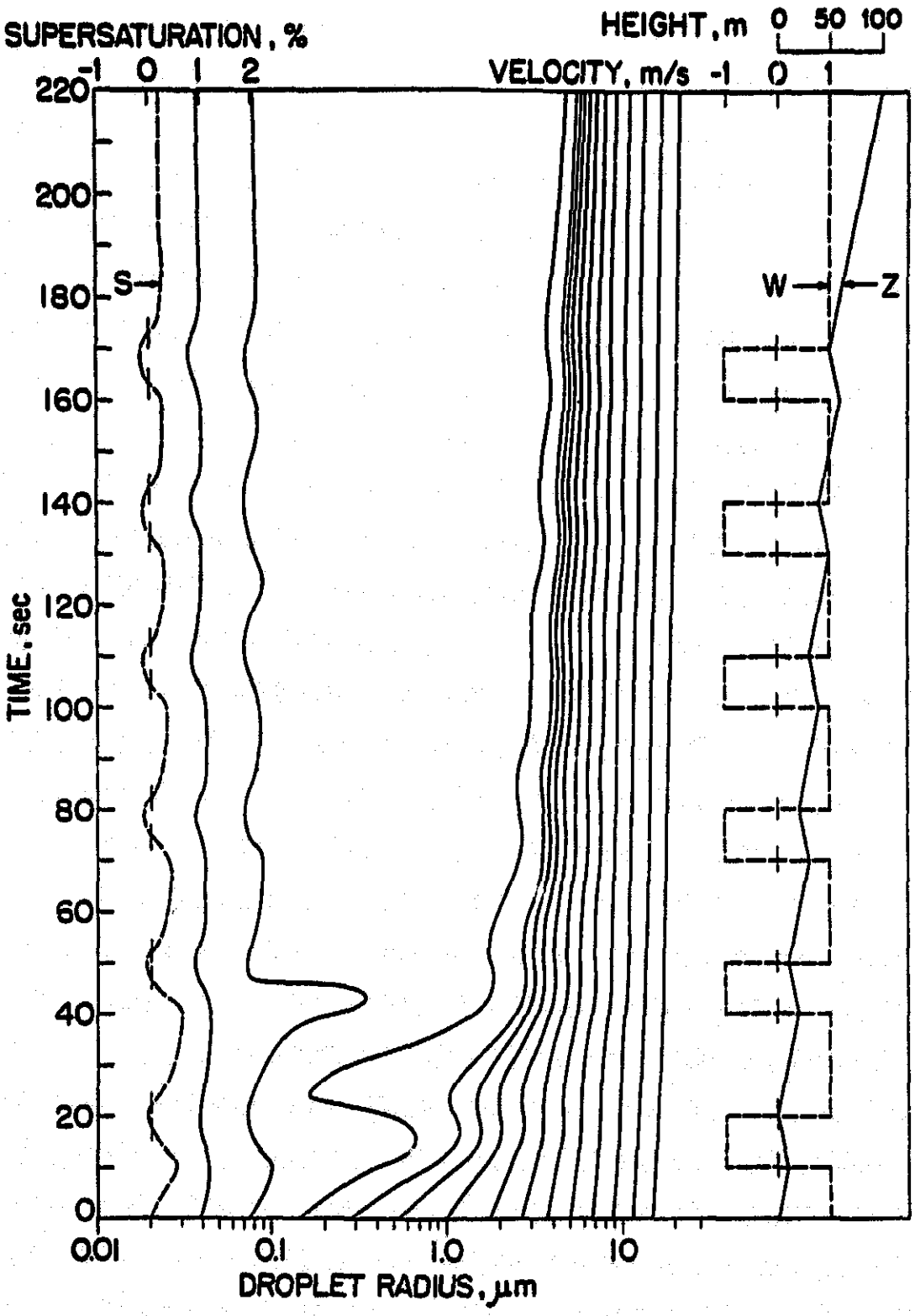

Figure 13. Growth of cloud droplets for indicated square wave velocity pattern. Only odd-numbered size classes are shown: Case 7.

in Figures 13-20, only the odd-numbered size classes have been included.) One result of the 10 meter shift between loops is that droplets of size class 3 (r_n = 0.023 μm) do not reactivate during the second loop.

Case 7 (Figure 13) is a series of six quick loops, with a maximum downdraft of -1 m/s. The effect is not nearly as dramatic as in the earlier cases.

Figures 14-20 represent the behavior of the droplets in a sinusoidal updraft. The effect of the fluctuating motion is small; the usual pattern is an oscillation of the size of the smallest droplets in direct response to the changing supersaturation. For the case of a maximum updraft of 1 m/s and a simulated eddy diameter of 25 meters (Figure 14), droplets of size class 3 are deactivated after some 165 seconds and thereafter carried along as haze particles. In this case, therefore, the water previously associated with class 3 droplets is released to promote growth of the larger droplets. This result indicates a process, which in a natural continuum of nucleus sizes must always be present, but which shows up only occasionally in a simulation based upon discrete size classes. It appears, however, that the transfer of water mass from the small to the larger sizes for this case is not great enough to affect the cloud droplet spectrum appreciably.

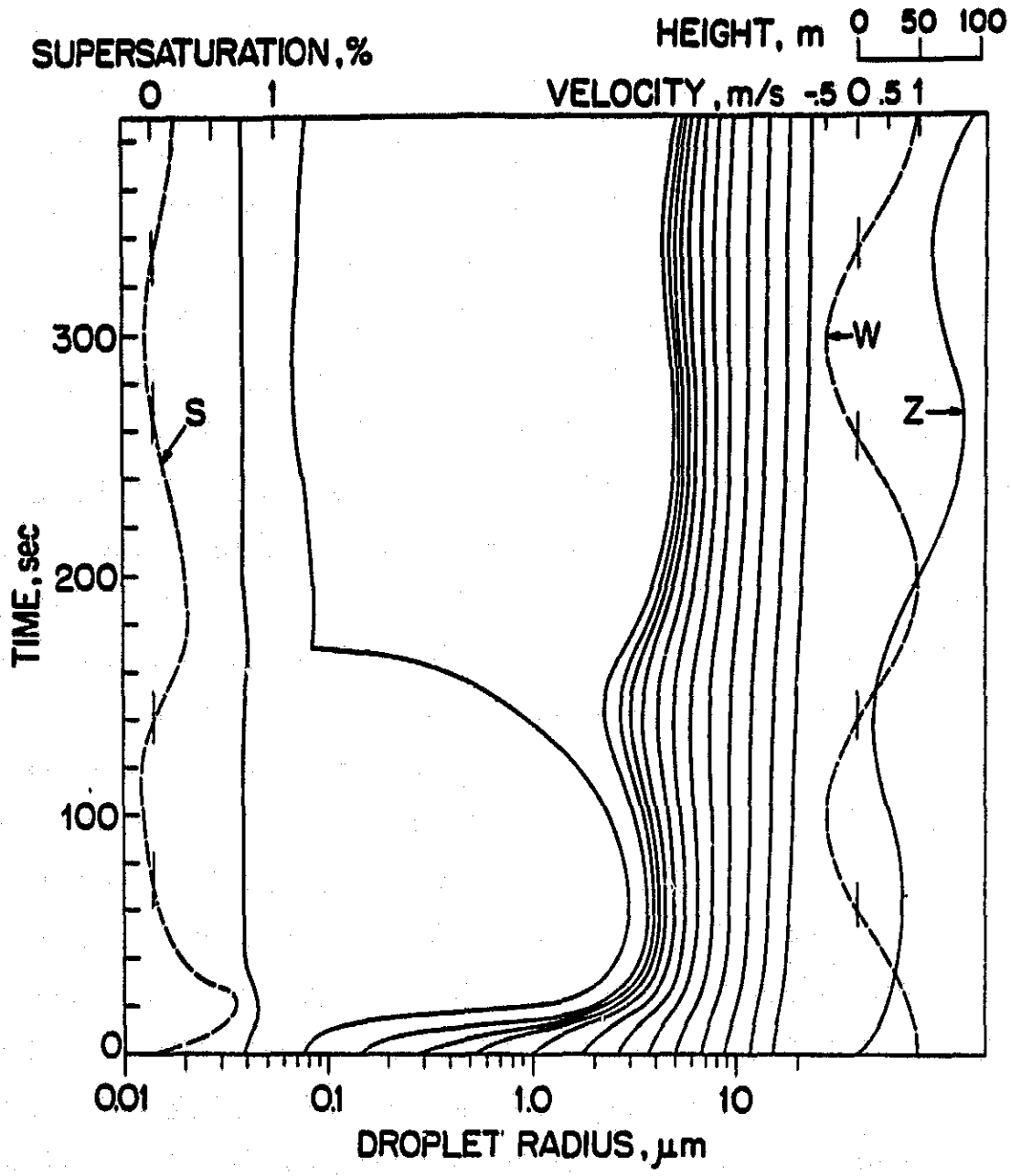

Figure 14. Growth of cloud droplets for indicated sinusoidal velocity pattern. Only odd-numbered size classes are shown: Case 8.

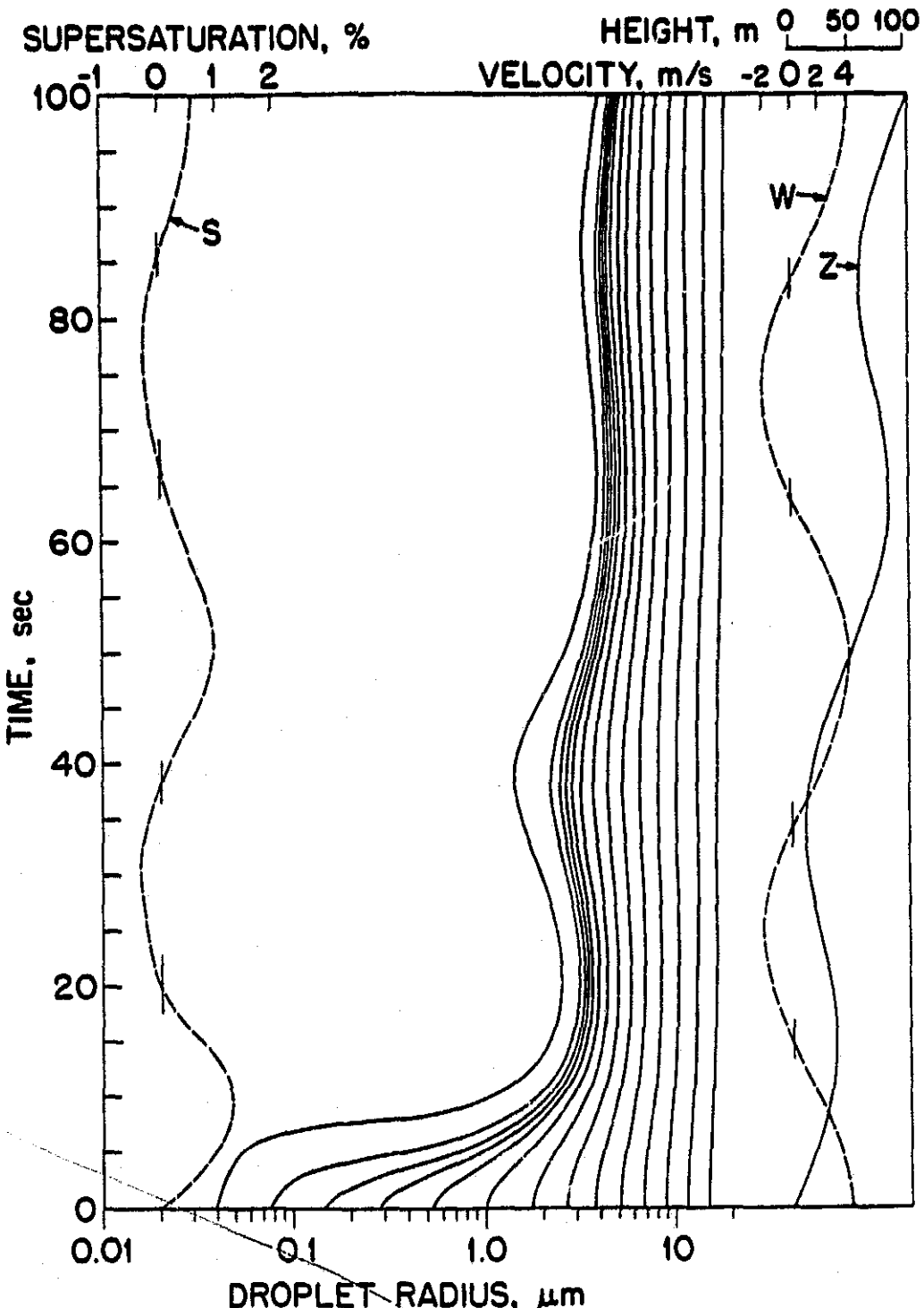

Figure 15. Growth of cloud droplets for indicated sinusoidal velocity pattern. Only odd-numbered size classes are shown: Case 9.

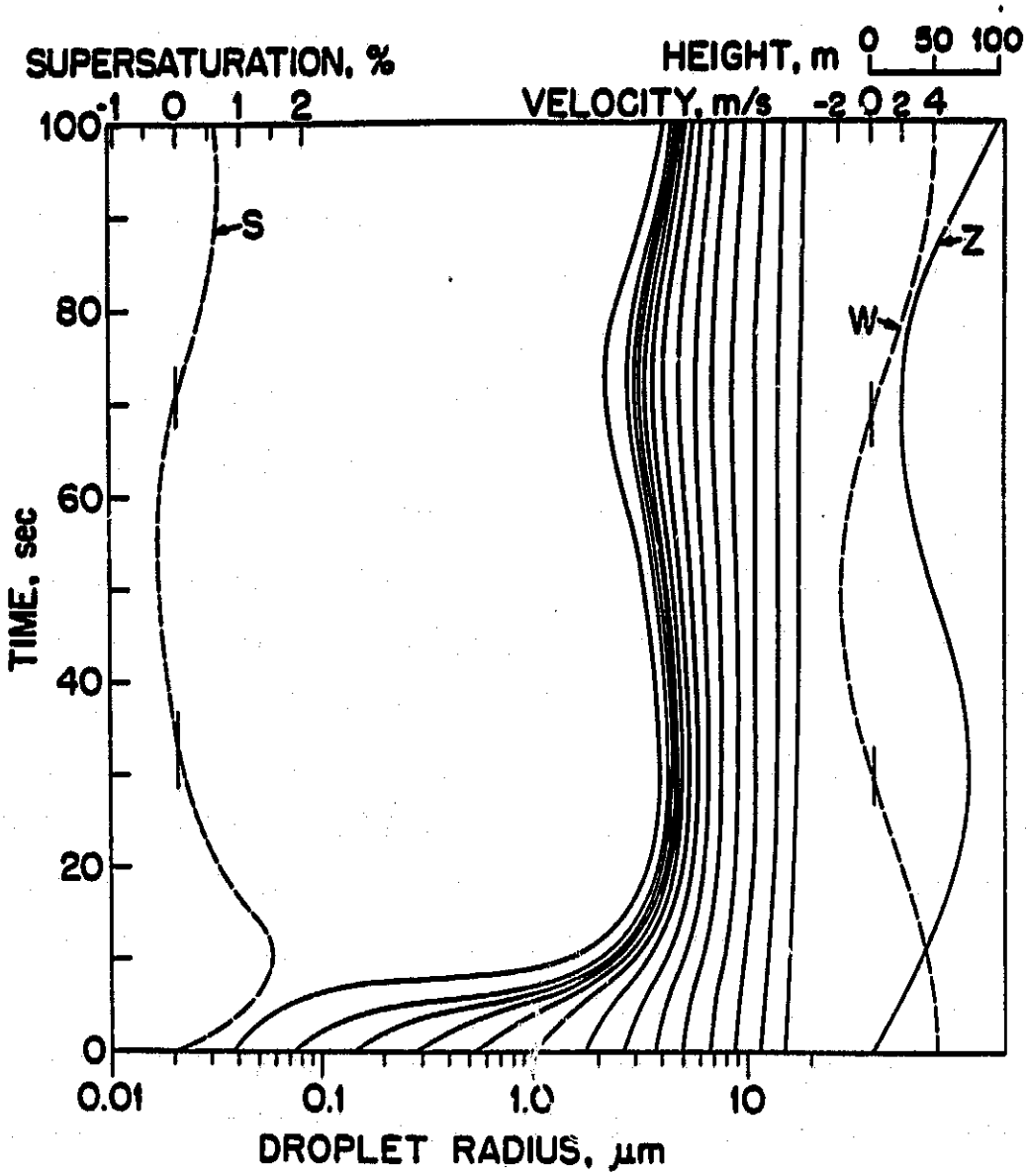

Figure 16. Growth of cloud droplets for indicated sinusoidal velocity pattern. Only odd-numbered size classes are shown: Case 10.

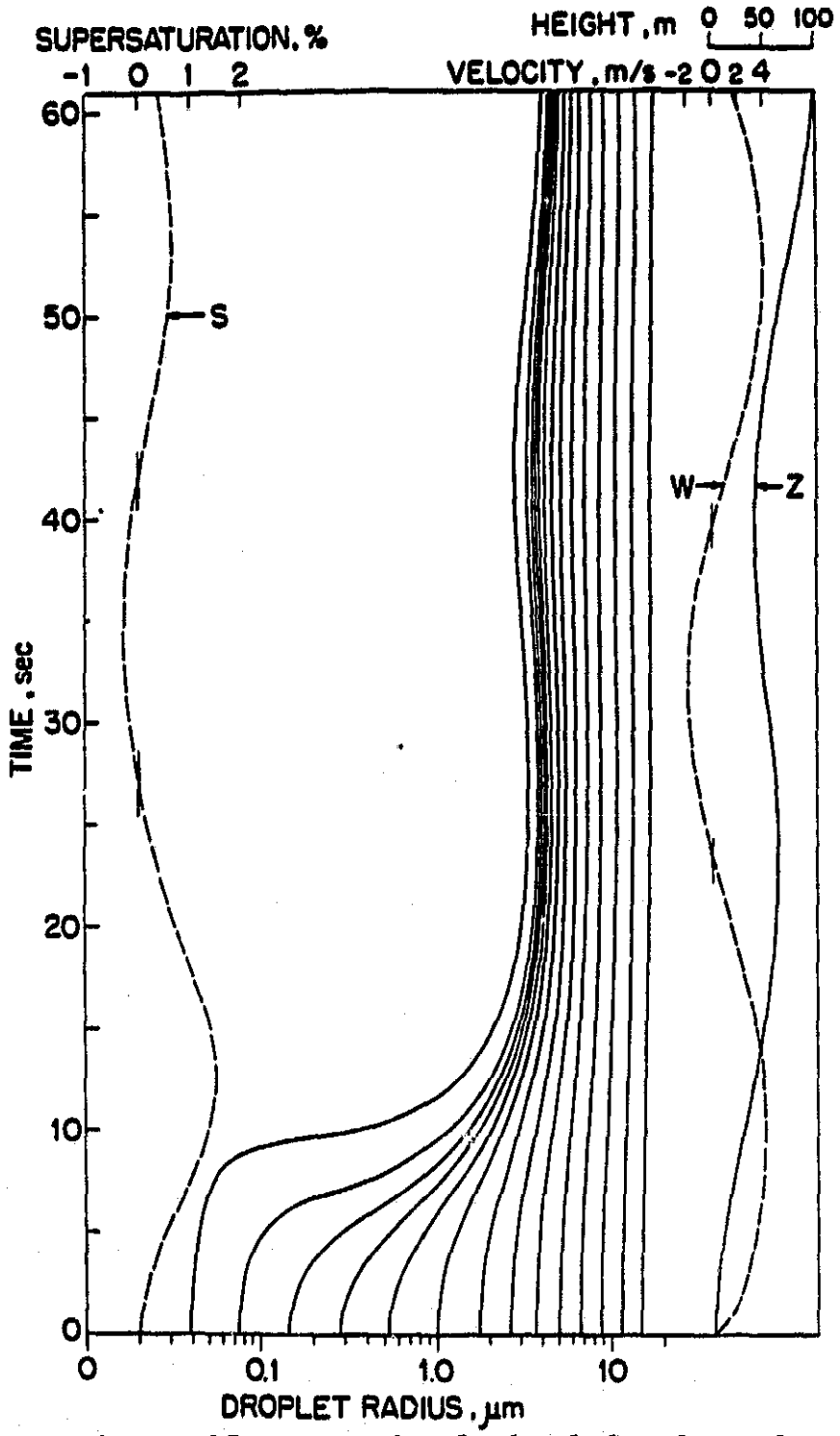

Figure 17. Growth of cloud droplets for indicated sinusoidal velocity pattern. Only odd-numbered size classes are shown: Case 11.

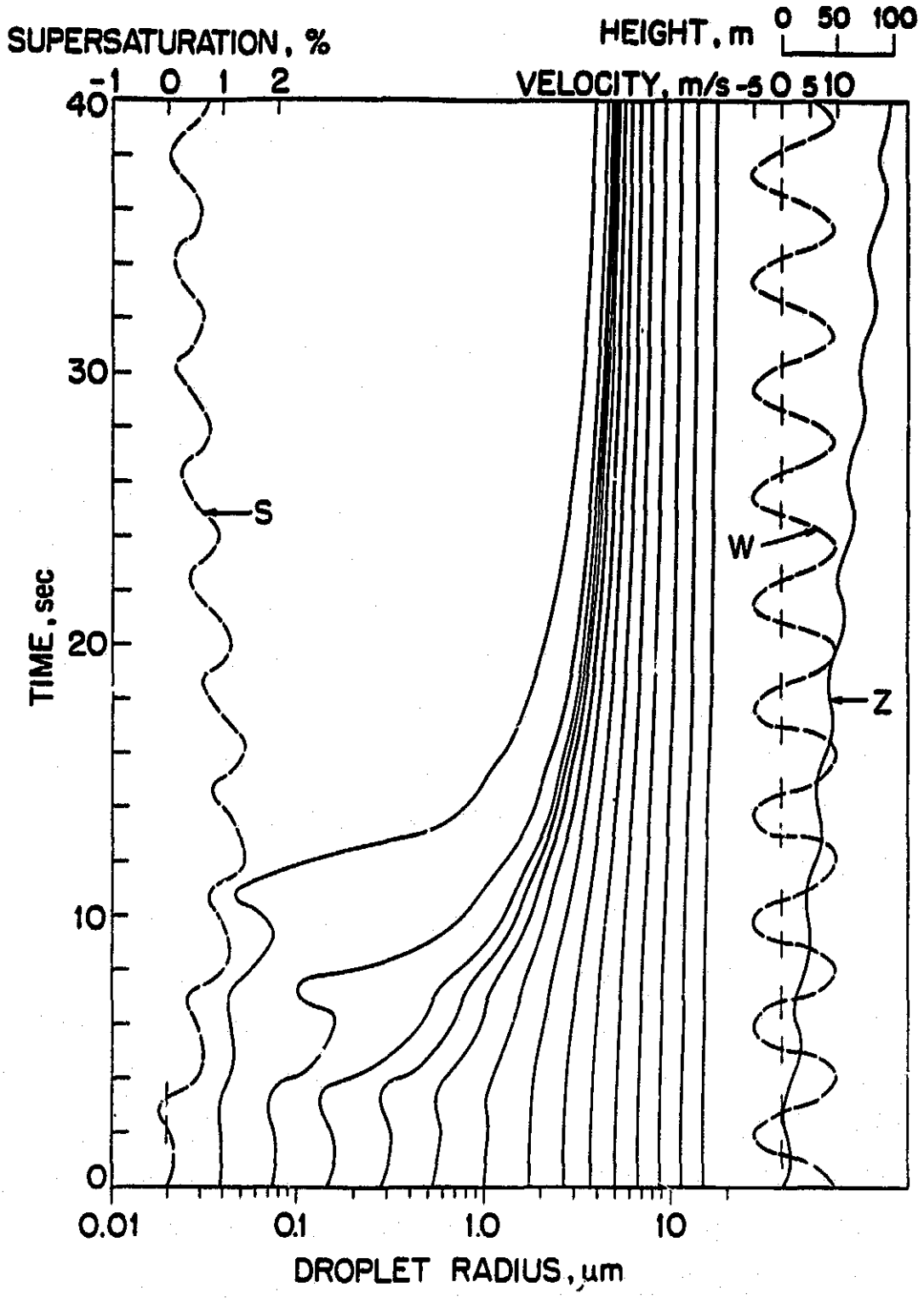

Figure 18. Growth of cloud droplets for indicated sinusoidal velocity pattern. Only odd-numbered size classes are shown: Case 12.

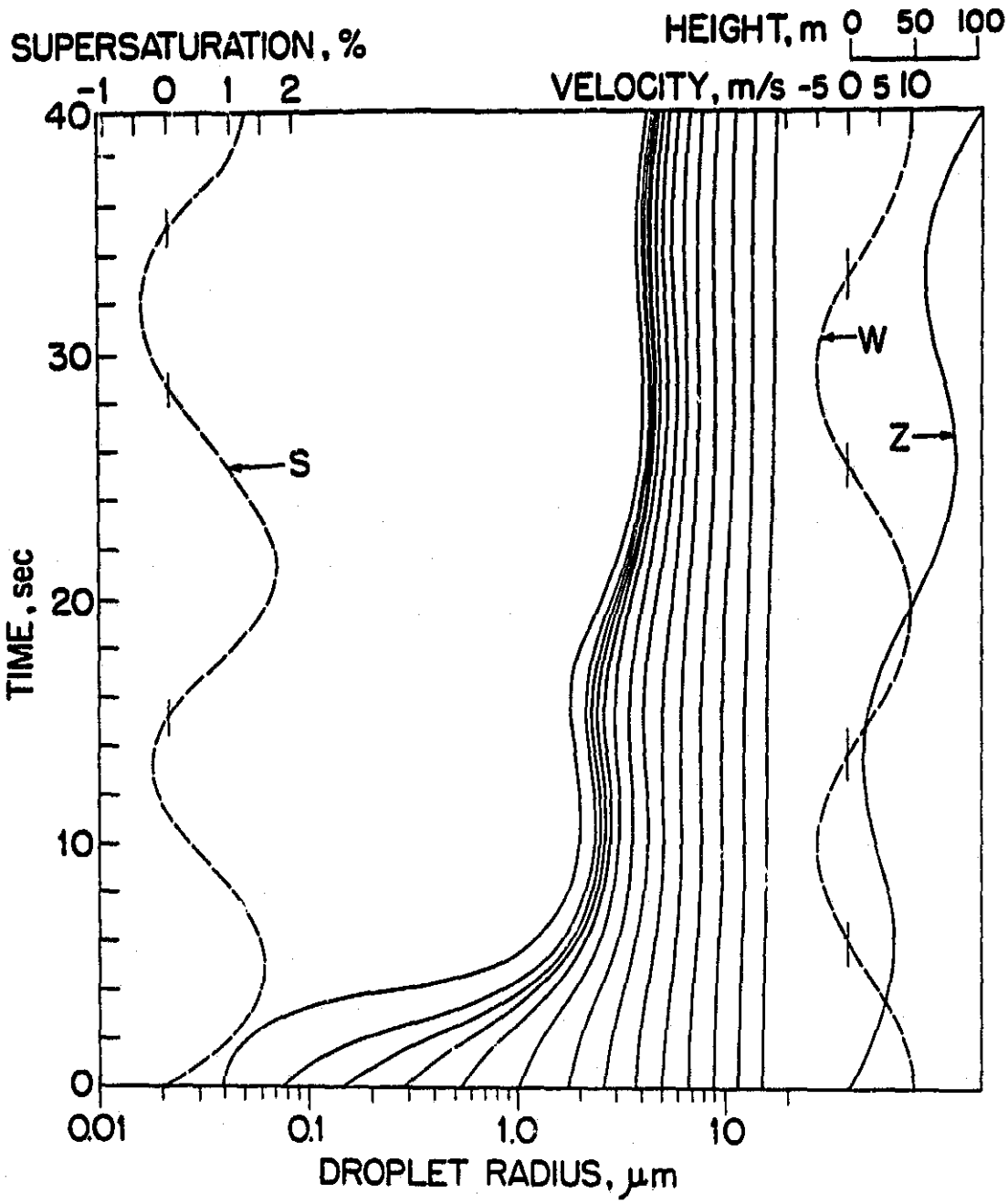

Figure 19. Growth of cloud droplets for indicated sinusoidal velocity pattern. Only odd-numbered size classes are shown: Case 13.

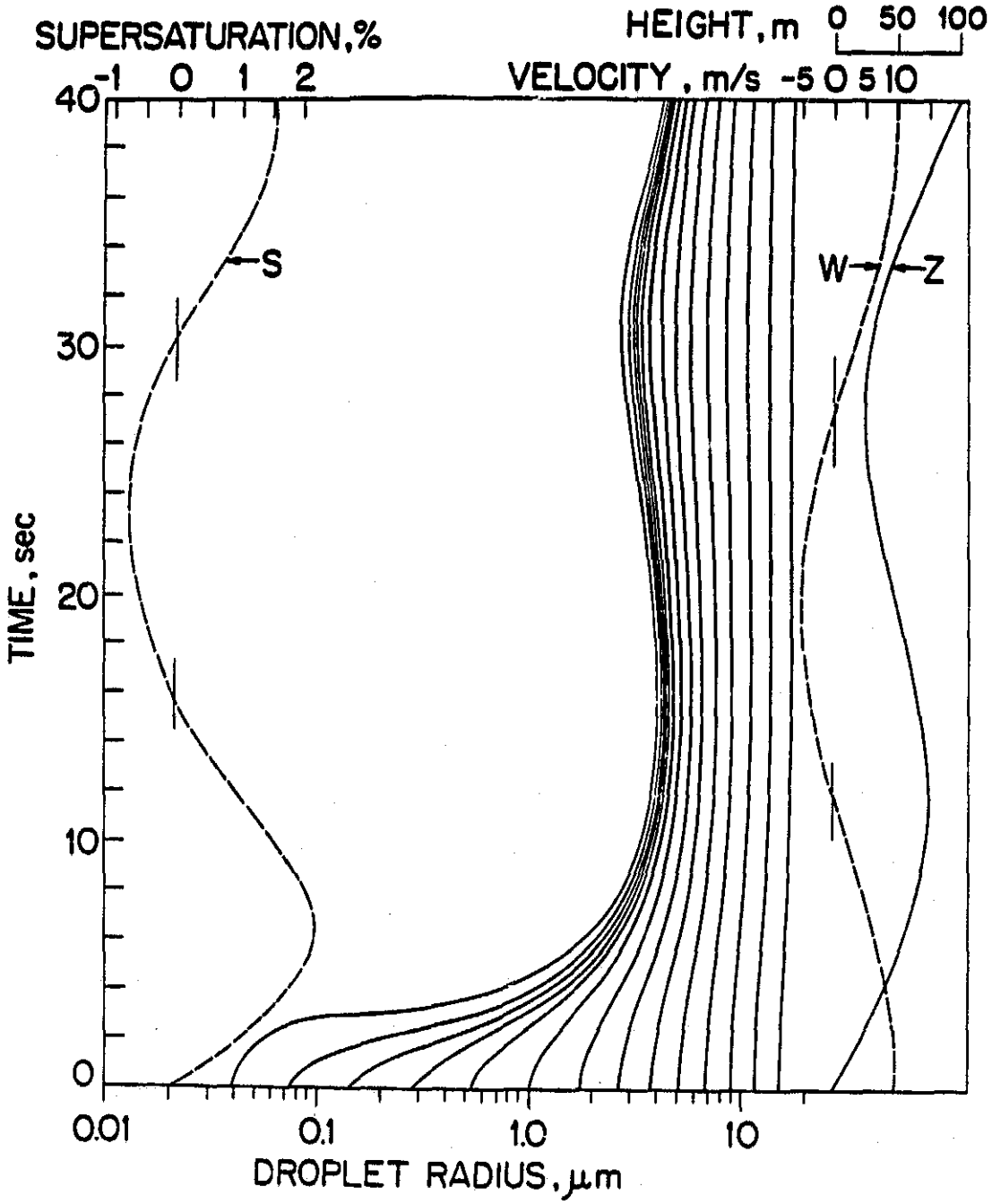

Figure 20. Growth of cloud droplets for indicated sinusoidal velocity pattern. Only odd-numbered size classes are shown: Case 14.

c. Dispersion of the droplet size distribution

To describe the droplet size distribution, three statistical parameters are useful: the mean radius, $\bar{r}$, the standard deviation, σ; and the coefficient of dispersion about the mean, $\delta = \sigma/\bar{r}$. The values at the 100-meter level or all fourteen cases are listed in Table IV. It is significant that the dispersion is increased substantially for the square wave velocity patterns, Cases 4-7. In Cases 4 and 5 in particular, the dispersion is more than double that produced by the steady updraft Case 1. For the sinusoidal velocity variations, the mean radius and dispersion decrease with increasing eddy diameter. For example, the dispersion produced by a steady updraft of 10 m/s is 0.060. With an eddy diameter of 5 meters, it is increased to 0.083. However, with eddy diameters of 25 and 50 meters, the dispersion decreases to 0.056 and 0.055 respectively.

Warner (1969a) measured the dispersion of droplet size distributions in Australian cumuli; these are shown in Figure 21. His measurements show that the dispersion averages about 0.2 at the cloud base, increases to a peak of about 0.45 at a height of 1.5 km above cloud base, and thereafter decreases somewhat. None of the values of the dispersion in this study is as high as 0.2. Other factors may be involved, but Warner's measurements were in maritime clouds, and the nucleus size distribution for this study is more descriptive

Table IV

Mean radius, $\bar{r}$, standard deviation, σ, and dispersion, δ, of droplet distributions 100 meters above cloud base.

Case No.	Figure No.	$\bar{r}$ (μm)	σ (μm)	δ
1	3	5.36	.384	.072
2	4	4.83	.308	.067
3	5	4.15	.250	.060
4	10	5.27	.783	.149
5	11	5.27	.760	.144
6	12	5.84	.722	.124
7	13	5.56	.606	.109
8	14	5.59	.456	.082
9	15	4.85	.383	.079
10	16	4.83	.351	.073
11	17	4.85	.357	.074
12	18	4.83	.402	.083
13	19	4.73	.265	.056
14	20	4.59	.252	.055

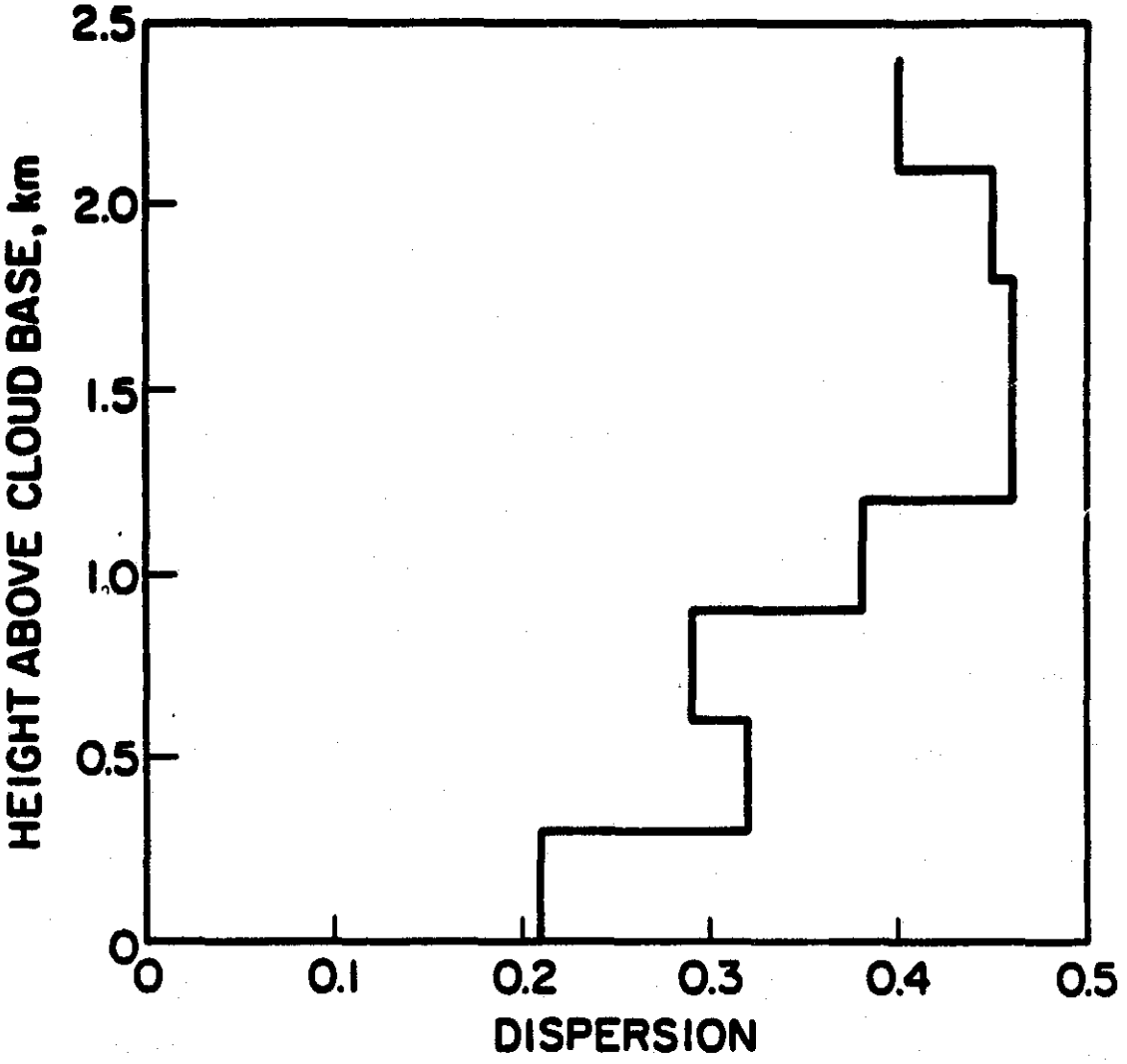

Figure 21. Coefficient of dispersion of cloud droplets, from Warner (1969a).

of continental clouds. Fitzgerald (1972) showed that the dispersion depends on the original nucleus size distribution. With a particle distribution similar to the one used here, Fitzgerald calculated a dispersion of 0.074 at the 244-meter level. With a less steep nucleus size distribution (fewer small particles, more large particles) his calculated dispersion was 0.28 at the 200-meter level. What is of interest in this study is how the dispersion and droplet size distribution are altered by turbulent motion.

d. Droplet size distribution

Some droplet size distributions are illustrated in Figures 22-25. The number of droplets per unit volume per unit radius interval is

$$\frac{dn_i}{dr} = \frac{2N_i\rho_d}{r_{i+1} - r_{i-1}}$$

in which N_i = number of droplets/gm air in i^{th} size class, and

ρ_d = dry air density.

Since our interest is with the cloud droplets, the mode due to nonactivated haze droplets is not shown in the figure. Also, it has been omitted from the calculation of the dispersion.

Figures 22 and 23 include the droplet size

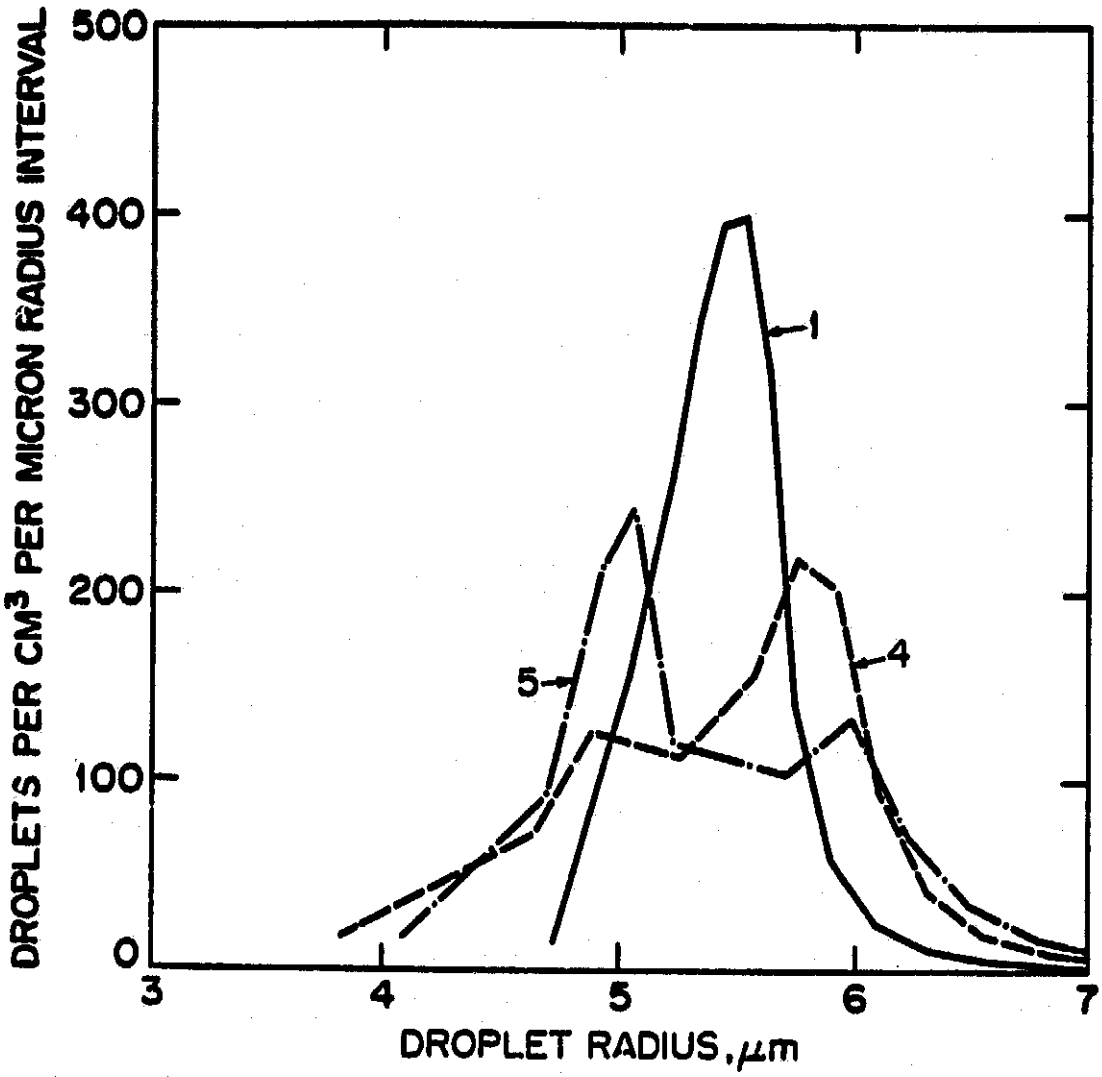

Figure 22. Droplet size distributions 100 meters above cloud base. Curve labels refer to case number.

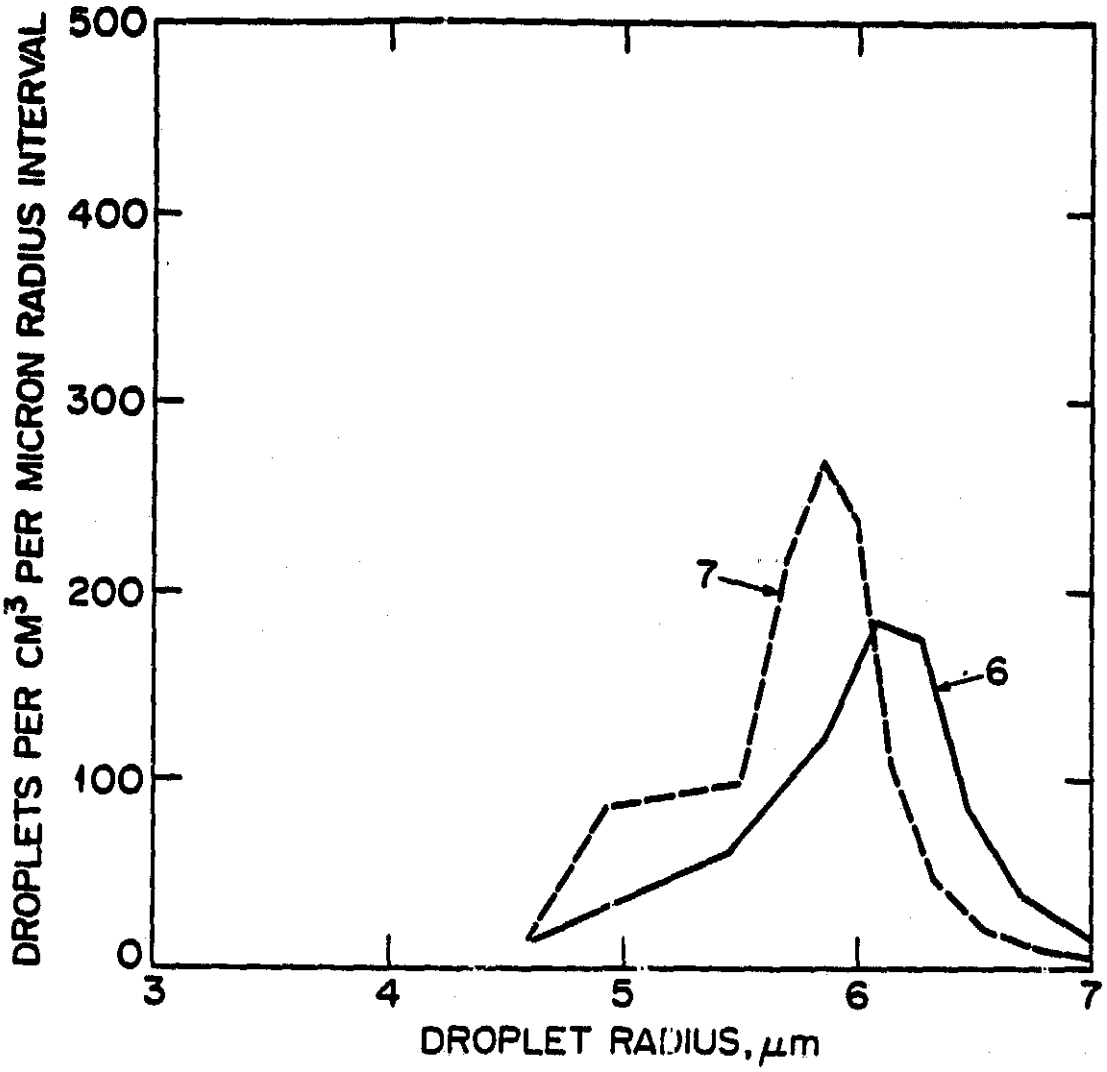

Figure 23. Droplet size distributions 100 meters above cloud base. Curve labels refer to case number.

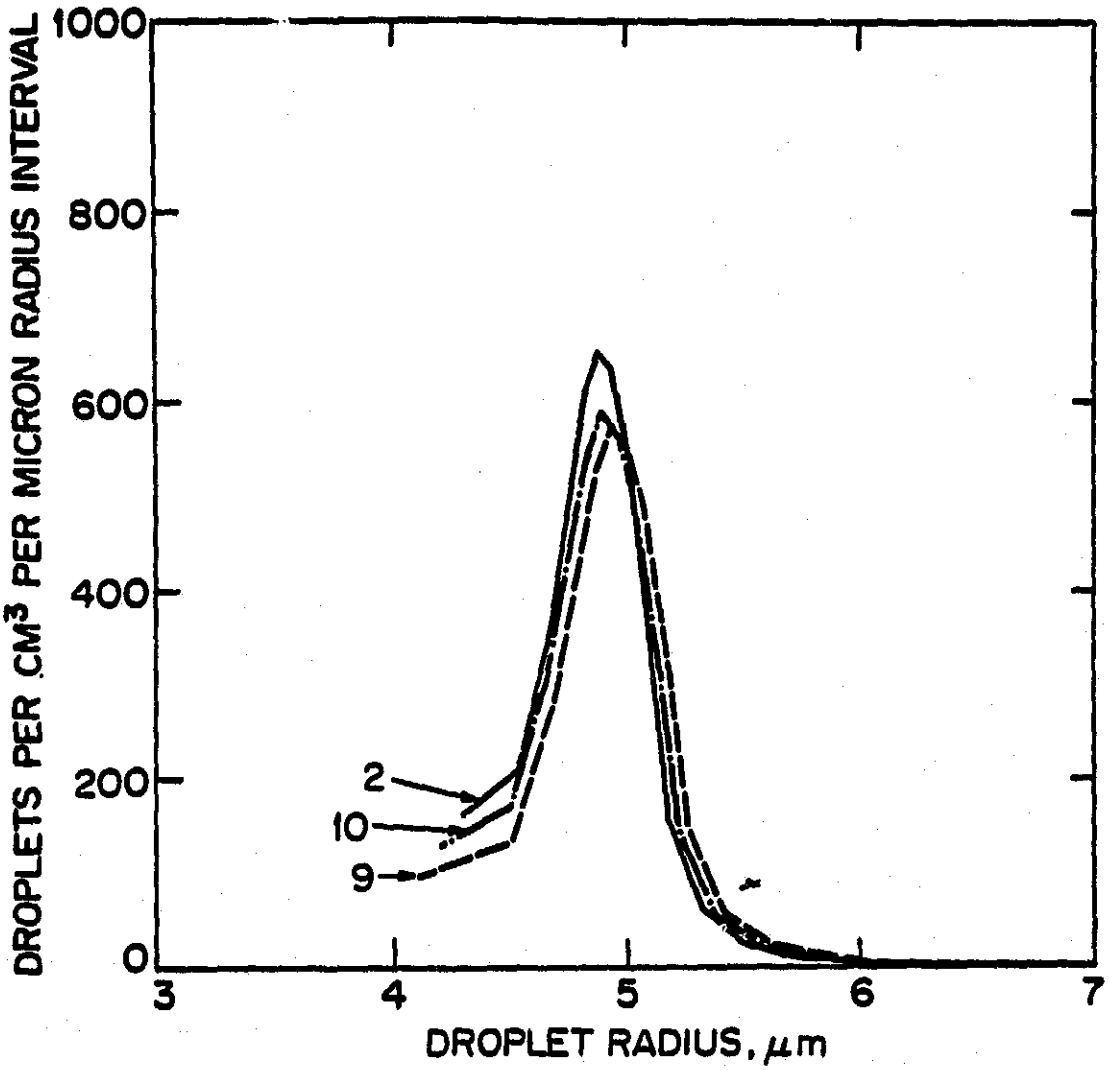

Figure 24. Droplet size distributions 100 meters above cloud base. Curve labels refer to case number.

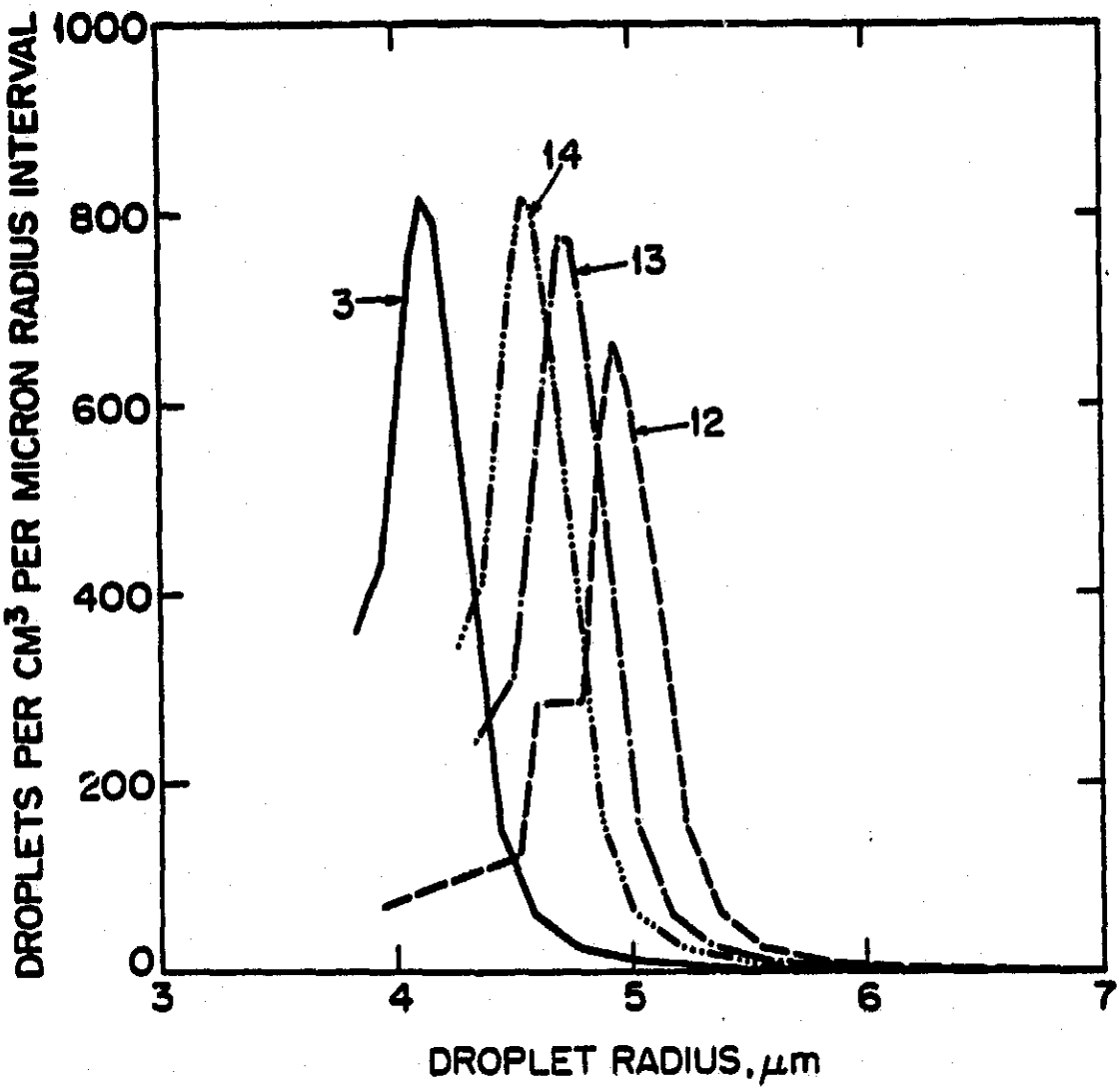

Figure 25. Droplet size distributions 100 meters above cloud base. Curve labels refer to case number.

distributions for a steady updraft of 1 m/s and for the cases (4-7) of alternating steady up and down motion. Figures 24 and 25 show droplet size distributions for steady updrafts of 4 and 10 m/s and corresponding sinusoidal velocity patterns. There are some striking differences between the droplet size distributions of the two vertical velocity groups. In the sinusoidal cases, the droplet size distributions have about the same shape as those produced by the steady updraft.

Turbulence simulated by alternate steady up and down motions changes the shape of the droplet size distribution dramatically. In each case, the maximum value is less than that obtained in the steady updraft. In addition, the distributions are broader, with some displaying a bimodal character.

The trend of the shape of the droplet size distribution is interesting. For Case 1, the mean droplet radius is 5.36 μm. For Case 4, which has a single loop, the mean radius is slightly less, 5.27 μm, despite the fact that it took 2.2 times as long to reach the 100-meter level. Also, the distribution is bimodal, with a major maximum near 5.8 μm-radius and a minor maximum near 4.9 μm-radius. When the droplets undergo a second loop (Case 5), the mean droplet radius remains the same, but the modes are reversed. The major maximum shifts to near 5.1 μm-radius and the minor maximum moves to near 6.0 μm-radius.

The velocity pattern for Case 6 differs from that of Case 5 only slightly; the second loop is centered 10 meters higher than the first. However, the resulting droplet size distribution is quite different. The mean droplet radius moves upward to 5.84 μm, and there is only one mode, near 6.1 μm-radius. The droplet size distribution for Case 7 does not resemble those of Cases 4 and 5 either, but that is not surprising since Case 7 involved small fast eddies.

The fact that alterations to the droplet size distribution occurred with the square wave velocity patterns and not with the sinusoidal velocity patterns is not considered to be attributable to the fact that the square wave patterns make no allowance for acceleration. Square wave velocity patterns are used because there is more control over the downdraft speed, the height where downward motion begins, etc. The next sections look at Cases 4, 5, and 6 in more detail to suggest why these cases increased the dispersion and others did not.

e. Single loop: Case 4

To review, the velocity pattern is this: the parcel is lifted from the cloud base at 1 m/s, lowered to the cloud base at -0.2 m/s, and raised again to the 100-meter level at 1 m/s.

Figure 26 shows the equilibrium supersatura-

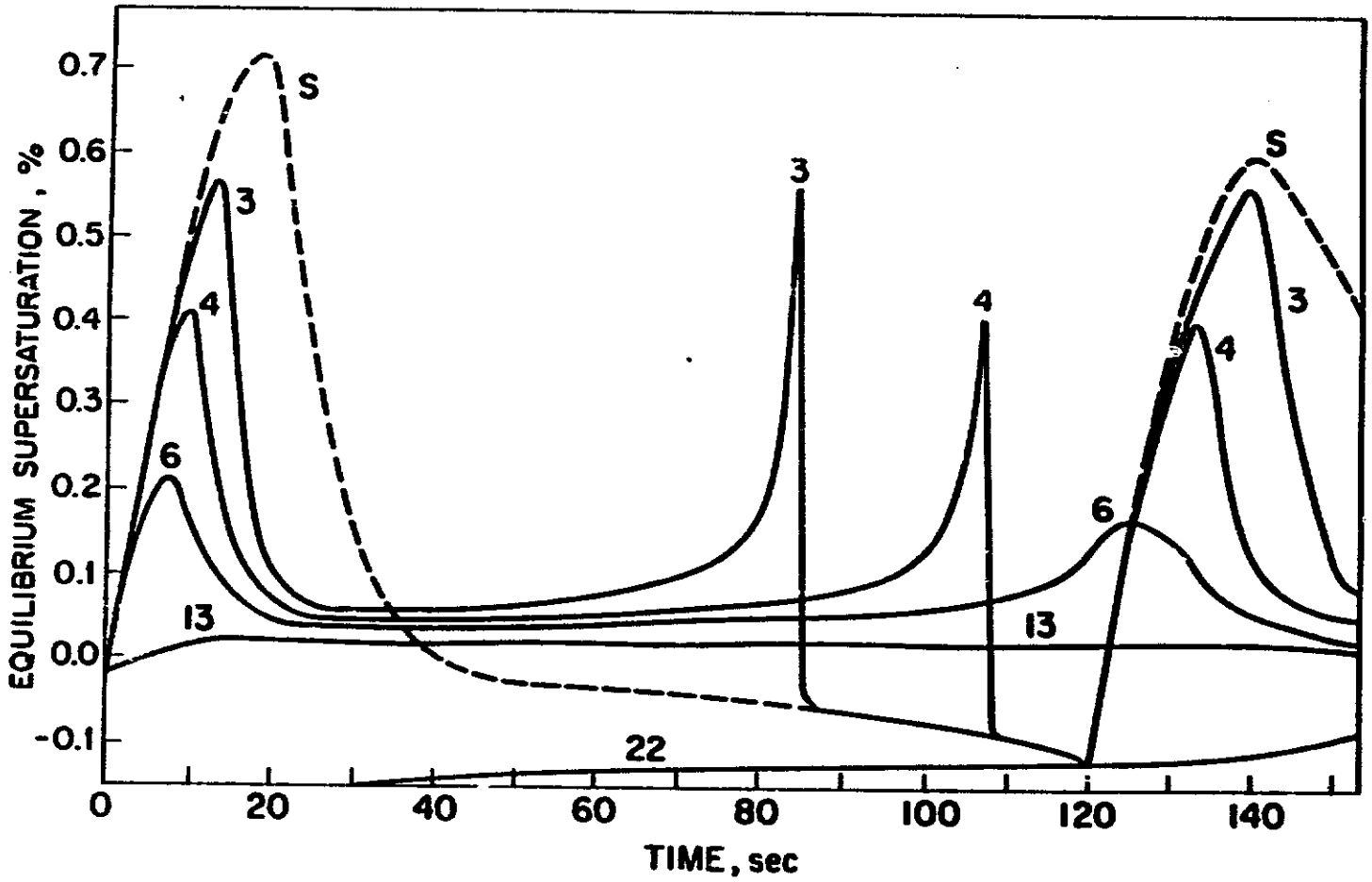

Figure 26. Equilibrium supersaturation for selected droplets: Case 4. Curve labels are the droplet size classes. Dashed line is the ambient supersaturation.

tion (e_r/e_s-1.0) for a few droplets for the first 150 seconds or so. The ambient supersaturation (e_a/e_s -1.0) is dashed in. A droplet grows whenever its equilibrium vapor pressure is less than the ambient value. A peak in a curve represents the critical supersaturation for droplets of the indicated size class.

The processes of selective activation and selective evaporation are seen here. Droplets of size class 6 (r_n = 0.04 μm) are among the first to activate and those of size class 13 (r_n = 0.20 μm) are the largest to activate. During downward motion (20-120 seconds), it is some 16 seconds before any droplets evaporate. The smallest droplets (size class 3) deactivate first. They evaporate for 48 seconds before they evaporate below critical radius, but once they do, they deactivate and reach equilibrium with the environment in less than a second. Before droplets of size class 6 can deactivate, the ambient supersaturation increases again due to renewed uplift, and the droplets resume growth. Since they did not deactivate, they did not pass through the critical point and the second maximum in the curve for size class 6 is not as high as the first.

The ambient supersaturation reached a low value of -0.117%. This was high enough that droplets of size class 22 (r_n = 1.31 μm) and larger did not evaporate during the cycle.

The radial growth rate of the droplets is

shown by Figure 27. Selective evaporation is quite evident.

The resulting size distribution 0, 20, and 100 m above cloud base are shown in Figure 28. At the bottom of the loop (t = 120 s, z = 0 m), most of the droplets are larger than they were originally (0 s, 0 m). The second time the parcel reaches the 20-meter level (140 s, 20 m) the mean size is slightly larger than it was just prior to downward motion (2.23 vs. 2.09 μm) and the dispersion is some 1.4 times as large (0.406 vs. 0.281). Further, a bimodal nature has developed. Subsequent lifting to the 100-meter level (220 s, 100 m) does not void the bimodal character. For comparison, the distribution at 100 meters for the steady updraft Case 1 (100 m, 100 s) is included.

f. Double loops: Cases 5 and 6

The effect of multiple loops is investigated with Cases 5 and 6. In Case 5, there is a second loop between the 20 and 0-meter levels. For Case 6, the second loop is between the 30 and 10-meter levels. In Case 5, the second loop initially increases the dispersion. At 20 meters, the dispersion for Case 5 (260 s, 20 m) is 0.48, and for Case 4 (140 s, 20 m) is 0.41. At the 100-meter level, the dispersion for Case 5 (0.76) is only slightly less than that for Case 4 (0.78). (See Table V for a summary of some statistics of Cases 1, 4, 5

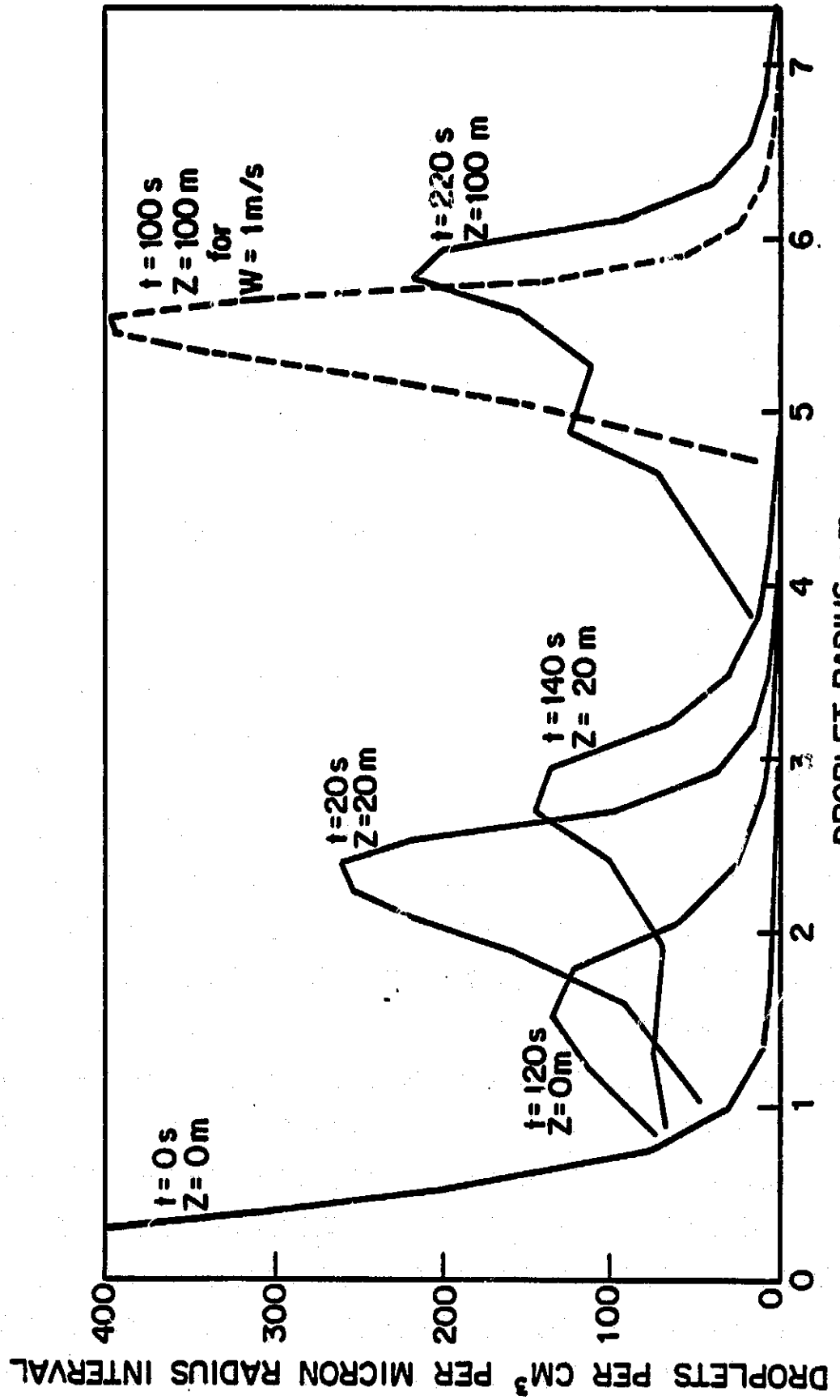

Figure 28. Droplet size distributions at several times and heights: Case 4.

TABLE V

Selected statistics for Cases 1,4,5 and 6.

	Case	1	4	5	6
first loop	height at top of loop, z_1	-	20	20	20
	$\bar{r}(z_1)$, μm	-	2.09	2.09	2.09
	$\sigma(z_1)$	-	.28	.28	.28
	time spent in downdraft, sec	-	100	100	100
	minimum S, %	-	-.117	-.117	-.117
	height at bottom of loop, z_2	-	0	0	0
	$\bar{r}(z_2)$, μm	-	1.55	1.55	1.55
	$\sigma(z_2)$		.647	.647	.647
	time spent in updraft, sec	-	100	20	30
	maximum S, %	-	.591	.591	.591
second loop	height at top of loop, z_3	-	-	20	30
	$\bar{r}(z_3)$, μm	-	-	2.23	2.92
	$\sigma(z_3)$	-	-	.41	.36
	time spent in downdraft, sec	-	-	100	100
	minimum S, %	-	-	-.144	-.059
	height at bottom of loop, z_4	-	-	0	10
	$\bar{r}(z_4)$	-	-	1.68	2.54
	$\sigma(z_4)$	-	-	.85	1.02
rise to 100 meter level	time spent in updraft	100	100	100	90
	maximum S, %	.713	.591	.611	.411
	$\bar{r}$(100 m), μm	5.36	5.27	5.26	5.84*
	σ(100 m)	.38	.78	.76	.72

*droplets in size classes 3 and 4 did not reactivate in Case 6.

and 6). However, the shapes of the size distribution curves are different (Figure 22). The effect of the second loop is best shown by Figure 29. Here, the mass of water on each size class is shown relative to that for Case 1. It can be seen that the effect of one loop, Case 4, is to remove some of the water from the small droplets (size class <7), without eliminating the smallest droplets, and move it to the higher size classes. In Case 5, even more water has been removed between size classes 5 to 8 and moved upscale.

In Case 6, the droplets had more time to recover before descending for the second time. As a result, the mean droplet radius before the second descent was larger (2.9 μm) than for Case 5 (2.2 μm). After the second loop, the maximum supersaturation attained in the final updraft (0.41%) was not high enough to reactivate size classes 3 and 4.

g. Effect of mixing parcels of cloud air

For a final experiment, parcels of air at the 100-meter level from several cases are mixed to see the effect on the dispersion. The results are in Table VI. When a parcel from Case 4 (square wave velocity pattern) is mixed with one or more parcels from sinusoidal cases the dispersion decreases. The dispersion increases when two sinusoidal cases are mixed together, and decreases slightly from the most disperse case when three are

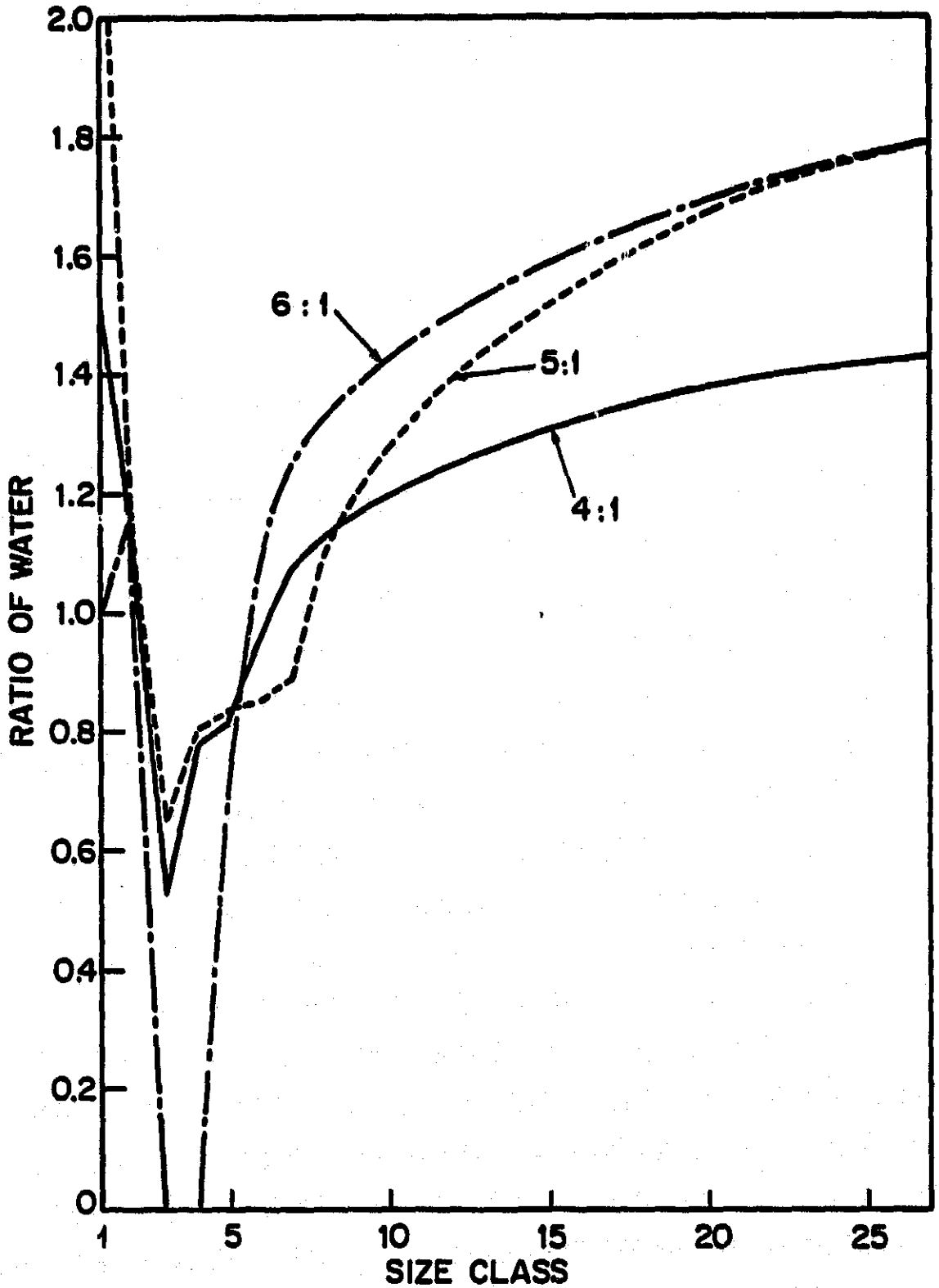

Figure 29. Mass of water associated with each size class for Cases 4, 5, and 6 relative to that of Case 1. Height is 100 meters above cloud base.

Table VI

Coefficient of Dispersion
for Mixed Parcels of Cloud Air

Case Numbers of Parcels Mixed	Individual Dispersions	Mixed Dispersion
1,4	.0716, .1486	.1163
4,14	.1486, .0549	.1328
8,12	.0815, .0832	.1105
8,14	.0815, .0549	.1209
4,8,14	.1486, .0815, .0549	.1334
12,13,14	.0832, .0561, .0549	.0696

mixed. Apparently, mixing of cloud air is not an effective means to broaden the droplet size distribution.

3.4 Conclusion

The effect of a fluctuating updraft on a distribution of droplets is complicated and not obvious. Some explanation of the behavior of a droplet size distribution can be made on the basis of this study. Ostensibly, there are at least three aspects which influence the droplet size distribution: the maximum and minimum values of the supersaturation, the height (or time) at which the parcel first undergoes downward motion, and the time spent in downward motion.

Figure 30 illustrates an important point. It shows the total mass of water associated with each droplet size class at several times for Case 4. Roughly 60% of the total liquid water is condensed on droplets of size classes 7(r_n =0.05 μm) through 11(r_n = 0.12 μm). Droplets in those size classes are activated in all 14 cases of this study. They are fairly slow to react to change in the environment; it takes 99 seconds of downward motion to deactivate the smaller droplets of size class 5(r_n = 0.035 μm) in Case 4.

Small droplets near equilibrium react quickly to environmental changes. A trajectory which affects only those droplets has only a small effect on the distribution

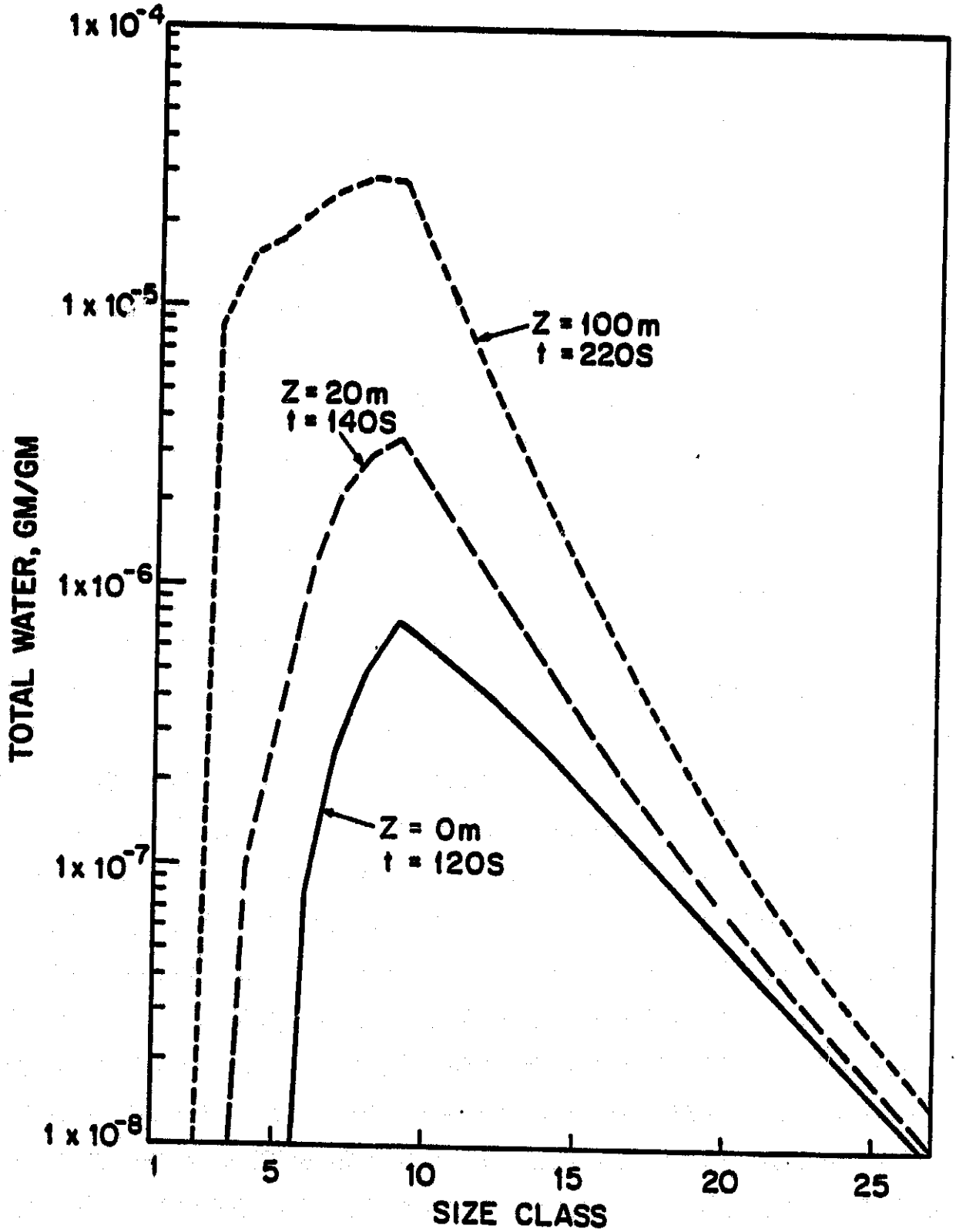

Figure 30. Total mass of water/(gm air) on each size class at indicated height and time: Case 4.

as a whole. An example of this situation is Case 12, with 5-meter diameter eddies and a maximum updraft velocity of 10 m/s. At first, small droplets oscillate in size in response to the changing supersaturation. Once they are activated, however, none of the droplets undergoes evaporation. Conversely, Case 14 with a 50-meter diameter eddy has a very low minimum supersaturation (-.717%) so that even the largest droplets begin to evaporate although the time spent in the downward motion field is only about 15 seconds.

The optimum situation for broadening the droplet size spectrum seems to occur when a long time is spent in an environment of a small undersaturation, as in Cases 4-6. In each, the parcel first undergoes downward motion after 20 seconds and continues on a downward path for 100 seconds with a minimum supersaturation of -0.12%. Under these conditions large droplets continue to grow and small ones grow toward equilibrium. The main difference is that the droplets of intermediate size, which are sluggish in their response to the environment but at the same time account for most of the liquid water, have sufficient time to evaporate significantly. It is apparently these droplets that are important in directing the flux of liquid water within the droplet spectrum and are responsible for the broadening of the droplet size distribution.

If droplets penetrate farther into the cloud before reversing direction, the mean radius increases and the parcel must spend a longer time in downward motion in order to significantly evaporate droplets with large amounts of water on them and therefore have a meaningful effect on the size distribution.

The pattern of growth of the cloud droplet population appears to be influenced by three fairly distinct groups of droplets within the population: small droplets near equilibrium which react quickly with changes of the environment but have a small effect on the final droplet distribution; large droplets which continue to grow throughout the downward motion; and intermediate sizes which account for a large fraction of the cloud liquid water.

The characteristic time for a growing or evaporating droplet is a complicated function of its physical and chemical nature and the environmental conditions. For this reason it is difficult to predict accurately what a given distribution of droplets will do under particular circumstances.

It has been demonstrated, however, that turbulence does indeed have a direct influence on a distribution of droplets. It can be expected that the degree of the modification of a droplet population differs throughout the various regions of a cloud.

CHAPTER IV

EXPLICIT MODEL

4.1 Introduction

Comprehensive modelling of air pollution scavenging requires a model capable of representing co-condensation of multiple vapors and energies of chemical reactions. One example is the transformation of gaseous sulfur dioxide to sulfate particles in the presence of water droplets and natural ammonia.

The classical, or implicit, model represents cloud droplet activation and growth upon condensation nuclei. It ignores any chemical reactions and vapors other than H_2O and depends upon simplifying assumptions to arrive at a single expression for droplet growth (Mason, 1957).

When two or more vapors whose condensates may form a solution are present, however, they jointly determine the equilibrium pressure of each component over the solution, and the simplifications of the implicit model are not applicable. The explicit model is designed to meet these problems.

Several authors have considered the heteromolecular nucleation (multimolecular formation) of droplet embryos, for example NH_3-H_2O (Lewis, 1969), H_2SO_4-H_2O (Doyle, 1961; Nair and Vohra, 1975; Hamill, 1975;

Hamill et al., 1977), and HCl-H_2O (Lewis 1968; Stauffer and Kiang 1974). In addition, Kiang et al., (1975) have investigated the H_2SO_4-HNO_3-H_2O ternary system. These papers deal specifically with the formation of embryos, say $r < 0.1$ μm. The focus in most of these references is on, though not limited to, the stratosphere and extra-terrestrial atmospheres. There are two approaches: analysis of equilibrium phase diagrams, and heteromolecular nucleation theory (Byers, 1965) extended to multicomponent systems.

The nucleation theory applies to the initial formation of small droplets in equilibrium with the environment. In contrast, the explicit model developed here extends the theory to the further growth of the droplets by co-condensation of the vapors without presupposing the condition of equilibrium.

The explicit model is applied here for the condensation of water only so that the results may be compared directly to those of the implicit model as an initial test. Considerations for the expansion of the model for more complicated systems follows.

4.2 Energy Budget of a Droplet

Considering all the known energy sources and sinks for a droplet, the energy balance is

$$Q_T = Q_L + Q_K + Q_M + Q_R + Q_\sigma + Q_F + Q_D + Q_\zeta \qquad (4.1)$$

where

$$Q_T = mc_r \frac{dT_r}{dt} \qquad \text{internal energy} \qquad (4.1a)$$

$$Q_L = L \frac{dm}{dt} \qquad \text{latent heat} \qquad (4.1b)$$

$$Q_K = -4\pi r K F_k V (T_r - T_a) \qquad \text{conductive transfer} \qquad (4.1c)$$

$$Q_M = -c_w (T_r - T_a) \frac{dm}{dt} \qquad \text{mixing} \qquad (4.1d)$$

$$Q_R = -16\pi r^2 \sigma_R T_a^3 (T_r - T_a) E \qquad \text{radiative transfer} \qquad (4.1e)$$

$$Q_\sigma = -\frac{d}{dt}(4\pi r^2 \sigma) \qquad \text{surface energy} \qquad (4.1f)$$

$$= -4\pi r^2 \left[\frac{1}{m}\left(\frac{2\sigma}{3}\left(1 + \frac{\mu}{\rho_r}\frac{\partial \rho}{\partial \mu}\right) - \mu \frac{\partial \sigma}{\partial \mu}\right)\frac{dm}{dt}\right.$$

$$\left. + \left(\frac{\partial \sigma}{\partial T} - \frac{2\sigma}{3\rho_r}\frac{\partial \rho}{\partial T}\right)\frac{dT_r}{dt}\right]$$

$$Q_F = \frac{2/9\ r^2 m g^2 (\rho_r - \rho_d)}{\mu_f} \qquad \text{friction} \qquad (4.1g)$$

$$Q_D = \frac{\mu}{m}\frac{dh}{d\mu}\frac{dm}{dt} \qquad \text{dilutior} \qquad (4.1h)$$

and

Q_ζ represents any other energy terms which might pertain to a particular system.

In the above expressions,

ρ_d is the air density

ρ_r is the density of the droplet

μ_f is the molecular viscosity of air

σ_r is the Stefan-Boltzmann constant

E is effective emissivity of the droplet

h is the enthalpy of dilution

and all other symbols are defined as before.

The mixing term arises from the assumption that the vapor condenses at the air temperature and then mixes completely with the droplet. The radiation term is an approximate formulation based upon the Stefan-Boltzmann law (Sedunov, 1974). The exact nature of the radiation exchange of a droplet is unknown, hence the inclusion of the factor E. The surface energy term includes the relationships of temperature and molality to the density and surface free energy. The friction term is related to the change of potential energy. It is strictly valid only when droplet settling is considered, but it is included here for completeness. The dilution term is the change of energy as a result of dilution by the condensing vapor. It is small for most salt solutions but can be important for acids.

A study of the magnitudes of each of these terms indicates that Q_K and Q_L are three to five orders of magnitude larger than the others. However, these two terms are of opposite sign and their residual determines the order of magnitude of terms that should be retained. This is comparable to Q_T. The calculations show that

of the energy terms only the frictional term, Q_F, can safely be dropped from further consideration in the early stages of cloud formation. Q_F is of the order of 10^{-10} Q_T or less for droplets smaller than 30 μm-radius.

4.3 Droplet Growth Equation

The droplet growth equation is

$$\frac{dm}{dt} = \frac{4\pi r D F_v V}{R_v} \left(\frac{e_a}{T_a} - \frac{e_r}{T_r}\right) \tag{4.2}$$

Because the droplet temperature is explicitly determined in the explicit model, (4.2) is used directly.

4.4 Integration Technique

Various attempts were made to determine the best method for solving the system (4.1), (4.2). The first method was to integrate (4.1) and (4.2) simultaneously by a Runge-Kutta technique. It was found to be highly unstable for time steps larger than 10^{-6} seconds because in the energy balance, an error in Q_K or Q_L of 1% leads to an error of about 10,000% in Q_T. Clearly, direct differencing of Q_K and Q_L should be avoided.

A second approach was an expansion of the method of Storebø and Dingle (1972). It was assumed (see Dingle, 1976) that a two-step process would adequately represent the microphysics. First, all the vapor which would

condense during a time step was allowed to condense at the beginning of the time step. Secondly, the heat gained as a result of condensation of the vapor was transferred to the environment by conduction and radiation, so that a mean temperature over the time step could be found. Since the mass increase of the droplet depended on this average temperature, the two steps were iterated to find the solution. This method was quite complicated, and since it was not clear that a second volatile component could be added to the system, it was abandoned.

The integration technique decided upon is simple, relatively stable, and can include any number of reacting gases and heat sinks. To begin, the energy balance (4.1) is rewritten as

$$T_r - T_a = [-Q_T + Q_L + Q_\sigma + Q_D + Q_\zeta] / (4\pi r K F_k V + c_w \frac{dm}{dt} + 16\pi r^2 \sigma_R E T_a^3) \qquad (4.3)$$

By this device, the large terms Q_K and Q_L are divided rather than subtracted. This properly emphasizes the minor contributions of the other terms and more easily maintains computational stability.

After the first time step, the rate of change of droplet temperature in Q_T and Q_σ is estimated from the previous time step, leaving only one differential equation (4.2) to be stepped forward for each droplet.

At time $t^{(0)}$, $dT_a^{(0)}/dt$ is calculated by setting the time rate of change of the vapor during the previous step, $dx^{(-1)}/dt$, equal to zero. For each size category, the initial droplet temperatures are found by the following process:

i. set $\{T_{r_i}\}^{(0)} = T_a^{(0)}$, where the curved brackets indicate an estimated value;

ii. using the estimated droplet temperatures, estimate from (4.2) the growth rate of each droplet, $\{dm_i/dt\}^{(0)}$;

iii. with these, calculate the droplet temperatures by (4.3) to get $[T_{r_i}]^{(0)}$, where the square brackets indicate a calculated value;

iv. compare the estimated and calculated droplet temperatures; if the absolute value of $\{T_{r_i}\}^{(0)} - [T_{r_i}] \geq 10^{-10}$, then $\{T_{r_i}\}^{(0)}$ is re-adjusted by a relaxation technique and steps ii, iii and iv are repeated.

At a subsequent time $t^{(k)} = t^{(0)} + \Delta t^{(0)} + \Delta t^{(1)} + \ldots \Delta t^{(k-1)}$, the known variables are $T_a^{(k)}$, $p_a^{(k)}$, and all $m_i^{(k)}$. The vapor mixing ratio $x^{(k)}$ is calculated from the water conservation equation (2.3). The rate of consumption of vapor during the previous time step is approximated by

$$\frac{dx^{(k-1)}}{dt} = \frac{x^{(k)} - x^{(k-1)}}{\Delta t^{(k-1)}} .$$

The derivatives of pressure (2.1) and air temperature (2.2) can then be readily calculated.

To compute the growth rate, it is necessary to find the temperature of each droplet. This is done by estimating the droplet temperature by extrapolation from the previous time step with a function ψ such that

$$T_{r_i}^{(k)} = T_a^{(k)} + (T_{r_i}-T_a)^{(k-1)} + \psi_i^{(k-2)} \Delta t^{(k-1)}$$

where the definition of ψ_i is presented below. A procedure similar to that used at time $t^{(0)}$ is used to iterate (4.2) and (4.3) to find the droplet temperatures and dm_i/dt. Under normal conditions, steps ii, iii, and iv, above, need to be repeated only once or twice.

The function ψ_i is then recalculated for use during the next time step as

$$\psi_i^{(k-1)} = [(T_{r_i}-T_a)^{(k)} - (T_{r_i}-T_a)^{(k-1)}]/\Delta t^{(k-1)}.$$

The rate of change of droplet temperature is estimated with

$$\frac{dT_{r_i}^{(k-1)}}{dt} = (T_{r_i}^{(k)} - T_{r_i}^{(k-1)})/\Delta t^{(k-1)}.$$

Since ψ, dT_r/dt, and dx/dt are averaged slopes over the previous time step $\Delta t^{(k-1)} = t^{(k)}-t^{(k-1)}$, rather than actual derivatives calculated at $t^{(k)}$, the superscript

must be in keeping with the convention adopted here.

For the zeroth time step (k=1), $\psi_i^{(-1)}$ is defined to be equal to zero. That is to say, that $dT_r^{(0)}/dt = dT_a^{(0)}/dt$.

Finally, the pressure, air temperature, and droplet masses are stepped forward using a Hamming modified predictor-corrector subroutine. This is a fourth-order technique which does not require computation of derivatives within the time step as does the Kutta-Simpson method. On the other hand, it is not self starting, and a modified Runge-Kutta method suggested by Ralston (1962) is used to integrate from $t^{(0)}$ to $t^{(2)}$.

The method outlined above allows for variable time steps and can readily include another volatile component.

4.5 Review of Implicit and Explicit Equations

There are three major differences between the equations of the implicit and explicit models. They are summarized below.

i. The implicit model depends on the assumption that the energy arising from the condensation of the vapor onto the droplet surface is conducted away to the environment. All other energy sources and sinks are assumed negligible. On the other hand, all energy sources and sinks comparable in magnitude to the heat storage term or larger may be included in the explicit model. The growth rate of a droplet depends on the droplet

temperature by means of the droplet equilibrium vapor pressure, e_r. An error in the droplet temperature results directly in an error in the droplet growth rate.

In the case of ammonium sulfate particles, the difference between the implicit and explicit computations is not significant. Situations do exist, however, in which the "minor" energy terms can be of importance, particularly if chemical reactions are taking place. Also, if there is a second condensing vapor, the latent energy of condensation of that vapor must enter the calculations.

ii. The second assumption of the implicit model is somewhat less obvious. The correct expression for the droplet growth rate is given by (4.2), rewritten as

$$\frac{dm}{dt} = \frac{4\pi r D F_v V}{T_a} (e_a - e_r \frac{T_a}{T_r}). \qquad (4.4)$$

In the implicit model, it is assumed that the droplet temperature is nearly equal to the air temperature so that (4.4) can be adequately approximated by

$$\frac{dm}{dt} = \frac{4\pi r D F_v V}{T_a} (e_a - e_r). \qquad (4.5)$$

Inasmuch as the approximation is made within a difference term, the error introduced should not be assumed negligible. When vapor condenses onto a droplet, then $T_r > T_a$, and (4.5) underestimates the true growth rate. Similarly,

when a droplet is evaporating, $T_r < T_a$ and $e_a < e_r$, so that the rate of evaporation is underestimated by the implicit model.

It is of interest to estimate the magnitude of the error. If (4.4) is taken to be the correct growth rate, then the error introduced in the implicit model is

$$\varepsilon = \frac{e_r \frac{T_a}{T_r} - e_r}{e_a - e_r \frac{T_a}{T_r}} .$$

Ignoring droplet curvature and solute effects, the droplet equilibrium vapor pressure is, from (2.8),

$$e_r = e_s(T_a)\left[1 + \frac{T^*(T_r - T_a)}{(T_a - 35.86)^2}\right].$$

Since the supersaturation is $S = e_a/e_s - 1$, the error is approximately

$$\varepsilon = \frac{1 + \left[\frac{T^*(T_r - T_a)}{(T_a - 35.86)^2}\right] (T_a - T_r)}{(S+1)T_r - \left[1 + \frac{T^*(T_r - T_a)}{(T_a - 35.86)^2}\right]T_a} .$$

The error therefore depends upon the supersaturation and the droplet temperature elevation, $T_r - T_a$. For a solution droplet, the error also depends on the droplet size and molality. Estimates show that for average cloud conditions the error ranges from zero to a few percent.

iii. The third difference between the two models is the most important. In the implicit model, the approximate energy balance equation is substituted into the droplet growth rate equation to arrive at a single differential equation. If there are important energy terms other than those for water vapor condensation and thermal conduction, or if there is another vapor present, the substitution of the energy balance equation into the growth rate equation is not practical.

The explicit model is the only approach which allows chemical reactions within the droplet and the simultaneous condensation of multiple vapors.

4.6 Results with Explicit Model

a. Droplet size distribution

The explicit model is used under the same conditions as Cases 1 and 4 of the implicit model. The droplet size distribution 100 meters above cloud base after a steady uplift of 1 m/s (Case 1) is shown in Figure 31. It is clear that both models, though they differ in detail, give nearly identical results for this case.

It has been shown that the implicit growth rate equation underestimates the true droplet growth rate. Spot checks of the output of the explicit model show that if assumption ii above were made, the growth rate at the 20-meter level would be 1.7% slower for droplets

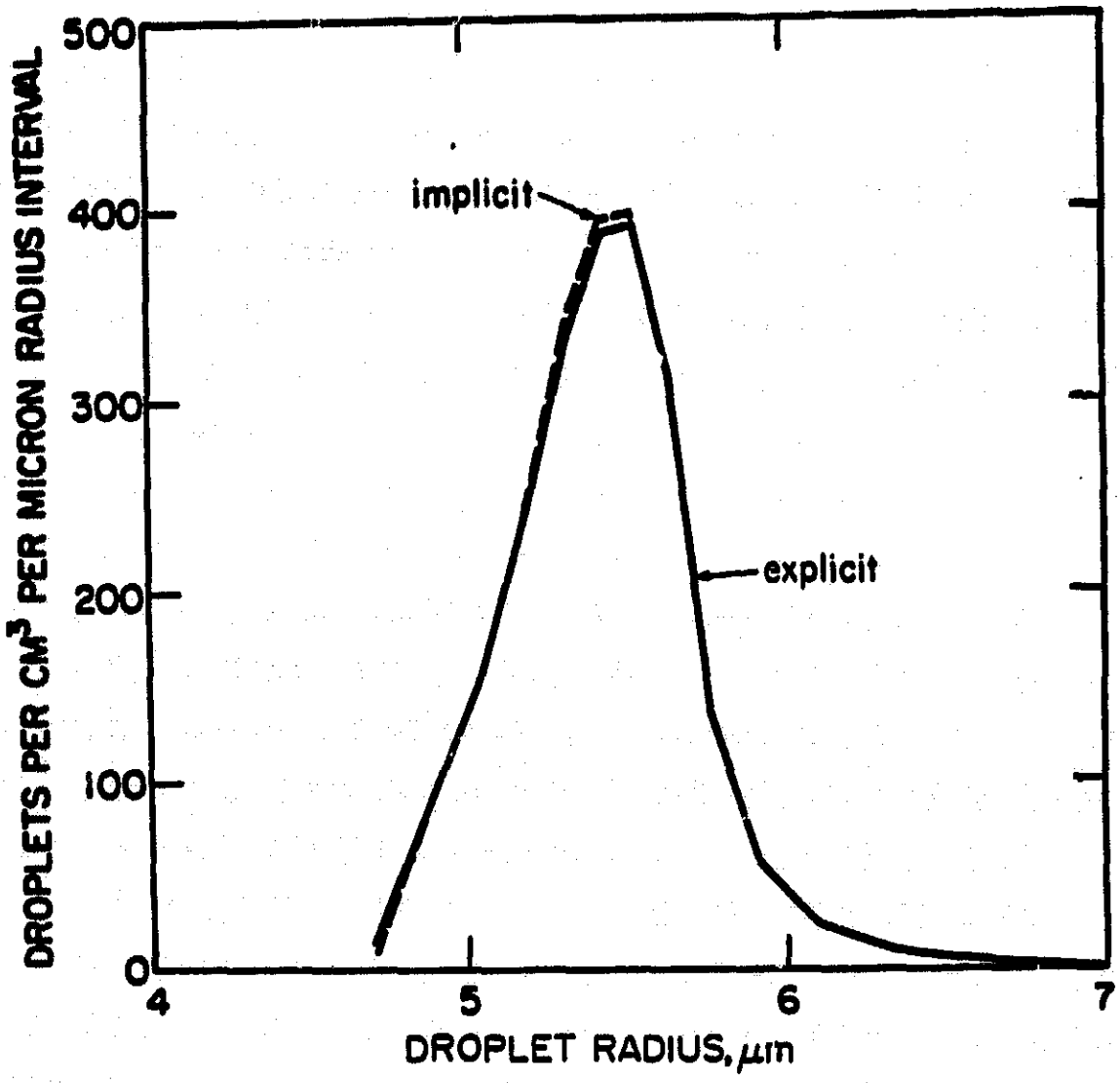

Figure 31. Droplet size distributions computed by implicit and explicit models for Case 1. Height is 100 meters above cloud base.

of size class 3 and 6.7% slower for droplets of size class 27. At the 100-meter level the growth rates would be slower by 4.3% and 5.6%, respectively. Because the explicit model predicts a faster droplet growth rate, the rate of consumption of vapor is enhanced, and the supersaturation is slightly lower. The maximum supersaturation reached by the explicit model is 0.708%, just barely less than the 0.713% obtained by the implicit model, but enough to compensate. Apparently, the errors introduced by the implicit model are not important in this case.

Only the very early period of cloud droplet growth is represented. As anticipated, the explicit model results in slightly more water in the larger droplet sizes. The small increase noted is in the direction required to produce a broader droplet spectrum and to promote rain generation. The effect is likely magnified at greater heights.

For the oscillating updraft, Case 4, the droplet size distributions predicted by the two models are slightly different (Figure 32). The reason for the difference is that droplets of size class 3 are not reactivated during the final ascent so that more water is available and is taken up by the larger droplets. This illustrates one of the difficulties that arises from the necessity of using a discrete, rather than a continuous, droplet size distribution. Cloud models must have a sufficient

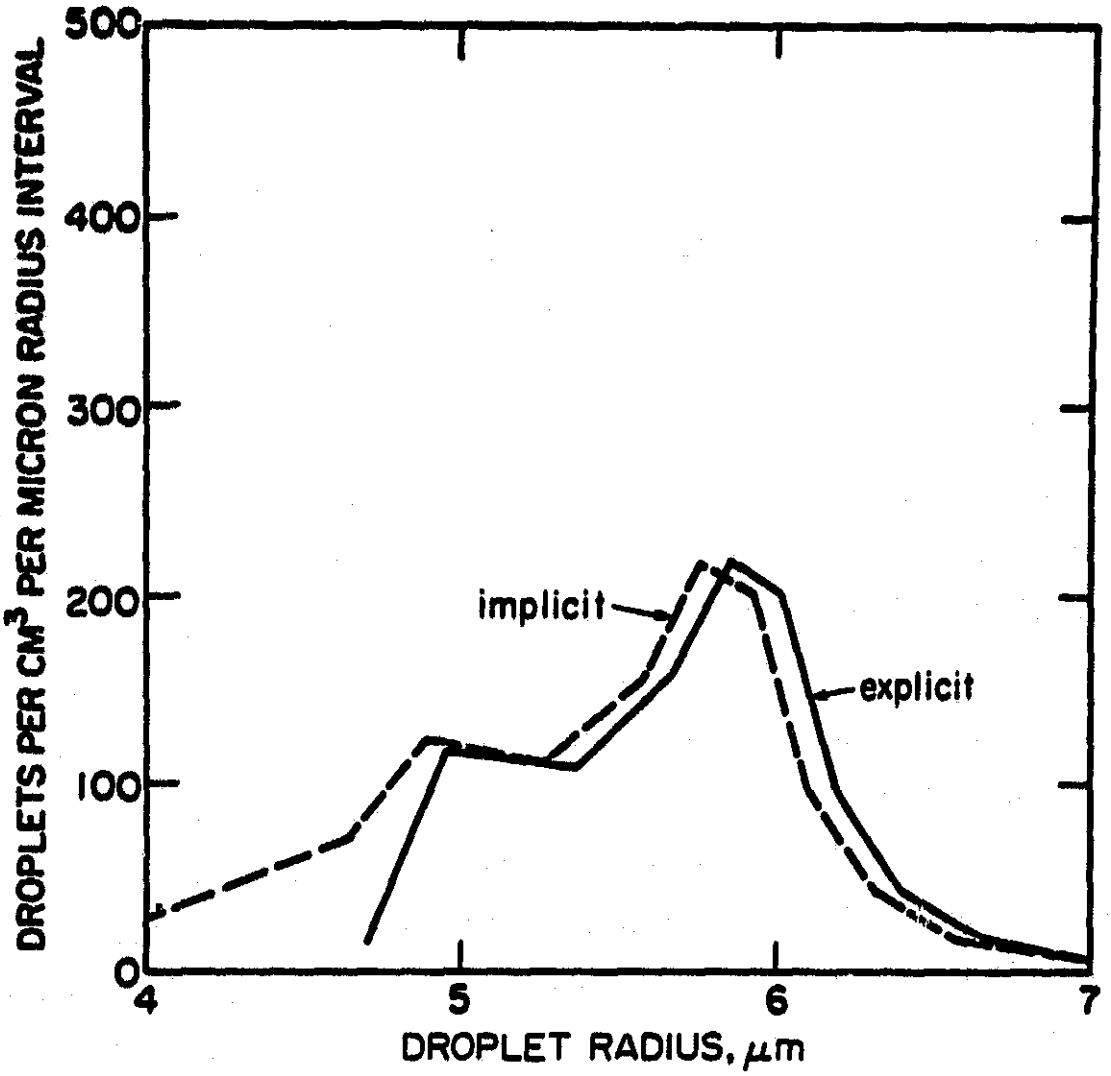

Figure 32. Droplet size distributions computed by implicit and explicit models for Case 4. Height is 100 meters above cloud base.

number of droplet size categories to assure that the results are not greatly distorted because of the finite increments used in specifying the nucleus size distribution. The difference between the curves of Figure 32 may have been reduced by choosing more size categories in the region of the smallest activated category. The distributions at 20 meters for Case 4 (not shown) are nearly identical.

b. Droplet temperature elevation

The temperature elevation, $(T_r - T_a)$, is shown in Figures 33 (Case 1) and 34 (Case 4). The droplet temperatures of the implicit model which may be calculated from (2.9) are not discernible from these. Throughout the modelling time, the largest droplets are the warmest and the smallest, the coolest. The greatest temperature elevations occur near the height of maximum supersaturation (∿18 meters).

c. Droplet equilibrium supersaturation

The droplet equilibrium supersaturation is defined at zero growth rate. From (2.10) the droplet equilibrium supersaturation for the implicit model is

$$S_{eq}^{i} = 1 - a \exp\left(\frac{2\sigma_r}{r\rho_r R_v T_a}\right) .$$

According to the explicit model, the droplet equilibrium

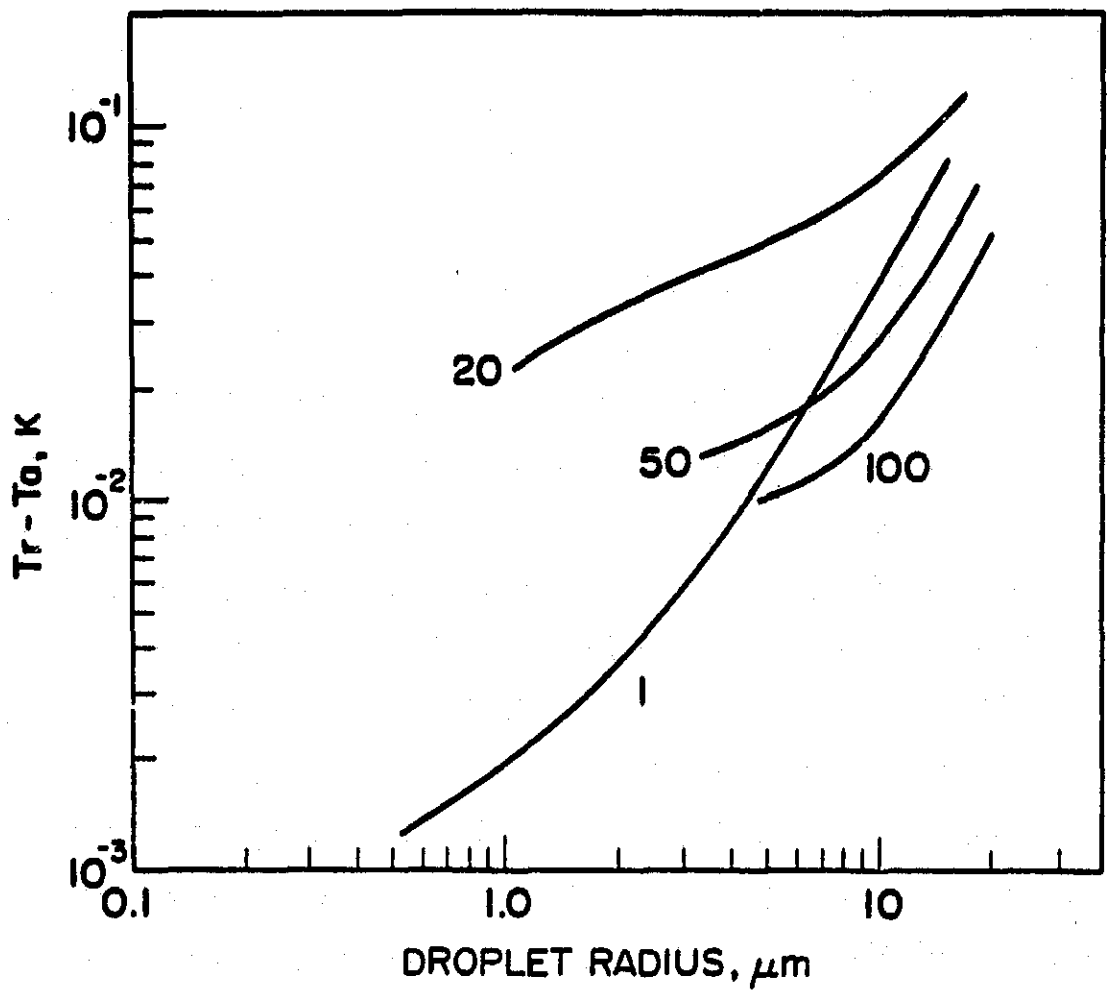

Figure 33. Droplet temperature elevation with respect to the ambient air: Case 1. Curve labels are time in seconds from cloud base.

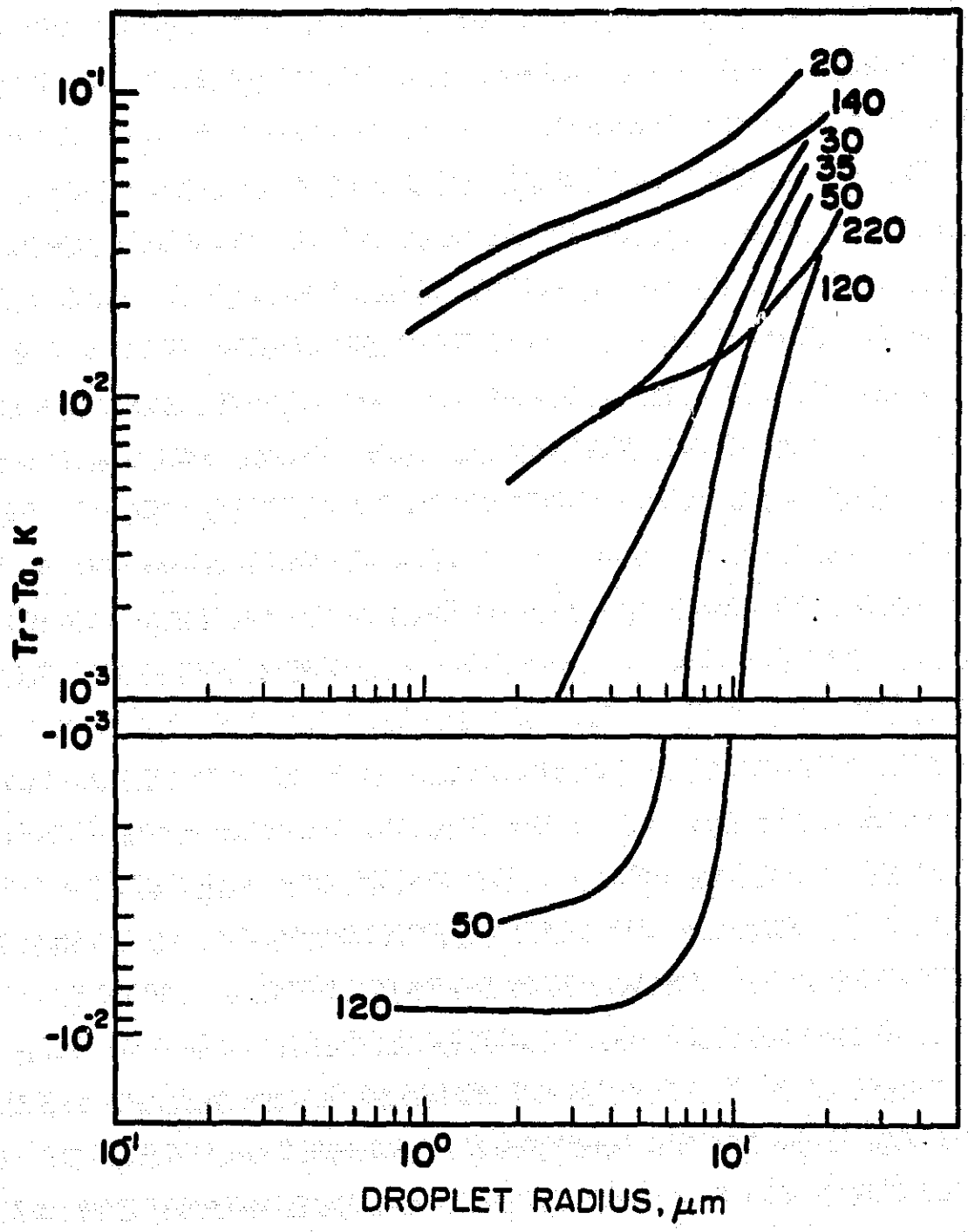

Figure 34. Droplet temperature elevation with respect to the ambient air: Case 4. Curve labels are time in seconds from cloud base.

supersaturation is, from (4.2),

$$S_{eq}^{x} = 1 - a \exp\left(\frac{2\sigma_r}{r\rho_r R_v T_r}\right) \frac{e_s(T_r)}{e_s(T_a)} \quad .$$

The difference is that in the implicit model, the air temperature is used to compute the droplet equilibrium vapor pressure. The explicit model requires the actual droplet temperature. Since the droplet equilibrium vapor pressure is exponentially dependent on the droplet temperature, the droplet equilibrium supersaturation is different for the two models (Figure 35). The values at the 20-meter level are between those of the 0- and 100-meter levels for the implicit model; for the explicit model, the values at the 20-meter level are the highest. This is a direct consequence of the fact that the droplet temperature elevations are the greatest near the 20-meter level, where the maximum supersaturation and growth rates occur.

The shapes of the curves are themselves interesting. At 20 meters with the implicit model, the smallest droplets, of size class 3, have the greatest value of equilibrium supersaturation. At this point, these droplets have just surpassed their critical supersaturation. With the explicit model at 20 meters, the maximum equilibrium supersaturation is associated with somewhat larger droplets. It increases because of increasing droplet temperature and finally decreases because of increasing droplet radius and increasing molality.

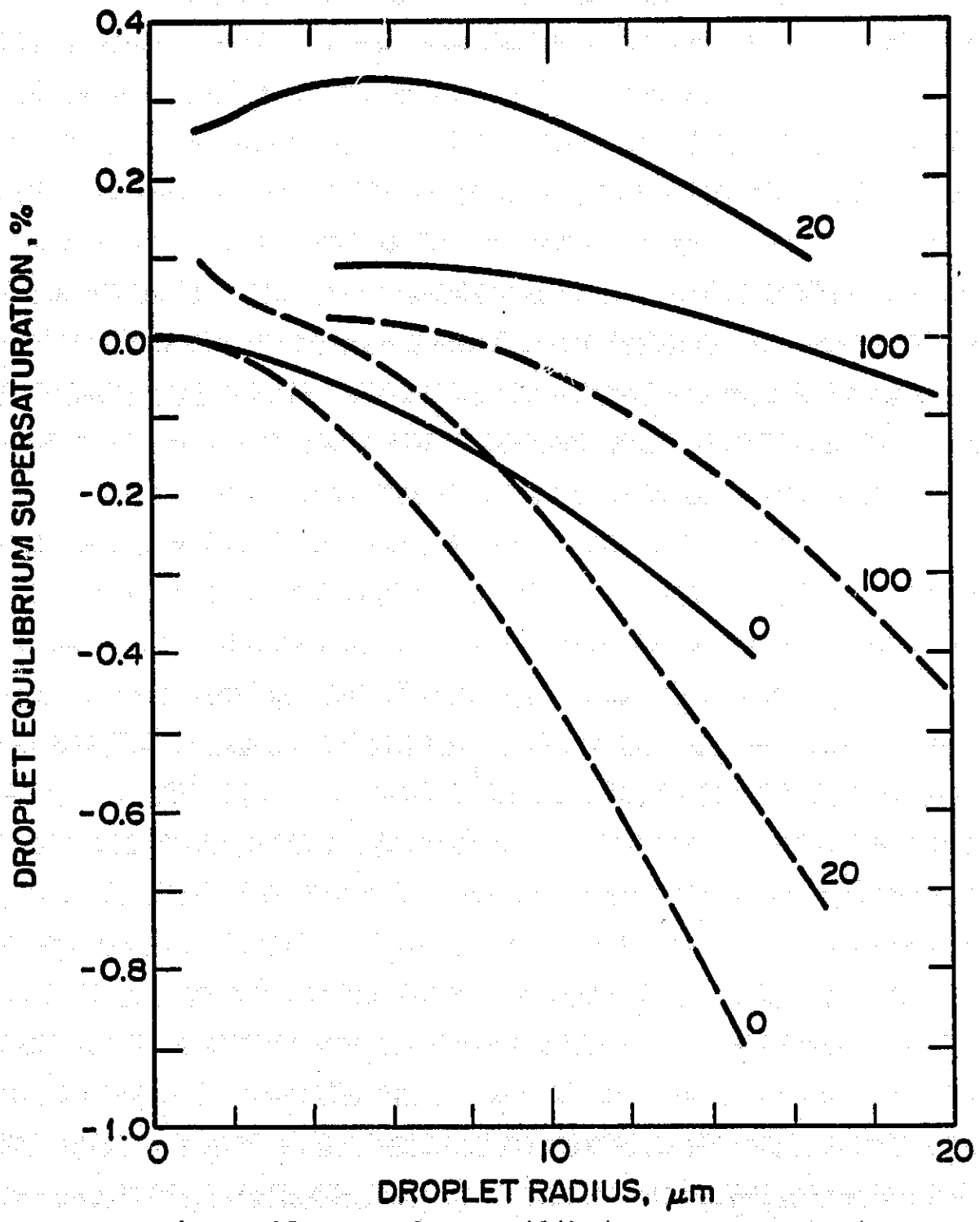

Figure 35. Droplet equilibrium supersaturation: Case 1. Curve labels are meters above cloud base. ——— Explicit model. - - - Implicit model.

Both the trend and the shape of the curves are different for the explicit model because a new dimension has been included in the computation of the droplet equilibrium supersaturation: the droplet temperature.

The implicit model uses the air temperature to calculate the droplet equilibrium vapor pressure. Even so, the accuracy of the growth rate equation used in the implicit model is not jeopardized by the substitution. This is because the air temperature and the droplet temperature are related by means of the Murray formulation (2.8) before arriving at the growth rate equation (2.10). The droplet temperature appears implicitly.

d. Energy terms

The values of the energy terms relative to the internal energy, Q_T, are shown in Figure 36. As $Q_L \approx -Q_K$, it is clear that Q_L and Q_K dominate. For the radiation term, the effective emissivity, E, is assigned the value 1.0. For Q_D, it is assumed that the enthalpy of dilution is -2.385×10^{10} ergs/mole of ammonium sulfate.

4.7 Conclusion

The explicit model is a workable alternative method for computing the growth or evaporation of droplets by vapor diffusion. For a simple system such as

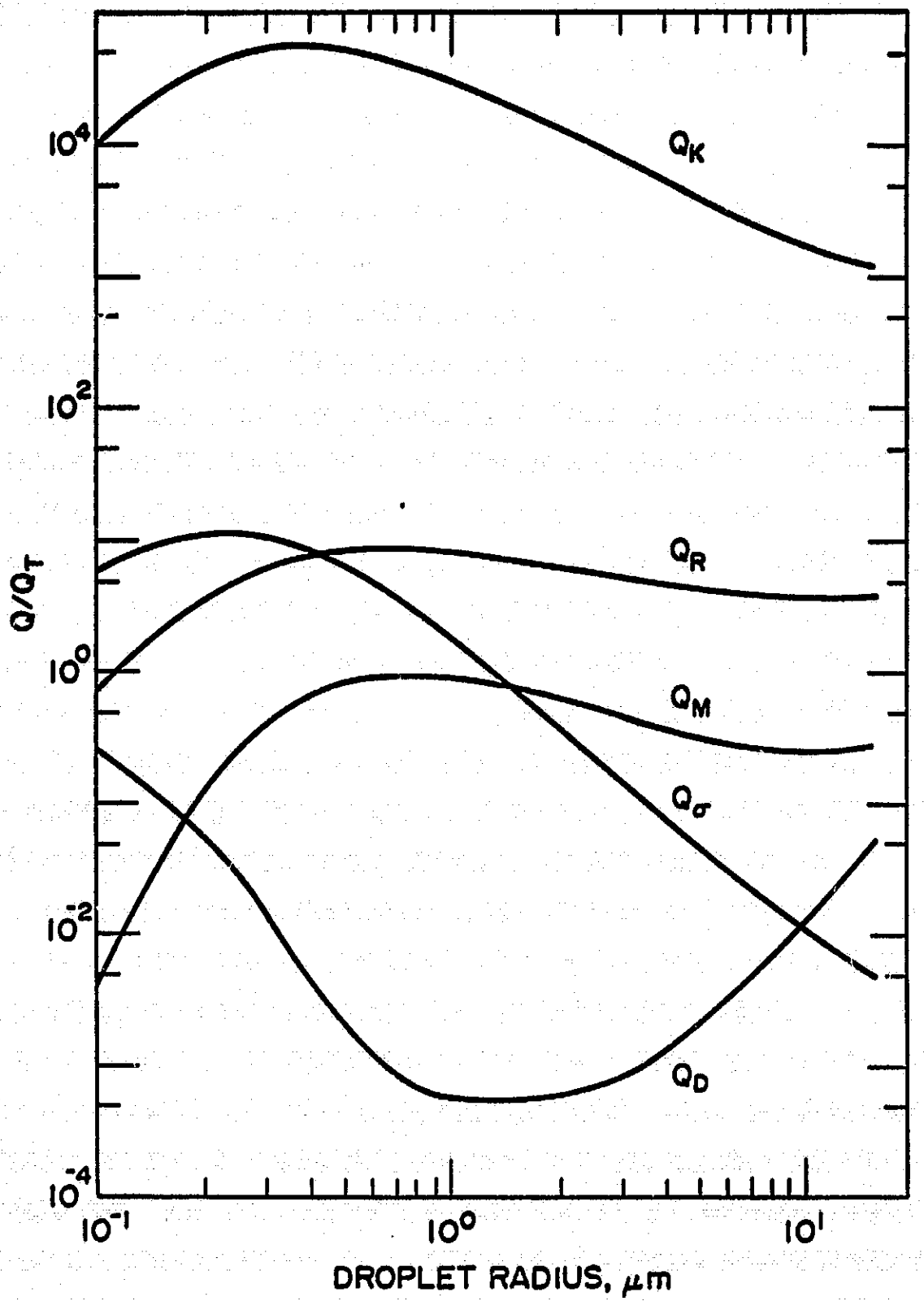

Figure 36. Indicated energy term relative to internal energy, Q_m, 10 meters above cloud base in a steady updraft of 1 m/s.

ammonium sulfate droplets, both the implicit and the explicit models predict comparable results up to at least the 100-meter level.

The explicit model makes direct use of the droplet temperature. By rearranging the energy balance equation, the set of equations includes one for the instantaneous droplet temperature elevation, rather than the time rate of change of the droplet temperature. This helps maintain computational stability by not requiring extreme accuracy in the calculation of minor energy terms.

For droplets of ammonium sulfate solution, all of the energy terms except Q_K and Q_L are unimportant and may be dropped without serious consequence. Indeed, without the extra energy terms, the explicit model essentially reduces to the implicit model.

It is the capability of considering all energy sources and sinks that makes the explicit model useful. To include more volatile liquids, it is assumed that $dm_r = dm_1 + dm_2 + \ldots$, where the subscript, r, refers to the bulk droplet, and the numbered subscripts represent the various components. This can be done because the energy terms are additive. Such a system allows for simultaneous diffusion of all components in both directions.

Some special information is required of each component, for example the diffusivity of each. The

sticking coefficient, α, used in the Fuchs' correction for vapor diffusion may be difficult to find in published data. The saturated vapor pressure over the solution can be used instead of the activity, if available. In addition, it is necessary to consider energies of chemical reactions and changes of phase of each component.

CHAPTER V

CONCLUDING REMARKS

5.1 Summary

Much research of the early growth of droplets within a cumulus congestus has been done before. A major shortcoming of models is the divergence between computed and observed droplet size distributions. In particular, droplet size distributions are observed to be broader than those calculated. Several schemes have been introduced to explain the observed distribution, chiefly turbulence and entrainment.

Turbulence has been characterized by, among others, random walk, mixing of parcels with different trajectories, and sinusoidal updraft velocities. This study uses a closed, adiabatic parcel of cloud air and imposes some simple predefined fluctuating velocity pattern to determine if there is any feedback from the action of dynamic turbulence alone to a distribution of cloud droplets.

Two types of velocity patterns are used: sinusoidal and alternating steady up and down motion. The latter is used because it is easier to control the period and amplitude of oscillation. The important point is that downward motion is included in the velocity pattern. Fourteen cases in all are studied: three steady updraft speeds of 1, 4, and 10 m/s; four cases of square wave oscillations; and seven cases with sinusoidal velocity

patterns of various eddy sizes and speeds. The study is restricted to the lowest 100 meters of cloud height.

Careful study of the steady updraft cases revealed that while small droplets can remain in near equilibrium with the environment, larger droplets tend to lag behind their equilibrium size because of their relatively long characteristic times for growth.

There are two consequences. First, large nuclei are not the first to become activated (surpass critical radius) and in fact may not be activated at all because of their large critical radius. Small droplets, on the other hand, do not become activated until their critical supersaturation is exceeded. Consequently, only a certain part of the nucleus distribution becomes activated and each droplet size has associated with it an equilibrium supersaturation which may be more than or less than zero.

Secondly, as a result of the fact that the vapor gradient to a droplet varies over the spectrum, droplets do not grow according to the inverse radius.

The result of these consequences is that if a parcel of cloud air is forced to descend, some droplets evaporate while others may continue to grow. Whether renewed updraft leads to a broader spectrum than before depends on many things. The transfer of water to droplets of large nuclei depends on the behavior of the portion of the spectrum which contains the bulk of the liquid water. If droplets in this region of the spectrum

undergo cycles of substantial evaporation and condensation, and at the same time the larger droplets grow throughout the cycle, then the droplet size distribution can be broadened.

If eddies are too small, then those droplets holding most of the liquid water do not evaporate to release the water for consumption by the large droplets; hence there is little effect on the droplet size distribution.

If an eddy size is too large, large droplets gain considerable mass of water at the expense of newly deactivated small droplets; subsequent uplifting results in a lower maximum supersaturation than before, and the small droplets do not reactivate. Consequently, the net effect is to increase the mean radius with no substantial increase of the breadth of the spectrum.

Also, if the downdraft speed is too high, all the droplets evaporate and recover with little hysteretic change.

Turbulence within a cloud has a wide range of eddy sizes and frequencies. The question that arises is this: does there exist a domain, or domains, of the turbulent energy spectrum that maximizes the breadth of the droplet size distribution, along with domains that produce narrow size distributions? The implication of this study is that such domains do exist.

A clear relationship between the droplet size distribution and eddy size and frequency has not been found since the underlying determinant is the ambient supersaturation and distribution of the droplet equilibrium supersaturation. In this study, the greatest increase in dispersion (107%) occurs when the parcel is lifted from the cloud base for 20 seconds at 1 m/s, lowered to the cloud base at -0.2 m/s, and lifted to the 100-meter level at 1 m/s. The maximum supersaturation during the first uplift is 0.71%. The minimum is -0.12% and the second maximum is 0.59%.

An adiabatic model as used here can increase the dispersion of a droplet population. It is not restricted to the cloud boundaries, but rather requires a certain oscillation of ambient supersaturation. These variations do occur in natural clouds, but not isotropically. Thus, different regions of a cloud, with different scales of turbulence, can have varying effects on the droplets therein.

Turbulence as described in this model lowers the ambient supersaturation and causes selective evaporation of the droplets, as does entrainment, but it does not at the same time dilute the vapor or introduce fresh particles. Further, an entrainment model which introduces cloud environment air and/or particles in a step-wise fashion may reduce the ambient supersaturation too much over a short period of time and lead to unrealistic results.

The model used for the study of turbulence is similar to one attributed to Mason (1957) in which the droplet temperature is dropped from the equation by substitution of a simplified heat balance equation for the droplet. The result is a single analytical expression for the growth rate of an individual droplet. Since the droplet temperature does not appear, it is called here the "implicit model."

A separate approach is presented in which all energy sources and sinks of a droplet may be considered. Since consolidation of the differential equations for droplet size and temperature is not possible, it is called the "explicit model."

Though details differ, studies show that for a population of droplets containing a nucleus of ammonium sulfate, both models give nearly identical results. Therefore, for this situation, energy terms such as radiation, surface expansion, and dilution of the droplet are unimportant and the implicit model adequately computes the rate of droplet growth.

The advantage of the explicit model, though, is that it is the first capable of computing the growth of solution droplets in the presence of more than one volatile component. Such a model is beneficial to the studies of air pollution scavenging and acid rain.

5.2 Suggestions for Further Research

The report presented here is limited in purview and by no means exhausts the study of the influence of turbulence upon a distribution of droplets. Some suggestions for further study follow:

1. The computations are limited to the lower 100 meters of the cloud - the region in which droplets first become activated. Extension to higher levels is necessary.

2. It would be desirable to include entrainment to see if it would increase or inhibit the effect of turbulence. Detrainment as well, in which a parcel slides down the edge of a cloud and reenters the updraft, should be considered.

3. Although the nucleus distribution is chosen somewhat arbitrarily, the portion of the size distribution which undergoes cycles of evaporation and regrowth coincide with that which contains the bulk of the liquid water. Other distributions should be tested.

4. No attempt is made to investigate the details and scales of dynamics and turbulence of a cloud. Such examinations exist (e.g., Fankhauser, 1969, 1971; Shmeter, 1970; Ackerman, 1967; Warner, 1970) and it is important to link the scales of turbulence to the microphysics.

5. One use of microphysical modelling is to parameterize the microphysics for inclusion into cloud models.

Further, the explicit model is merely introduced here. Extensions of the study include the following:

1. The explicit model is shown to be capable of treating the growth of droplets by the diffusion of water vapor. The next logical step is to use it to study the growth of droplets in the presence of multiple vapors.

2. Although the Hamming method used to integrate the equations is successful, it is time consuming for this system of equations. Other methods (Fox, 1972; Enright, et al., 1975) may prove to be more efficient.

APPENDIX

FUCHS' CORRECTION FACTORS

A.1 Correction for Vapor Diffusion

A droplet is considered to grow by the condensation of water vapor molecules which migrate to the surface of the droplet. Maxwell's equation assumes that diffusion is a continuous process; this treatment is not valid when the size of the droplet is of the order of magnitude of, or smaller than, the mean free path length, λ. For droplets smaller than λ, the Maxwell equation predicts a growth greater than that predicted by kinetic theory.

Langmuir (1915), while studying the dissociation of hydrogen in a light bulb, used the concept of a boundary layer near the wall surface. Borovikov, et al., (1963) called the boundary layer a parietal layer. According to Fuchs (1959), the necessary correction factor to the Maxwell equation was first derived by Schaefer (1932). The solution by Fuchs, especially the correction for heat transfer, has been criticized (Fukuta and Walter, 1970) somewhat. Fukuta and Walter (loc. cit.) and Fitzgerald (1972) have given a detailed derivation of the correction factor.

It is assumed that Maxwell's equation predicts the correct diffusion rate up to a distance $\delta \approx \lambda$ from

the droplet. Inside this layer, it is assumed that the motion of molecules is determined by kinetic theory.

The rate of collision of molecules onto the droplet surface, from kinetic theory, is

$$\frac{dm_w}{dt} = 4\pi r^2 C_\delta \nu_{v\delta} \alpha_c$$

where C_δ = vapor concentration at a distance $R = \delta$

α_c = condensation coefficient, or "sticking coefficient," the fraction of striking molecules which condense onto the surface, and

$\nu_{v\delta}$ = 1/4 of the mean velocity of vapor at $R = \delta$. Numerically, it is equal to $(R_v T/2\pi)^{1/2}$.

Similarly, the rate of evaporation is

$$\frac{dm_w}{dt} = 4\pi r^2 C_r \nu_{vr} \alpha_e ,$$

where ν_{vr} = 1/4 of the mean velocity of vapor molecules leaving the surface, and

α_e = evaporation coefficient.

Fuchs and other authors assume that $\nu_{vr} = \nu_{v\delta} = \nu$ and $\alpha_e = \alpha_c = \alpha$. It is not physically obvious that $\alpha_e = \alpha_c$, particularly in the case of a dirty surface. Under equilibrium conditions $\rho_r \nu_{vr} \alpha_e = \rho_\delta \nu_{v\delta} \alpha_c$,

suggesting that $\alpha_e = \alpha_c$ under conditions of equilibrium.

Fitzgerald (1972) lists values of α determined by the experiments of various investigators. Most reports of α vary from 0.02 to 0.05. Others found values as high as 0.3. Fuchs (1959) assumes the Alty and Mackay (1935) value of α for pure water of 0.036, as does Fitzgerald.

With these assumptions, then, the net rate of condensation is

$$\frac{dm_w}{dt} = 4\pi r^2 (C_\delta - C_r) \nu_v \alpha. \qquad (A.1)$$

For continuity, this rate must equal the rate of vapor diffusion to the surface of radius $r + \delta$, viz.

$$\frac{dm_w}{dt} = 4\pi (r+\delta) D (C_a - C_\delta). \qquad (A.2)$$

Combining equations (A.1) and (A.2),

$$C_\delta = \frac{C_r \nu_v \alpha r^2 + (r+\delta) D C_a}{r^2 \nu \alpha + (r+\delta) D}.$$

Substitution into equation (A.2) yields the growth equation in the form

$$\frac{dm_w}{dt} = 4\pi r F_v D (C_a - C_r), \qquad (A.3)$$

where

$$F_v = \frac{1}{\frac{r}{r+\delta} + \frac{D}{r\nu_v \alpha}}$$

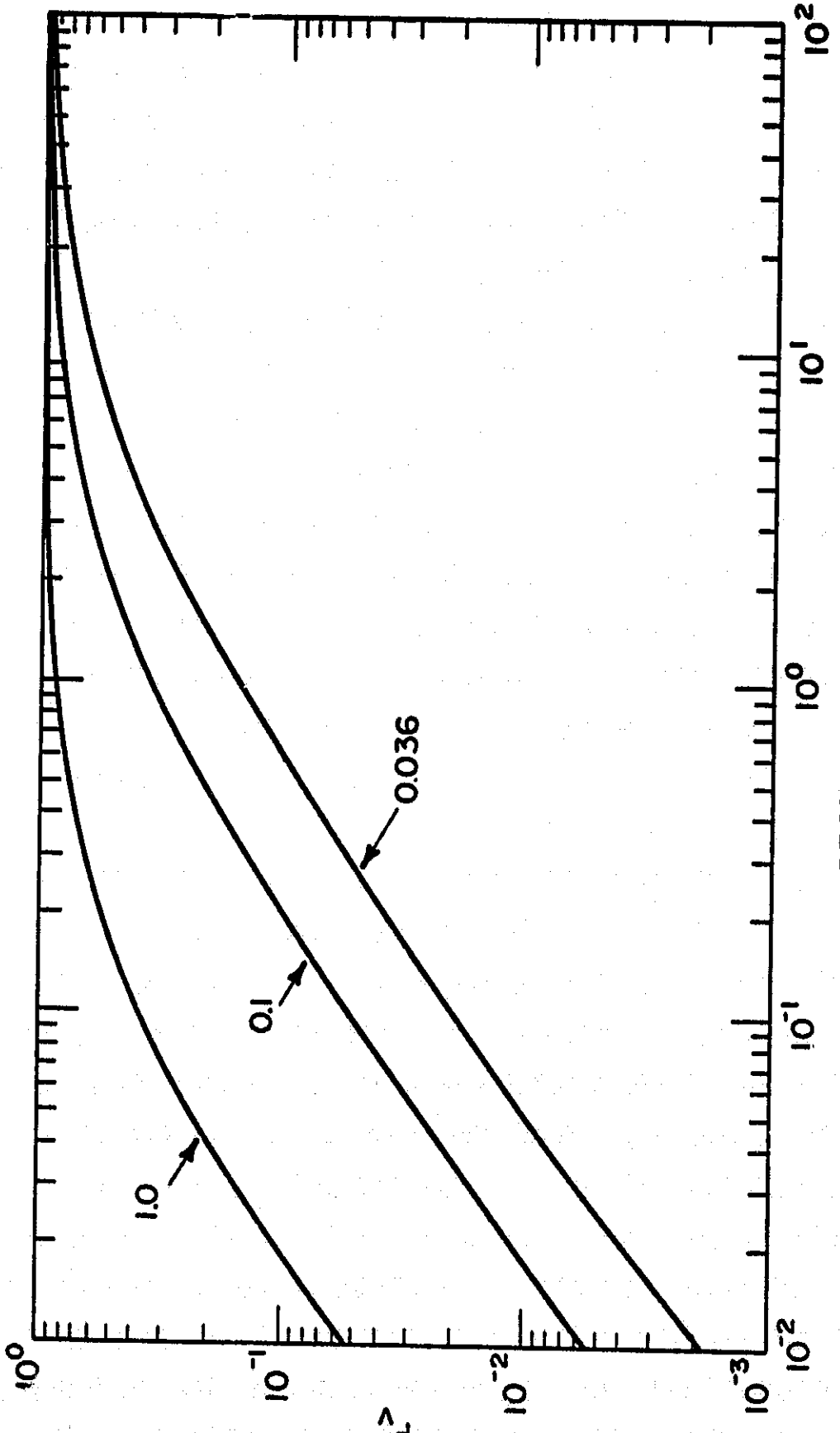

Figure 37. Correction factor for vapor diffusion at 10°C and 900 mb. Curve labels indicate value of condensation coefficient.

is the Fuchs correction to the coefficient of vapor diffusion. For this study, 0.036 is used for the condensation coefficient. Values of F_v at 10°C appear in Figure 37 .

A.2 Correction for Thermal Diffusion

Similar reasoning holds for the diffusion of sensible heat. For heat loss from the droplet,

$$\frac{dq}{dt} = 4\pi(r+\Delta)K(T_\Delta - T_a)$$

where K = thermal conductivity, and

Δ = thickness of parietal layer for heat diffusion.

The kinetic equation is

$$\frac{dq}{dt} = \pi r^2 \nu_d \rho_d c_{pd} (R_r - T_\Delta)\gamma. \qquad (A.4)$$

where

ν_d = ν for dry air molecules

ρ_d = density of dry air

c_{pd} = heat capacity at constant pressure for dry air, and

γ = accomodation coefficient.

It is assumed here that the vapor density in the parietal layer is negligible compared to that of dry air, and hence all the heat transfer is accomplished by the air molecules.

From the above equations,

$$T_\Delta = \frac{r^2 \rho_d \nu_d \gamma c_{pd} T_r + 4K(r+\Delta) T_a}{4K(r+\Delta) + \rho_a \nu_d \gamma c_{pd} r^2} .$$

Substitution into equation (A.4) yields

$$\frac{dq}{dt} = 4\pi r F_K K (T_r - T_a),$$

where

$$F_K = \frac{1}{\frac{r}{r+\Delta} + \frac{K}{r\rho_a \gamma c_{pd} \nu_d} \left(\frac{2\pi}{R_d T_r}\right)^{1/2}} \qquad (A.5)$$

is the Fuchs correction to the coefficient of thermal conductivity.

The accomodation coefficient is generally assumed to be close to unity. Howell (1949) and Fitzgerald (1972) used a value of 0.7 which is adopted here. The variance of F_K with droplet radius is shown by Figure 38.

A.3 Thickness of Parietal Layer

Fuchs (1964) gives a simplified derivation of δ (or Δ), since a rigorous derivation is difficult. Suppose there are two particles of radius r_i and r_j ($r_i \geq r_j$) and r_i is at rest. The small particles may leave the surface of the contact sphere (radius $r_i + r_j$) and go in any equally probable direction or distance

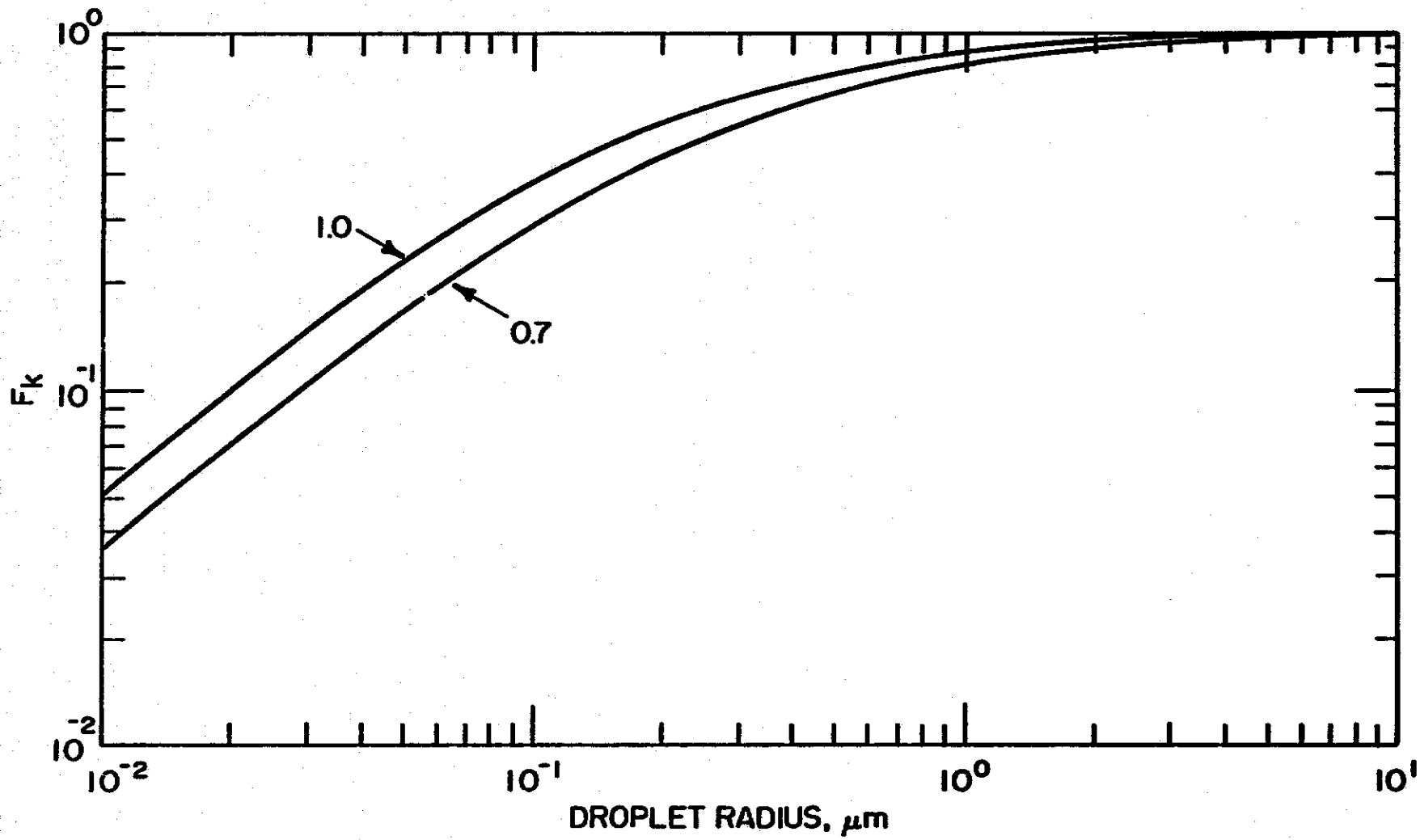

Figure 38. Correction factor for thermal diffusion at 10°C and 900 mb. Curve labels indicate value of thermal accomodation coefficient.

equal to the mean free path length, λ_j. The average distance normal to the surface is then

$$\delta = \frac{(r_i+r_j+\lambda_j)^3 - ((r_i+r_j)^2 + \lambda_j^2)^{3/2}}{3(r_i + r_j)\lambda_j} - (r_i+r_j).$$

For particles in relative motion, λ_j should be replaced with

$$\lambda = (\lambda_i^2 + \lambda_j^2)^{1/2}.$$

The mean free path of a vapor molecule is

$$\lambda_v = \lambda_0 \frac{Tp_0}{T_0 p} \left(\frac{M_a+M_w}{2M_a}\right)^{1/2} \left(\frac{2r_a}{r_a+r_w}\right),$$

where

λ_0 = mean free path length of air at T_0, p_0

M_a, M_w = molecular mass of air, water

r_a, r_w = radius of air, water molecule.

Similarly, the mean free path of an air molecule

$$\lambda_a = \lambda_0 \frac{Tp_0}{T_0 p}.$$

The thickness of parietal layers for vapor diffusion, δ, and thermal diffusion, Δ, are shown in Figure 39. The radius of air and water molecules are assumed negligible relative to that of the droplet.

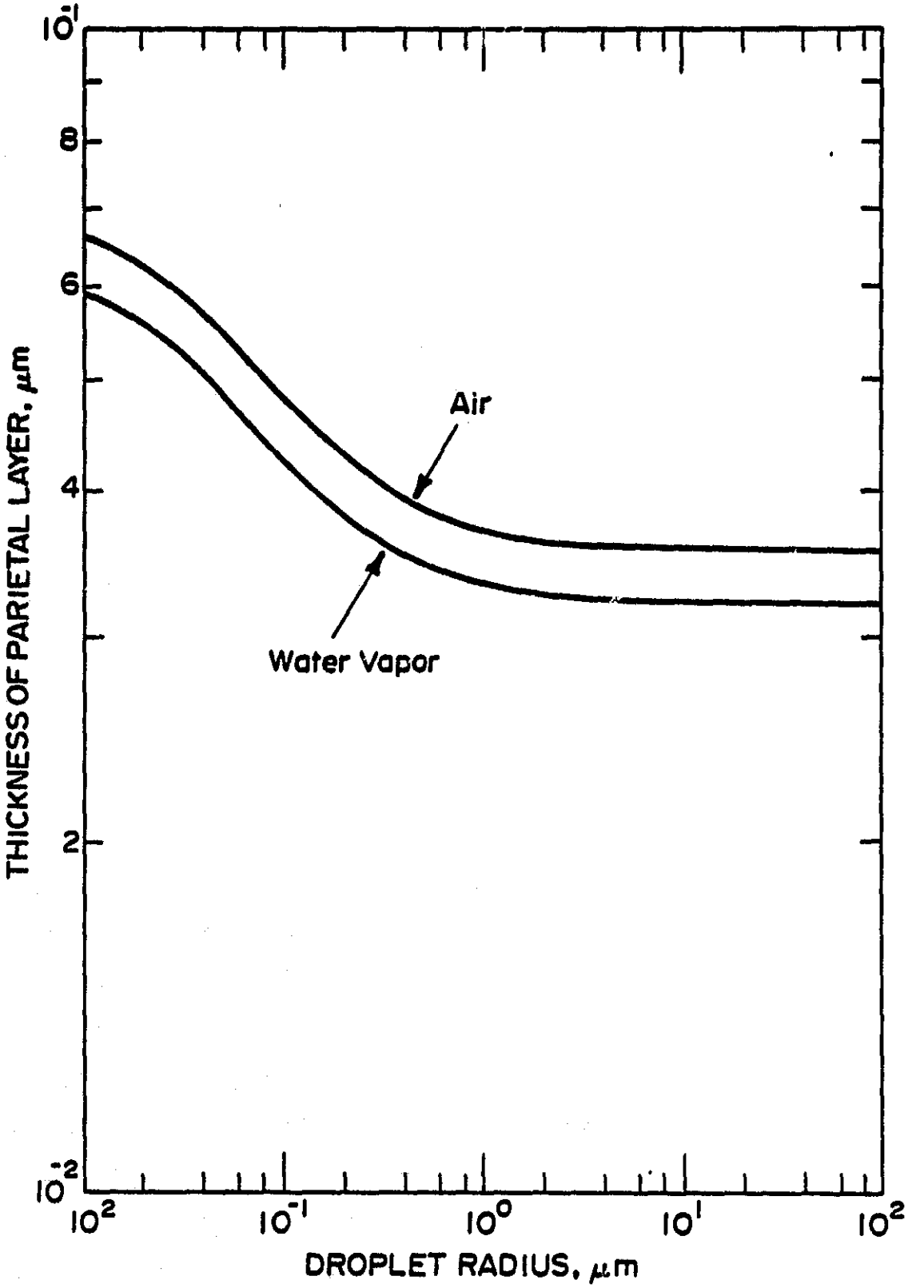

Figure 39. Thickness of parietal layer at 10°C and 900 mb. The mean free path lengths for air and water molecules are 0.071 and 0.064 μm, respectively.